LATVIJAS UNIVERSITĀTE
ĶĪMIJAS FAKULTĀTE

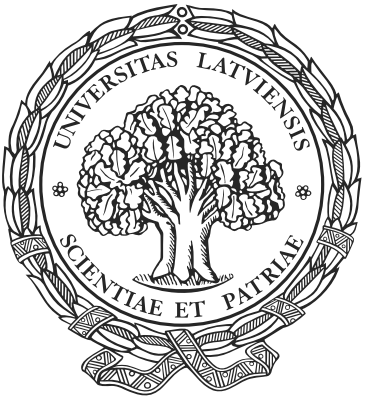

Toms Rēķis

Enantiomēru atpazīšana kristāliskā stāvoklī: izvēlētu mazu organisku molekulu enantiomēru veidoto cieto šķīdumu strukturālā un termodinamiskā daba

PROMOCIJAS DARBS

Doktora grāda iegūšanai ķīmijas nozarē
Apakšnozare: Fizikālā ķīmija

Rīga, 2018

I call any geometrical figure, or group of points, 'chiral', and say that it has chirality if its image in a plane mirror, ideally realized, cannot be brought to coincide with itself.

Sers Viljams Tomsons Lords Kelvins, 1894

Promocijas darbs izstrādāts Latvijas Universitātes Ķīmijas fakultātes Fizikālās ķīmijas katedrā, Maksa Planka Kompleksu tehnisku sistēmu dinamikas institūta Procesu inženierijas fizikālo un ķīmisko pamatu laboratorijā, Magdeburgā, Vācijā un Boloņas Universitātes Ķīmijas fakultātes Molekulāro kristālu inženierijas grupā, Boloņā, Itālijā laika posmā no 2014. gada līdz 2017. gadam.

Darbs sastāv no kopsavilkumiem latviešu un angļu valodās un no 4 zinātniskajām publikācijām. Darba forma: publikāciju kopa Ķīmijā, Fizikālajā ķīmijā.

Darba vadītājs: Vad. pētn., *Dr.chem.* Liāna Orola
Zinātniskie konsultanti: Vad. pētn., *Dr.chem.* Agris Bērziņš
Prof., *Dr.chem.* Andris Actiņš
apl. Prof., *Dr.rer.nat.* Haike Lorenca
Prof., *Dr.* Fabrīcija Grepioni

Recenzenti:
Dr.phys. Anatolijs Mišņovs (Latvijas Organiskās sintēzes institūts)
Prof., *Dr.chem.* Māris Turks (Rīgas Tehniskā universitāte)
Asoc. prof., *Dr.chem.* Pēteris Mekšs (Latvijas Universitāte)

Promocijas darba aizstāvēšana notiks 2018. gada 10. maijā, plkst. 14.00, Latvijas Universitātes Ķīmijas nozares promocijas padomes atklātā sēdē, Latvijas Universitātē, Ķīmijas fakultātē, Jelgavas ielā 1, 701. auditorijā.

Ar promocijas darbu var iepazīties LU Bibliotēkas Daudznozaru bibliotēkā: datorika, juridiskās zinātnes, teoloģija (Rīgā, Raiņa bulvārī 19).

ISBN 978-9934-556-33-3

ANOTĀCIJA

Darbā pētītas vairākas cietos šķīdumus veidojošas enantiomēru sistēmas. Izpētīta izvēlēto savienojumu enantiotīro un racēmisko formu kristālisko cietfāžu daudzveidība (polimorfisms un solvatomorfisms). Enantiomēru sistēmas raksturotas ar divkomponentu fāžu diagrammām, norādot uz termodinamiski stabilu un metastabilu cieto šķīdumu veidošanos pilnā un nepilnā enantiomēru sastāva apgabalā. Noteiktas arī kristāliskās struktūras, atklājot cietos šķīdumus ar enantioselektīvām un stereonespecifiskām kristalogrāfiskajām pozīcijām. Apkopojot eksperimentālos un literatūras datus, pārskatīta viena (enantioselektīvā) cieto šķīdumu tipa definīcija. Noteikta pētīto savienojumu cieto šķīdumu strukturālā daba, norādot gan uz no hirālā centra konfigurācijas neatkarīga ūdeņraža saišu tīkla lomu, gan uz stereonespecifiskām π···π mijiedarbībām. Visbeidzot, tika sintezēti divi jauni savienojumi, kuru enantiomēri veido cietos šķīdumus, tādējādi norādot, ka šādas ārkārtīgi reti sastopamas fāzes var tikt konstruētas un iegūtas apzināti.

Enantiomēru cietie šķīdumi, enantiomēru atpazīšana kristāliskā stāvoklī, divkomponentu fāžu diagrammas, *qvazi*–centrosimetriskas struktūras, nesakārtotas struktūras

SATURS

Anotācija 5
Ievads 7
Publicētie rezultāti 10
1. nodaļa. Promocijas darba teorētiskie pamati un pētītās sistēmas 12
1.1. Enantiomēru cieto šķīdumu termodinamiska raksturošana 12
1.2. Enantiomēru cieto šķīdumu strukturālā daba 13
1.3. Pētītās sistēmas 14
2. nodaļa. Rezultāti un to izvērtējums 16
2.1. Pimobendāna (**1**) enantiomēru veidotie cietie šķīdumi 16
2.2. Fenilpiracetāma (**2**) enantiomēru veidotie cietie šķīdumi 20
2.3. Naftalimīda atvasinājumu (**3**) enantiomēru veidotie cietie šķīdumi 24
Secinājumi 30
Literatūras saraksts 32
Pielikumi 67

CONTENTS

Abstract 39
Introduction 40
Results published 43
Chapter 1. Research background 45
1.1. Thermodynamic Characterization of Solid Solutions of Enantiomers 45
1.2. Structural Aspects of Solid Solutions of Enantiomers 46
1.3. Objects of investigation 47
Chapter 2. Results and discussion 49
2.1. Solid Solutions of Pimobendan (**1**) Enantiomers 49
2.2. Solid Solutions of Phenylpiracetam (**2**) Enantiomers 53
2.3. Solid Solutions of Naphthalimide Derivative (**3**) Enantiomers 57
Conclusions 63
References 65
Appendices 67

IEVADS

Hiralitātei ir liela nozīme dažādās zinātņu jomās. Hirāla savienojuma enantiomēri katrs atsevišķi nav izšķirami ahirālās vidēs[1]; bet, ņemot vērā atšķirīgas savstarpējās mijiedarbības, tas tā nav, ja sistēmā parādās citas hirālas daļiņas. Tas attiecas arī uz abu enantiomēru maisījumiem. Hiralitātei tāpēc ir būtiska nozīme tad, kad optiski aktīviem savienojumiem paredzēts mijiedarboties ar bioloģiskām sistēmām. Ļoti bieži farmācijā, agroķīmijā vai pārtikas industrijā tikai viens no enantiomēriem ir vēlams[2,3] tādēļ, ka otra izmantošana saistāma ar kaitīgu, potenciāli kaitīgu efektu, vai arī nevajadzīgu papildu vielas uzņemšanu vai lietošanu. Tomēr lielākoties sintēzē ir nesalīdzināmi vienkāršāk iegūt ekvimolāru (racēmisku) enantiomēru maisījumu, nevis molekulas to enantiotīrā formā. Līdz ar to tīru enantiomēru iegūšana ir liels izaicinājums gan organiskajā, gan fizikālajā ķīmijā[4].

Pēdējās desmitgadēs panākts ievērojams progress, attīstot enantioselektīvas un stereospecifiskas sintētiskās metodes. Tomēr vēsturiski tīri enantiomēri tikuši iegūti no racēmiskiem maisījumiem ar atdalīšanas metodēm. Uz kristalizāciju balstīta enantioatdalīšana joprojām ir ļoti populāra un pat vēlama industriālam pielietojumam, jo tā ir robusta un ievērojami lētāka metode. Šāda enantioatdalīšana ir lielākoties iespējama, veidojot diastereomērus aduktus (sāļus, kokristālus vai pat kovalentus savienojumus), bet arī tieša atdalīšana no racēmiska maisījuma ir iespējama[4]. Fundamentāli pētījumi par stereoselektivitāti un stereospecifiskumu tāpēc ir svarīgi, lai sistematizētu un racionalizētu dažādu kristālisko fāžu veidošanās dabu. Pie tam, tā kā pēdējā laikā īpaši tiek pētīta molekulāro kristālu potenciālā pielietojamība molekulārajās iekārtās[5], fundamentāla zinātība par enantioselektivitāti un enantiospecifiskumu kristāliskā stāvoklī ir noderīga kristālu inženierijas jomā.

Lai arī abi enantiomēri ir simetriski, tie nav kongruenti objekti, un tāpēc tie ir dažādi elementi kristāliskās struktūras veidošanā. No tā izriet, ka no šādām dažādām (bet pēc būtības identiskām) molekulām var veidoties daudzveidīgas cietfāzes. Kristalizējot racēmiskus maisījumus, iespējams rasties trīs dažādiem produktiem: 1) racēmiskie savienojumi (veidojas ~90% gadījumos); 2) konglomerāti (~10% gadījumos); 3) enantiomēru cietie šķīdumi (<1% gadījumos)[6]. Racēmiskais savienojums ir fāze, kuras sastāvā ir abi enantiomēri. Jēdziens "racēmiskais savienojums" būtībā uztverams kā termins abu enantiomēru veidotam molekulārām savienojumam attiecībā 1:1. Retāk racēmisku maisījumu kristalizācijā šādi racēmiskie savienojumi gan neveidojas. Tā vietā katrs enantiomērs kristalizējas atsevišķā kristāliskā struktūrā, un iegūto mehānisko maisījumu sauc par konglomerātiem. Abas fāzes ir spoguļfāzes viena otrai. Visbeidzot, ļoti reti novēro enantiomēru cieto šķīdumu veidošanos.

Racēmisko savienojumu, konglomerātu un cieto šķīdumu novērtētā statistiskā izplatība[6] norāda uz to, ka visbiežāk kristalogrāfiskās molekulu pozīcijas ir stingri stereospecifiskas. Racēmiskajos savienojumos *per se* pastāv strikta enan-

tiomēru kārtība, un konglomerātu veidošanās gadījumā katrā struktūrā ir tikai viens no enantiomēriem. Savukārt reti sastopamie enantiomēru cietie šķīdumi, kuros divi komponenti (enantiomēri) kristāliskā stāvoklī netiek atpazīti, nav tipiski molekulāriem kristāliem – sistēmām, kurās pirmām kārtām parasti eksistē trīsdimensionāla translācijas simetrija.

Tā kā enantiomēru cietie šķīdumi ir tik reta parādība, tie ir maz pētīti. Tomēr tie slēpj atbildes par stereoselektivitātes un stereospecifiskuma mehānismiem molekulārajos kristālos. Sākotnējos šādu sistēmu pētījumos enantiomēru cietie šķīdumi tika raksturoti galvenokārt ar divkomponentu fāžu diagrammām[6]. Attīstoties rentgendifraktometriskajām metodēm un datu apstrādes programmām, ir bijusi iespēja noteikt vairāku cieto šķīdumu struktūras, kurās uzskatāmi novērojama abu enantiomēru veidota nesakārtotība[7–11], līdz ar to ir bijusi iespēja analizēt šādu fāžu strukturālo dabu, kas pamatā aprakstīta jau gadu desmitus atpakaļ Šiona *et al.* un Kitaigorodska darbos[12,13].

Joprojām nav metodžu, kas ļautu paredzēt enantioselektivitāti un enantiospecifiskumu kristāliskā stāvoklī, kas tādējādi dotu iespēju plānot stereospecifisku kristalizācijas procesu, izvairoties no liela eksperimentālā darba apjoma. Līdz ar to nav iespējams arī paredzēt enantiomēru cieto šķīdumu veidošanos vai arī mērķtiecīgi sintezēt hirālas molekulas, kas veidotu šādas jauktās kristāliskās fāzes. Enantiomēru cietie šķīdumi gan varētu būt interesanti pielietojumam tā sauktajās molekulārajās ierīcēs, jo tie ir vienas fāzes kristāliski materiāli ar iespēju (atkarībā no sastāva) smalki regulēt fizikālķīmiskās īpašības, piemēram, nelineārās optikas īpašības.

Šī pētījuma **mērķis** ir izpētīt hirālu mazu organisku molekulu daudzkomponentu sistēmas, kurās novērojama enantiomēru neatpazīšana kristāliskā stāvoklī ar nolūku noteikt enantiomēru cieto šķīdumu veidošanās strukturālos un termodinamiskos aspektus, lai būtu iespējams peredzēt cieto šķīdumu veidošanos vai mērķticīgi tos iegūt.

DARBA UZDEVUMI

1. Raksturot fenilpiracetāma enantiomēru sistēmu, konstruējot divkomponentu fāžu diagrammu un veicot detalizētus kristālisko fāžu struktūras pētījumus.
2. Raksturot pimobendāna enantiomēru sistēmu, konstruējot divkomponentu fāžu diagrammu.
3. Ar rentgendifrakcijas un termiskās analīzes metodēm raksturot plašo pimobendāna enantiomēru cieto šķīdumu sistēmu.
4. Veikt enantiotīra un racēmiska pimobendāna cietfāžu struktūru pētījumu.
5. Izpētīt cieto šķīdumu veidošanās iespējamību 2–(hinuklidin–3–il)–1,8–naftalimīda enantiomēru sistēmā, veicot racēmiska un neracēmiska sastāva kristālu struktūru pētījumus.
6. Sintezēt jaunus aizvietotus 2–(hinuklidin–3–il)–1,8–naftalimīda at-

vasinājumus, kuri veidotu enantiomēru cietos šķīdumus.

ZINĀTNISKĀ NOVITĀTE

1. Kopumā tika noteiktas 9 jaunas enantiomēru cieto šķīdumu struktūras, kas ir aptuveni tikpat, cik atrodams zinātniskajā literatūrā līdz šim. Noteiktās struktūras tika izmantotas, lai vēl detalizētāk racionalizētu enantiomēru cieto šķīdumu veidošanās strukturālo dabu.
2. Konstruētas divu sistēmu divkomponentu fāžu diagrammas, raksturojot pētīto cieto šķīdumu termodinamisko dabu, kā arī norādot uz šādu sistēmu sarežģītību (tai skaitā polimorfu enantiotropu saistību un vairāku metastabilu cieto šķīdumu veidošanās iespējamību).
3. Izpētīta plaša pimobendāna enantiomēru cieto šķīdumu sistēma, kas ietver ne tikai nesolvatētas, bet arī solvatētas fāzes. Tādējādi tas ir pirmais zinātniskajā literatūrā aprakstītais gadījums, kurā enantiomēru cieto šķīdumu veidošanās iemeslus iespējams izskaidrot molekulārā līmenī. Tas parāda, ka cieto šķīdumu veidošanās ne vienmēr ir saistīta ar molekulārās un kristāliskās struktūras specifisku īpatnību mijiedarbi.
4. Tika veikts detalizēts enantiomēru cieto šķīdumu skalēmisku kristālu struktūru pētījums, kas literatūrā sastopams reti, jo pārsvarā aprakstītas enantiotīro un racēmisko robežgadījumu cieto šķīdumu struktūras. Skalēmisko kristālu struktūrās novērotās īpatnības pierāda atsevišķu enantiomēru cieto šķīdumu piederību II tipam (ar enantioselektīvām kristalogrāfiskajām molekulu pozīcijām), kuri literatūrā nereti piedēvēti I cieto šķīdumu tipam.
5. Sintezēti divi jauni savienojumi, kuru enantiomēri veido cietos šķīdumus. Šādas cietfāzes, kurās enantiomēri netiek pilnībā atpazīti līdz šim nav tikuši mērķtiecīgi sintezēti.

PRAKTISKĀ NOZĪME

1. Pimobendāna (ražo A/S "Grindeks") cieto šķīdumu pētījuma rezultāti ļāva atrisināt kvalitātes kontroles problēmas pimobendāna A formas ražošanas procesā.
2. Fenilpiracetāma (ražo A/S "Olainfarm") cieto šķīdumu pētījuma rezultāti ļāva risināt patentēšanas problēmas enantiotīra savienojuma gadījumā.
3. Racionalizēti enantiomēru cieto šķīdumu veidošanās strukturālie aspekti, tādējādi paverot iespēju kristālu inženierijā veidot pievilcīgus molekulāru kristālu materiālus ar smalki regulējamām (no enantiomēru sastāva atkarīgām) īpašībām.

PUBLICĒTIE REZULTĀTI

Publikācijas, konferenču tēzes un patenti

1. Rekis, T., Bērziņš, A., Sarceviča, I., Kons, A., Balodis, M., Orola, L., Lorenz, H., Actiņš, A., A maze of solid solutions of pimobendan enantiomers: an extraordinary case of polymorph and solvate diversity. *Cryst. Growth Des.* **2018**, 18(1), 264–273.

   T. Rēķis izstrādāja 40% no eksperimentālā darba apjoma, izstrādāja plānu un uzrakstīja publikāciju, noformēja pētījuma rezultātus atbilstoši žurnāla prasībām, kā arī sagatavoja atbildes uz recenzentu jautājumiem un aizrādījumiem.

2. Rekis, T., d'Agostino, S., Braga, D., Grepioni, F., Designing solid solutions of enantiomers: lack of enantioselectivity of chiral naphthalimide derivatives in the solid state. *Cryst. Growth Des.* **2017**, 17(12), 6477–6485.

   T. Rēķis izstrādāja 70% no eksperimentālā darba apjoma, izstrādāja plānu un uzrakstīja publikāciju, noformēja pētījuma rezultātus atbilstoši žurnāla prasībām, kā arī sagatavoja atbildes uz recenzentu jautājumiem un aizrādījumiem.

3. Rekis, T., Bērziņš, A., Džabijeva, D., Nakurte, I., Orola, L., Actiņš, A., Structure and Stability of Racemic and Enantiopure Pimobendan Monohydrates: On the Phenomenon of Unusually High Stability. *Cryst. Growth Des.* **2017**, 17(4), 1814–1823.

   T. Rēķis izstrādāja 70% no eksperimentālā darba apjoma, sniedza ieguldījumu publikācijas rakstīšanā (80%), noformēja pētījuma rezultātus atbilstoši žurnāla prasībām, kā arī sniedza ieguldījumu, sagatavojot atbildes uz recenzentu jautājumiem un aizrādījumiem.

4. Rekis, T., Bērziņš, A., Orola, L., Holczbauer, T., Actiņš, A., Seidel-Morgenstern, A., Lorenz, H., Single Enantiomer's Urge to Crystallize in Centrosymmetric Space Groups: Solid Solutions of Phenylpiracetam. *Cryst. Growth Des.* **2017**, 17(3), 1411–1418.

   T. Rēķis izstrādāja 90% no eksperimentālā darba apjoma, izstrādāja plānu un uzrakstīja publikāciju, noformēja pētījuma rezultātus atbilstoši žurnāla

prasībām, kā arī sagatavoja atbildes uz recenzentu jautājumiem un aizrādījumiem.

5. Rekis, T., Bērziņš, A., Orola, L., Actiņš, A., Seidel-Morgenstern, A., Lorenz, H., On the formation of phenylpiracetam solid solutions: thermodynamic and structural considerations. *Proceedings 23rd Int Workshop on Industrial Crystallization (BIWIC 2016)* **2016**, 106-111.

6. Rēķis, T., Oša, G., Bērziņš, A., Actiņš, A. Pimobendāna polimorfās kristāliskās A formas iegūšanas paņēmiens. *Patents A61K31/501*, **2013**

Konferences

1. T. Rekis, A. Bērziņš, L. Orola, A. Actiņš, A. Seidel-Morgenstern, H. Lorenz, On the formation of phenylpiracetam solid solutions: thermodynamic and structural considerations. *23rd International Workshop on Industrial Crystallization (BIWIC 2016)*, Magdeburga, Vācija, **2016**

2. T. Rekis, G. Oša, A. Bērziņš, L. Orola, I. Sarceviča, A. Actiņš, H. Lorenz, The chaos in a solid solution decreased in the presence of a solvent: the case of racemic pimobendan. *14th European Powder Diffraction Conference (EPDIC 2016)*, Bari, Itālija, **2016**

3. T. Rekis, A. Bērziņš, L. Orola, I. Sarceviča, G. Oša, I. Heinmaa, R. Prekup, A. Actiņš The chaos in a solid solution decreased in the presence of a solvent: the case of racemic pimobendan. *8th Crystal Forms @ Bologna*, Boloņa, Itālija, **2015**

4. T. Rēķis, G. Oša, A. Bērziņš, L. Orola, I. Sarceviča, A. Actiņš Time dependent systematic unit cell parameter change of pimobendan polymorph. *7th Crystal Forms @ Bologna*, Boloņa, Itālija, **2013**

5. T. Rēķis, L. Orola, O. Sežanova, A. Bērziņš, A. Actiņš. Polymorphic and solvatomorphic forms of pimobendan. *University of Latvia 70th conference*, Rīga, Latvija, **2012**

1. NODAĻA
PROMOCIJAS DARBA TEORĒTISKIE PAMATI UN PĒTĪTĀS SISTĒMAS

1.1. ENANTIOMĒRU CIETO ŠĶĪDUMU TERMODINAMISKA RAKSTUROŠANA

Cietie šķīdumi ir izostrukturālas fāzes, kas sastāv no vismaz diviem komponentiem ar mainīgu sastāvu. Konstruējot divkomponentu fāžu diagrammas, iespējams noskaidrot cieto šķīdumu veidošanās iespējamību, kā arī tos raksturot, piemēram, nosakot termodinamisko stabilitāti un komponentu sajaukšanās attiecību robežas. 1.1. attēlā redzamas pamata fāžu diagrammas, kurās iesaistīti cietie šķīdumi.

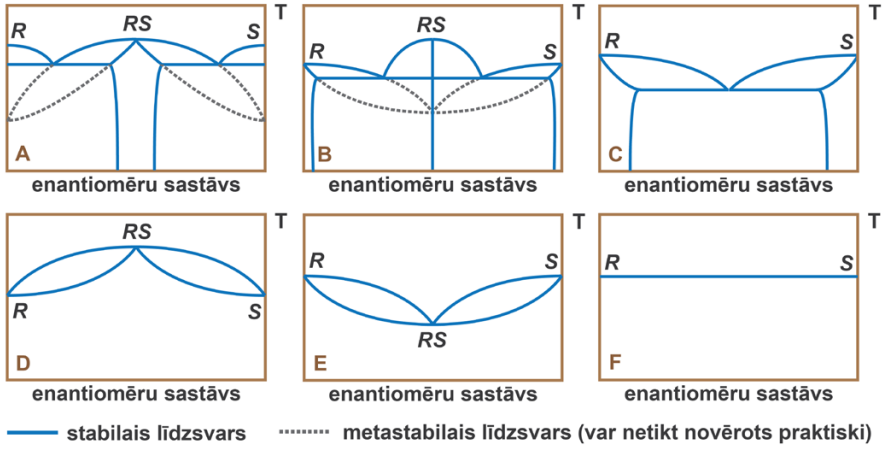

1.1. att. **Divkomponentu sistēmu fāžu diagrammas sistēmām ar cieto šķīdumu veidošanos (A–C ar daļēju un D–F pilnīgu komponentu sajaukšanos).**

Literatūrā ziņots par enantiomēru sajaukšanos racēmiskā sastāva apgabalā[14], enantiotīrā sastāva apgabalā[12,15,16] kā arī visā kompozīcijas diapazonā[7,8,10,11,17–19]. Fāžu diagrammu konkrētam savienojumam definē cietfāžu termodinamiskā daba. Piemēram, ja cietais šķīdums novērojams racēmiskā sastāva apgabalā (1.1. attēls A), tad eksistē racēmiska fāze RS, kurai piemīt struktūras īpatnība aizvietot enantiomērus ar pretējiem, tādējādi veidojot skalēmiska sastāva fāzes – cietos šķīdumus. Enantiomēru sajaukšanās tomēr nav novērojama visā sastāva apgabalā, jo eksistē stabila strukturāli atšķirīga enantiotīra fāze S (jeb R). Sajaukšanās apgabala platumu un citas kvantitatīvas fāžu diagrammas īpašības nosaka cietfāžu RS un

S (jeb R) fizikālķīmiskās īpašības – kušanas entalpijas un kušanas temperatūras. Gadījumā, kad sajaukšanās novērojama enantiotīra sastāva tuvumā (1.1. attēls B un C), eksistē cietfāze S (vai R) ar struktūras īpatnību veidot cieto šķīdumu. B gadījumā racēmiskā sastāvā eksistē stabila cietfāze RS. Attēlotais metastabilais līdzsvars var netikt arī novērots. C gadījumā, savukārt, ierobežota sajaukšanās skaidrojama ar to, ka pie noteikta sastāva cietā šķīduma struktūra vairs nav termodinamiski stabila, un tā vietā veidojas mehānisks divu fāžu (cieto šķīdumu ar robežgadījuma sastāvu) maisījums. Gadījumi D, E un F attēlo enantiomēru sajaukšanos visā kompozīciju apgabalā, attiecīgi veidojot neideālus cietos šķīdumus ar maksimālo un minimālo kušanas temperatūru racēmiskam sastāvam, un ideālu cieto šķīdumu. Cietfāzes RS un S (jeb R) šajos gadījumos ir izostrukturālas.

1.2. ENANTIOMĒRU CIETO ŠĶĪDUMU STRUKTURĀLĀ DABA

No struktūrālā skatu punkta enantiomēru atpazīšanu cietajos šķīdumos var raksturot ar diviem cieto šķīdumu tipiem: 1) enantionespecifisku (I tips); 2) enantioselektīvu (II tips). I tips ir definēts šādi: kristālā, kurš satur x daudzumu R molekulu un $(1-x)$ daudzumu S molekulu, varbūtība atrast molekulu R kristalogrāfiskajā molekulu pozīcijā ir x, un varbūtība atrast molekulu S ir $(1-x)$[12].

II tips šajā pētījumā attiecināts uz struktūrām, kurās vērojama noteikta no struktūras īpatnībām izrietoša enantioselektivitāte. Oriģinālajā Šiona *et al.* definīcijā nepātraukta enantiomēru sajaukšanās tika piedēvēta tikai daļai kristalogrāfisko molekulu pozīciju, kas attiecīgi racēmiska sastāva gadījumā paredzēja sakārtotu racēmisko savienojumu. Tomēr, kā rāda literatūrā ziņotās nepārprotami enantioselektīvu cieto šķīdumu struktūras[7–11], ne vienmēr tiek iegūtas pilnībā sakārtotas racēmiskas struktūras, bet gan drīzāk attiecīgās struktūras tikai tiecas uz enantiospecifisko speciālgadījumu, kāds būtu sakārtots racēmiskais savienojums. Tādēļ II tipa cieto šķīdumu definīcija ir pārskatīta salīdzinājumā ar to, kas tika dota oriģinālajā petījumā gadu desmitus atpakaļ, iztirzājot enantiomēru cieto šķīdumu strukturālo dabu[12]. Oriģinālā definīcija drīzāk atbilst idealizētam enantioselektīva cietā šķīduma (II tipa) speciālgadījumam.

I tipa cietajos šķīdumos nav novērojama nekāda enantiomēru atpazīšana kristāliskā stāvoklī, savukārt II tipa cieto šķīdumu strukturālā daba ir sarežģītāka. Ņemot vērā fizikālus un ķīmiskus apsvērumus, vispārīgā gadījumā tīrs enantiomērs var kristalizēties tikai vienā no 65 Zonkes telpiskajām grupām (bez otrā veida simetrijas elementiem, kuri ir enantiogēni – inversijas centri, rotoinversijas asis, spoguļplaknes vai slīdplaknes)[20]. Visbiežāk gan II tipa cietajos šķīdumos ir novērojama šķietama centrosimetrija: vienas un tās pašas konfigurācijas molekulas ieņem dažādas konformācijas, kas dod aptuvenus spoguļattēlus savā starpā. Minētā strukturālā daba ir attēlota 1.2. attēlā.

Enantiotīra viela kristalizējas *kvazi*–centrosimetriskā struktūrā, līdz ar to trūkstošais enantiomērs tiek imitēts, struktūrā esošajam ieņemot atšķirīgas konformācijas. Skalēmiskās struktūrās lokāli būtu novērojami patiesi inversijas centri (vai citi otrā veida simetrijas operāciju lokusi). Racēmiskam sastāvam attēlo-

ti divi gadījumi – pilnībā sakārtota struktūra jeb racēmiskais savienojums (visas molekulas ieņem tikai vienu no konformācijām, struktūrā tikai patiesi otrā veida simetrijas elementi), kā arī nesakārtota struktūra. Jāievēro, ka šādās nesakārtotās struktūrās sastopami tikai konformēru pāri RI – SII un RI – SI, ja simetrijas lokuss kristalogrāfisko pozīciju pārim struktūrā ir otrā veida jeb enantiogēns (skat. 1.2. attēlu).

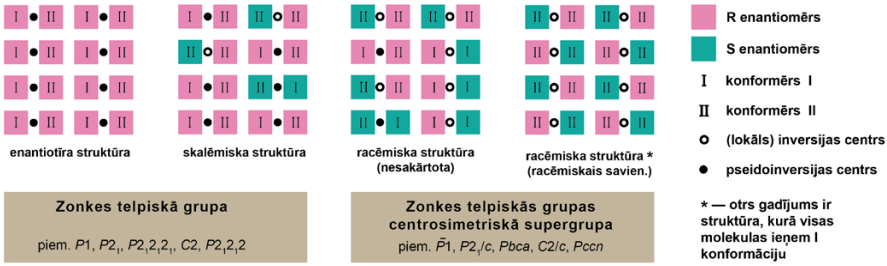

1.2. att. **II tipa cieto šķīdumu veidošanās garfisks attēlojums.**

Šis strukturālais nosacījums patiesībā atšķir cieto šķīdumu II tipu no I. Neatkarīgi no tā, vai racēmiska sastāva gadījumā ir vai nav novērojama nesakārtotība, šāds II tipa šķīdums aprakstāms ar centrosimetrisku Zonkes telpiskās grupas supergrupu. Nesakārtotas racēmiskās fazes gadījumā šī centrosimetriskā telpiskā grupa izriet no statistiskas simetrijas. Praksē nesakārtotu racēmisku kristālu asimetriskās vienības ir molekulu pāra, piem., RI – SII superpozīcija, tādējādi ar noteiktu varbūtību katrā kristalogrāfiskajā molekulu pozīcijā ir viens vai otrs konformērs (un enantiomērs). Enantiotīras struktūras nekad nav nesakārtotas (ja vien kāda statiska nesakārtotība neizriet no citiem apstākļiem), to asimetriskajās vienībās ir pāra skaits molekulu, kuras ieņem dažādas konformācijas, turklāt tās, kuru superpozīcija novērojama racēmiskajā struktūrā.

1.3. PĒTĪTĀS SISTĒMAS

Darba ietvaros tika pētīti pieci savienojumi (struktūrformulas dotas 1.3. attēlā).

Pimobendāns (**1**) (4,5–dihidro–6–[2–(*p*–metoksifenil)–5–benzimidazoil]–5–metil–3(2H)–piridazinons) ir farmaceitiski aktīva viela, ko lieto kā pozitīvo jonotropiķi un vazodilātoru, lai ārstētu sirdskaites gan veterinārajā, gan cilvēka medicīnā[21,22]. Viela tirgū pieejama racemāta veidā. Līdzīgi kā novērots vairumam hirālu savienojumu, arī pimobendāna enantiomēru farmakokinētika un farmakodinamika atšķiras[22,23]. Par racēmiska pimobendāna cietvielu formām iepriekš ziņots patentā[24], tai skaitā par dažiem polimorfiem un solvātiem (1,4–dioksāna, metanola, ūdens). Turklāt, pimobendāna cietvielu formu daudzveidību plaši pētījuši pētniecības grupas kolēģi, un informācija kā nepublicēti dati ir bijusi pieejama Ķīmijas fakultātes Fizikālās ķīmijas katedrā. Par pimobendāna polimorfu B ziņots zinātniskajā rakstā, kur noteikta tā struktūra no pulvera rentgendifrakcijas datiem[25].

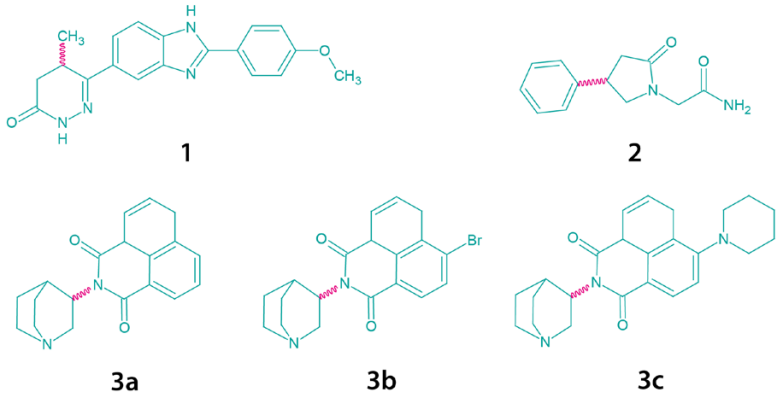

1.3. att. **Pētīto savienojumu struktūrformulas (1 – pimobendāns; 2 – fenilpiracetāms; 3 – naftalimīda atvasinājumi).**

Fenilpiracetāms (**2**) (2–(2–okso–4–fenilpirolidin–1–il)–acetamīds) ir mēreni nootropiska zāļu viela, kurai ir antiamnēzijas, antidepresanta, antikonvulsanta, anksiolītiskas īpašības un atmiņu uzlabojošs efekts[26–28]. Tās R enantiomērs var tikt lietots, lai ārstētu miega problēmas[29]. S enantiomērs, savukārt, var samazināt ķermeņa svara pieaugumu[30]. Iepriekš fenilpiracetāma molekulārā struktūra pētīta ar gāzes elektronu difrakcijas metodi un kvantu ķīmiskajiem aprēķiniem[31]. Informācija par cietvielu formu daudzveidību racēmiskam un enantiotīram savienojumam ir bijusi pieejama kā nepublicēti dati Ķīmijas fakultātes Fizikālās ķīmijas katedrā.

Visbeidzot tika pētītas trīs modeļvielas: 2–(hinuklidin–3–il)–1,8–naftalimīds (**3a**), 4–brom–*N*–(hinuklidin–3–il)–1,8–naftalimīds (**3b**), un 4–(piperidin–1–il)–*N*–(hinuklidin–3–il)–1,8–naftalimīds (**3c**). Racēmiska un enantiotīra sastāva struktūras naftalimīda atvasinājumam **3a** ziņotas literatūrā[32]. Ņemot vērā struktūras datus, tika paredzēts, ka savienojuma **3a** enantiomēri veido cietos šķīdumus[32]. Lai izpētītu šo enantiomēru sistēmu, savienojums **3a** tika sintezēts kā racēmiskā, tā arī enantiotīrā veidā. Turklāt, abi pārējie savienojumi (**3b** un **3c**) tika sintezēti no jauna kā racēmiskā, tā arī enantiotīrā veidā, ar nolūku mēģināt mērķtiecīgi iegūt vielas, kuru enantiomēri veido cietos šķīdumus.

2. NODAĻA
REZULTĀTI UN TO IZVĒRTĒJUMS

2.1. PIMOBENDĀNA (1) ENANTIOMĒRU VEIDOTIE CIETIE ŠĶĪDUMI

Racēmiskam un enantiotīram pimobendānam zināmi vairāki polimorfi: *rac*–**1**–A, *rac*–**1**–B, *rac*–**1**–C, *enant*–**1**–D, *enant*–**1**–E, *enant*–**1**–F, and *rac*–**1**–Gd (izostrukturālo solvātu *rac*–**1**–G izostrukturālais desolvāts). Zināmi arī 5 hidrāti: *rac*–**1**–H1 (monohidrāts), *rac*–**1**–H2 (monohidrāts), *rac*–**1**–H3 (hemihidrāts), *rac*–**1**–H4 (trihidrāts), and *enant*–**1**–H5 (monohidrāts), kā arī dažādi solvāti: *rac*–**1**–MS1 (metanola monosolvāts), *rac*–**1**–MS2 (metanola hemisolvāts), *rac*–**1**–DS1 (1,4–dioksāna monosolvāts), *enant*–**1**–DS2 (1,4–dioksāna monosolvāts) un *rac*–**1**–G (izostrukturālie solvāti ar vismaz 12 dažādiem šķīdinātājiem). Pimobendāna polimorfu un solvātu PXRD ainas attēlotas 2.1. attēlā.

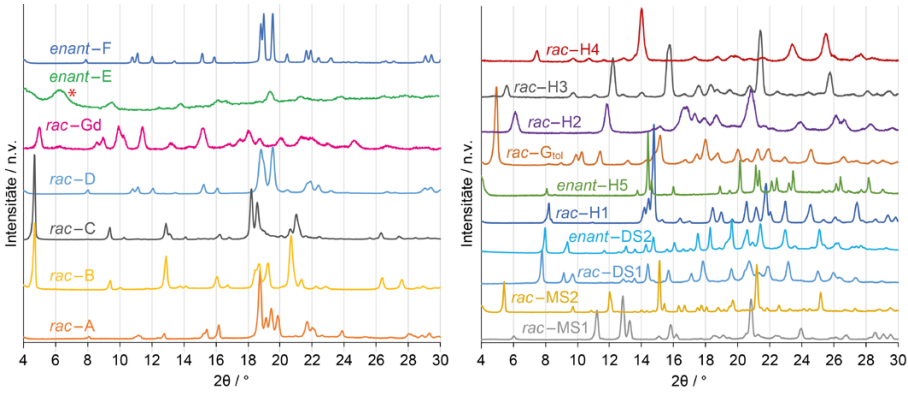

2.1. att. **Nesolvatētu (pa kreisi) un solvatētu (pa labi) pimobendāna kristālisko formu PXRD ainas (* – platais reflekss pie 6,3° 2θ *enant*–E gadījumā radies no karstumkameras polimēra plēves).**

Pētot nesolvatēto pimobendāna formas, tika atklāta sarežģīta cieto šķīdumu sistēma. Fāžu diagramma, kurā raksturotas nesolvatētas fāzes parādīta 2.2. attēlā. Pimobendāna enantiomēri veido divu cieto šķīdumu eitektisku sistēmu, līdz ar to kristāliskajā stāvoklī enantiomēri jaucas kā enantiotīrā tā racēmiskā sastāva apgabalos. Papildus novērojami divi metastabili cietie šķīdumi (**1**–δ un **1**–γ) racēmiska sastāva apgabalā.

Lai izzinātu zināmo enantiotīra un racēmiska pimobendāna solvātu enantioselektivitāti, tika pētīti pimobendāna enantiomēru skalēmiski maisījumi Pārsteidzošā kārtā visi vienkāršā ceļā eksperimentāli iegūstamie solvāti tika noteikti kā stereonespecifiski vai enantioselektīvi. Pagatavojot metanola hemisolvātu no skalēmiska pimobendāna, iegūto produktu PXRD ainas ir līdzīgas, kas ir rak-

sturīgi cietajiem šķīdumiem.

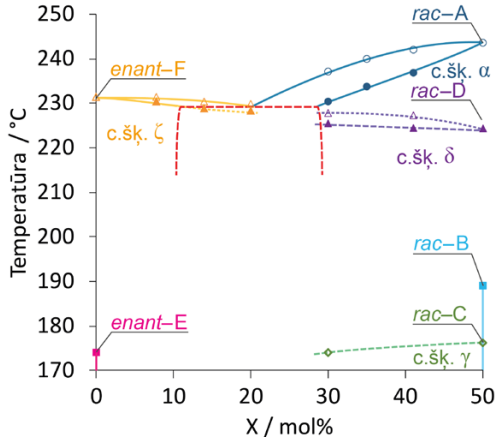

2.2. att. **Pimobendāna enantiomēru fāžu diagramma (pildīti marķieri – soliduss; tukši marķieri – likviduss; līnijas attēlotas uzskatāmībai; attēlota tikai puse no fāžu diagrammas).**

TG/DSC analīzes rezultāti paraugiem ar 30 un 50% enantiomēru sastāvu ir līdzīgi, turklāt tie norāda uz identisku masas zudumu, kas atbilst hemimetanolāta stehiometrijai (skat. 2.3. attēlu). Desolvatējot minētos metanola hemisolvātus iegūst formu **1**–C (cietais šķīdums 1–γ).

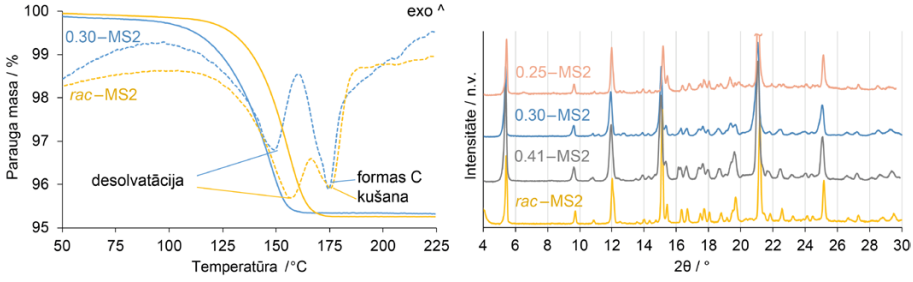

2.3. att. **Pimobendāna metanola hemisolvāta 1–MS2 TG (nepārtrauktās līnijas) un DSC (pārtrauktās līnijas) analīzes dati (pa kreisi) un PXRD ainas (pa labi).**

Līdzīgā veidā tika atrasts, ka arī vairāki citi pimobendāna solvāti veido cietos šķīdumus (metanola solvāts **1**–MS1; hidrāti **1**–H1, **1**–H3, **1**–H5; dioksāna solvāti **1**–DS1 un **1**–DS2; izostrukturālie solvāti **1**–G). Interesanti, ka monohidrāti *rac*–**1**–H1 un *enant*–**1**–H5 nav viena un tā paša cietā šķīduma robežgadījumi, bet tā vietā cietais šķīdums **1**–H1 ir stabils racēmiska sastāva apgabalā, un **1**–H5 – enantiotīra sastāva apgabalā. Arī 1,4–dioksāna monosolvāti *rac*–**1**–DS1 un *enant*–**1**–DS2 nav izostrukturāli, bet gan divi atšķirīgi cietie šķīdumi.

Tā kā vairumā gadījumu nebija iespējams izaudzēt monokristālus, struktūras tika noteiktas tikai dažām pimobendāna formām. Forma *rac*–**1**–A kristal-

izējas monoklīnās singonijas *C*2/*c* telpiskajā grupā (*Z*=8, *Z*'=1). Struktūra ir nesakārtota, asimetriskā vienība satur divas atšķirīgas konformācijas molekulas ar atrašanās varbūtību aptuveni 3:1. Tādējādi pimobendāna cietais šķīdums **1**–α atbilst II tipa cietajiem šķīdumiem, kuri uzrāda kristalogrāfisko pozīciju enantioselektivitāti.

Termodinamiski stabilākās enantiotīrās fāzes *enant*–**1**–F struktūra tika noteikta no pulvera rentgendifraktometrijas un ^{13}C cietvielu KMR datiem. Tika noskaidrots, ka struktūra kristalizējas trigonālās singonijas $P3_121$ (un $P3_221$) telpiskajā grupā (*Z*=6, *Z*'=1). No molekulu skaita asimetriskajā vienībā izriet, ka atbilstošais cietais šķīdums **1**–ζ (skat. 2.2. att.) ir I tipa, jo tā struktūrā nav vismaz 2 simetriski neatkarīgu molekulu. *Rac*–**1**–A un *enant*–**1**–F struktūrās ir identiski ūdeņraža saišu tīkli, attēlojami ar grafu kopu pierakstu $R_2^2(16)$ un $C_1^1(11)$ (skat. 2.4. att.).

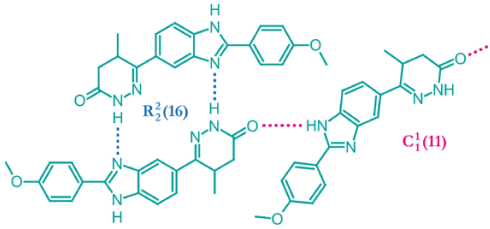

2.4. att. **Ūdeņražu saišu tīkla attēlojums *rac*–1–A un *enant*–1–F struktūrās.**

Atšķirības struktūrās novērojamas molekulu konformācijās un pakojumā. *Rac*–**1**–A struktūrā bezgalīgas $C_1^1(11)$ ķēdes, sapakotas paralēli, veido slāņus, kas savā starpā savienoti ar centrosimetriskiem $R_2^2(20)$ ūdeņraža saišu cikliem. *Enant*–**1**–F struktūrā $C_1^1(11)$ ķēdes veido stienīšus ar trešās kārtas vītņass simetriju. Stienīši savā starpā savienoti ar $R_2^2(20)$ ūdeņraža saitēm (skat. 2.5. att.).

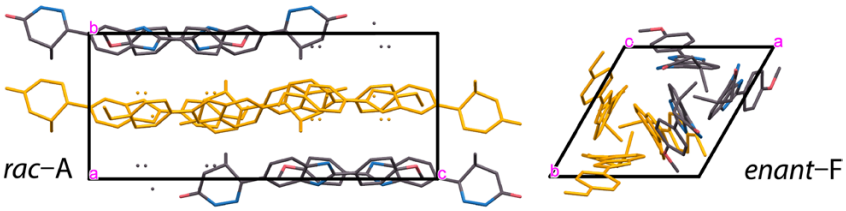

2.5. att. ***Rac*–1–A un *enant*–1–F struktūru attēlojums gar attiecīgi kristalogrāfiskajām a un c asīm. Slāņi un stienīši, kas izveidojušies ar $C_1^1(11)$ ūdeņraža saitēm, attēloti oranži.**

No monokristālu datiem tika noteiktas arī struktūras racēmiskajam un enantiotīrajam monohidrātam (*rac*–**1**–H1 un *enant*–**1**–H5). Racēmiskais pimobendāna hidrāts kristalizējas monoklīnās singonijas $P2_1/c$ (*Z*=4, *Z*'=1) telpiskajā grupā. Enantiotīrais hidrāts kristalizējas ortorombiskās singonijas $P2_12_12_1$ telpiskajā grupā (*Z*=4, *Z*'=1). Abu hidrātu asimetriskajās vienībās ietilpst viena ūdens

un viena pimobendāna molekula. Kristāliskā režģa parametri abiem hidrātiem ir ļoti līdzīgi, un pimobendāna konformācijas *rac*–**1**–H1 un *enant*–**1**–H5 struktūrās ir praktiski identiskas (skat. 2.6. att.).

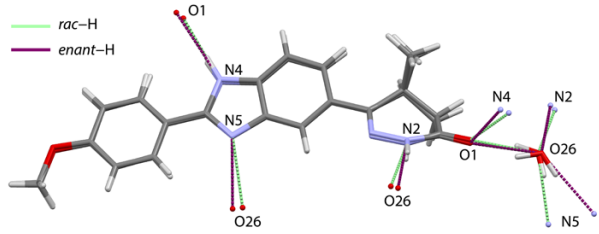

2.6. att. ***Rac*–1–H1 un *enant*–1–H5 struktūru asimetriskās vienības, attēlojot arī ūdeņraža saites.**

Abās kristāliskajās struktūrās novērojamas tieši tādas pašas $C_1^1(11)$ ķēdes kā *rac*–**1**–A un *enant*–**1**–F struktūrās (skat. 2.4. att.). Turklāt, neprotonētais benzimidazola fragmenta slāpekļa atoms (N5) ir savienots ar protonēto piridazinona cikla slāpekli (N2), bet ne ar tiešu ūdeņraža saiti, bet gan caur ūdens molekulu tiltiņiem. *Rac*–**1**–H1 struktūrā tādējādi (līdzīgi kā *rac*–**1**–A) novērojami centrosimetriski cikli (divas pimobendāna molekulas un divas ūdens molekulas veido $R_4^4(20)$ ciklus). *Enant*–**1**–H5 struktūrā ūdeņraža saišu ciklu nav, jo katra pimobendāna molekula caur ūdens tiltiņiem ir savienota ar divām atsevišķām pimobendāna molekulām. Abā struktūrās ir novērojami izostrukturāli slāņi, kas paralēli (004) plaknēm. *Rac*–**1**–H1 struktūrā R/S slāņi ir sapakoti pārmaiņus, kamēr *enant*–**1**–H5 struktūrā katrs otrais slānis ir spoguļattēls atbilstošajam slānim *rac*–**1**–H1 struktūrā (skat. 2.7. att.).

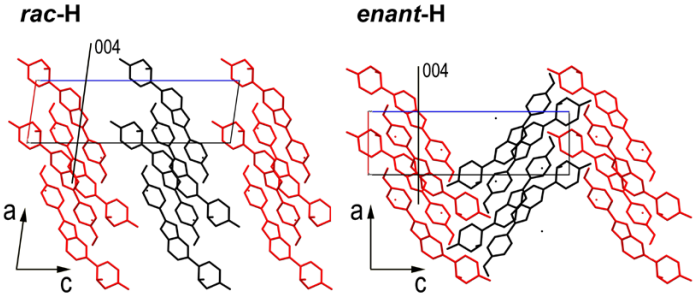

2.7. att. **Molekulu pakojuma attēlojums *rac*–1–H1 un *enant*–1–H5 struktūrās skatā gar kristalogrāfisko *b* asi (sarkanā krāsā iekrāsotie slāņi ir izostrukturāli, melnā krāsā – savstarpēji spoguļattēli).**

No visām 4 noteiktajām struktūrām strukturālie iemesli cieto sķīdumu pastāvēšanai uzskatāmi novērojami tikai *rac*–**1**–A gadījumā (divu konformēru superpozīcija, kas ir tipiski II tipa cietajiem šķīdumiem (skat. 1.2. att.)). Tomēr PXRD un TG/DSC analīzes norāda, ka arī pārējās trīs struktūras ir enantiotīrā vai racēmiskā sastava cieto šķīdumu robežgadījumi. Abām enantiotīrajām struk-

tūrām nav novērojami *kvazi*–centrosimetriskie pāri, kas ir tipiski II tipa gadījumā, turklāt, tā kā *Z'*=1, daļēja enantioselektivitāte pavisam noteikti nav iespējama, un **1**–F (**1**–ζ) un **1**–H5 tāpēc ir I tipa cietie šķīdumi. Cietais šķīdums **1**–H1 ir drīzāk II tipa, kas racēmiskajā sastāvā ir pilnībā sakārtots (skat. 1.2. att.), vai arī iespējama eksperimentāli grūti nosakāma nesakārtotība. Jāpiebilst, ka standarta monokristālu rentgendifrakcijas analīzē, piemēram, oglekļa atomus ar aizņemtības faktoru <10% ir grūti noteikt, jo nosakāmais elektronu blīvums ir mazs (aptuveni tāds pats kā ūdeņraža atomiem).

Pārsteidzoši lielais daudzums cieto šķīdumu, kas atrasti pimobendānam, liek secināt, ka strukturālie aspekti to veidošanās iespējamībai varētu būt nosakāmi molekulārā līmenī. Tā kā hirālais centrs ir fiksēts heterociklā, un atlikušie divi aizvietotāji ir ūdeņraža atoms un metilgrupa, tiek uzskatīts, ka enantiomēru neatpazīšanas iemesli struktūrās ir šādi – izmaiņas, kas tiek ieviestas struktūrā molekulārajā pozīcijā novietojot vienu vai otru enantiomēru nav būtiskas, jo: 1) hirālā centra aizvietotāju salīdzināmā izmēra dēļ nav sagaidāmi būtiski stēriskie traucējumi; 2) sagaidāms, ka maiņas dēļ tiek ietekmēts tikai dispersijas enerģijas loceklis, kam, tā kā struktūrā sagaidāms enerģētiski izdevīgs ūdeņraža saišu tīkls, acīmredzami ir maza ietekme kopējā režģa enerģijā.

2.2. FENILPIRACETĀMA (2) ENANTIOMĒRU VEIDOTIE CIETIE ŠĶĪDUMI

Pētot racēmisku un enantiotīru fenilpiracetāmu (**2**), noskaidrots, ka racēmiski paraugi kristalizējas vienā kristāliskajā formā (*rac*–**2**–A), savukārt, enantiotīra savienojuma gadījumā iegūstamas divas formas: *enant*–**2**–A un *enant*–**2**–B. Pulvera rentgendifrakcijas ainas visām trīs kristāliskajām formām dotas 2.8. attēlā.

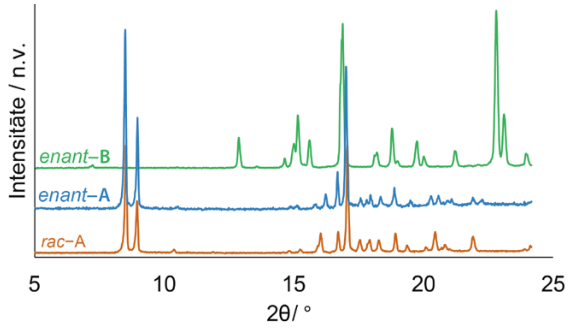

2.8. att. **Pulvera rentgendifrakcijas ainas racēmiska un enantiotīra fenilpiracetāma (2) kristāliskajām fāzēm.**

Gandrīz identiskās difrakcijas ainas *rac*–**2**–A un *enant*–**2**–A fāzēm norāda uz ļoti augstu strukturālo līdzību, un tomēr, ņemot vērā nelielas atšķirības, konglomerātu veidošanās šajā gadījumā var tikt izslēgta. Līdz ar to visticamāk abas fāzes ir cietā šķīduma ekstrēmi, kas tālāk apstiprināts arī ar divkomponentu fāžu diagrammu. DSC analīzes rezultāti (2.9. att.) norāda, ka fāzes *enant*–**2**–A kušanai

seko fāzes *enant*–**2**–B kristalizācija, kas ir novērojams kā eksotermisks efekts.

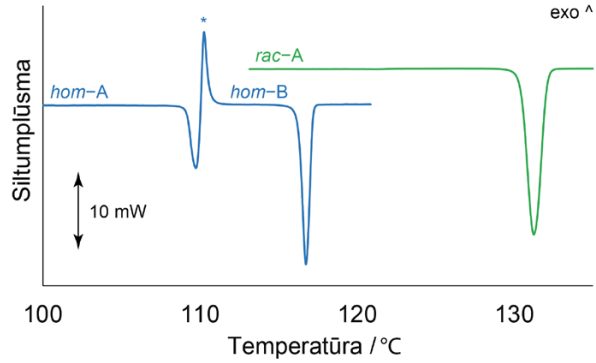

2.9. att. **Fenilpiracetāma (2) kirstālisko fāžu DSC līknes (kristalizācija atzīmēta ar zvaigznīti).**

Kušanas temperatūras un entalpijas vērtības uzskaitītas 2.1. tabulā. Fāzes *enant*–**2**–A kušanas entalpija tika izrēķināta, ņemot vērā, ka ar kušanu pārklājušamies eksotermiskā kristalizācijas efekta laukumam jābūt vienādam ar fāzes *enant*–**2**–B kušanas efekta laukumu.

2.1. tabula. **Fenilpiracetāma (2) kristālisko formu kušanas temperatūras un entalpijas (ΔH^f) dati**

Forma	Kušanas temp. / °C	ΔH^f / kJ·mol^{-1}
rac–**2**–A	130,4	30,0(3)
enant–**2**–A	109,2	25,1(6)
enant–**2**–B	116,3	22,4(3)

Tā kā eksistē divas viena komponenta fāzes (*enant*–**2**–A un *enant*–**2**–B), starp tām var pastāvēt vai nu monotropa, vai enantiotropa saistība. Šī saistība tika noteikta, izmantojot kušanas likumu[33], kā arī apstiprināta, veicot suspendēšanas eksperimentu. Tika noskaidrots, ka fāzes *enant*–**2**–A un *enant*–**2**–B ir enantiotropi saistītas. Fāžu pārejas punkts tika noteikts, balstoties uz termodinamiskiem apsvērumiem, aprēķinot Gibsa brīvo enerģiju starpību starp *enant*–**2**–A un *enant*–**2**–B kā funkciju no temperatūras, izmantojot izobārisko siltumpietilpību, kušanas temperatūru un kušanas entalpiju mērījumus. Pārejas līdzsvara temperatūra fāzēm *enant*–**2**–A un *enant*–**2**–B ir 70(7) °C.

Lai nepārprotami pierādītu, ka *enant*–**2**–A un *rac*–**2**–A ir cietā šķīduma ekstrēmi (attiecīgi **2**–$\alpha_{x=0}$ un **2**–$\alpha_{x=0,5}$), tika pētīta dažāda sastāva paraugu kušana, kā arī konstruēta divkomponentu fāžu diagramma (2.10. att.). Tāpat tika noskaidrots, ka arī *enant*–**2**–B ir kāda cietā šķīduma robežgadījums, proti, **2**–$\alpha_{x=0}$. Enantiomēru sajaukšanās pārrāvuma apgabals cietajiem šķīdumiem **2**–α un **2**–β ir mazs. Eitektiskās temperatūras tuvumā divfāžu apgabals eksistē starp enantiomēru sastāvu 2 un 9%. Tas ir tāpēc, ka pastāv liela kušanas temperatūru atšķirī-

ba starp racēmisko fāzi un enantiotīro fāzi *enant*–**2**–B. Līdz ar to likvidusa līnijas krustojas tālu no racēmiskā sastāva. Eitektiskais invariants novērojams 114,4 °C temperatūrā un enantiomēru attiecības aptuveni 3:97. Ņemot vērā šauro divfāžu apgabalu, kā arī eitektiskā punkta atrašanās vietu, precīzāk noteikt eitektisko sastāvu, piemēram, izmantojot Tamana trijstūri, nav iespējams.

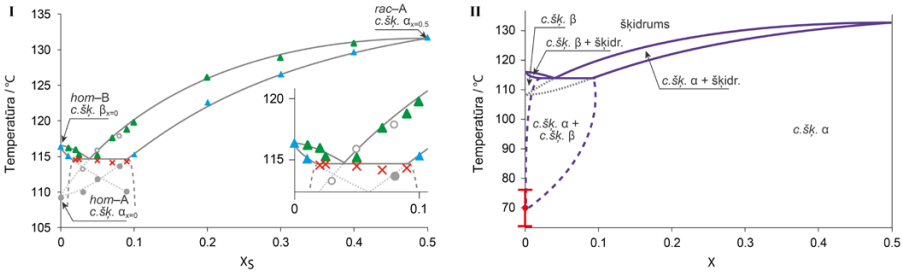

2.10. att. **Fenilpiracetāma enantiomēru divkomponentu fāžu diagramma. I: Attēlojot eksperimentālos punktus no DSC analīzes datiem (zaļie trijstūri – stabilā līdzsvara likviduss, zilie trijstūri – stabilā līdzsvara soliduss, sarkanie krusti – eitektikas signāli, pelēkie punkti – metastabilā līdzsvara likviduss un soliduss; līnijas ir acu gidi). II: Ieteiktā vispārīgā sistēmas fāžu diagramma, ņemot vērā enantiotropo pāreju (sarkanais punkts – pārejas līdzsvara temperatūra).**

Šajā sistēmā novēro arī cietā šķīduma **2**–α metastabilo līdzsvaru. Tā kā pastāv enantiotropa saistība, paraugiem, kuros viena enantiomēra moldaļa ir mazāka nekā 0,1 (cietā šķīduma **2**–α metastabilais apgabals), nav novērojama eitektikas kušana. Līdz ar to cietā šķīduma **2**–α solidusa un likvidusa turpinājumam atbilstošās fāzes ir vienkāršā ceļā eksperimentāli iegūstamas. Temperatūrās, kas ir zemākas par enantiotropās pārejas līdzsvara temperatūru, fenilpiracetāma enantiomēri cietā stāvoklī jaucas jebkurā attiecībā. Cietā šķīduma **2**–β eksistence varētu būt diskutabla, jo tas uzrādīts ļoti šaurā sastāva apgabalā, un tomēr, cietais šķīdums **2**–β tiek iegūts arī tā metastabilajā apgabalā, piesējot dažāda enantiomēru sastāva maisījumus ar formu *enant*–**2**–B.

Lai noskaidrotu fenilpiracetāma cieto šķīdumu strukturālo dabu, izdevās noteikt struktūras formām *enant*–**2**–A, *enant*–**2**–B un *rac*–**2**–A. *Enant*–**2**–A kristalizējas triklīnās singonijas *P*1 telpiskajā grupā (*Z*=4, *Z*'=4). *Enant*–**2**–B, savukārt, kristalizējas ortorombiskās singonijas $P2_12_12_1$ telpiskajā grupā (*Z*=8, *Z*'=2). Abas telpiskās grupas, ņemot vērā ķīmiskā sastāva ierobežojumu, ir Zonkes telpiskās grupas[20]. Tomēr, neievērojot hirālā oglekļa un dažu apkārtējo atomu pozīcijas, abām struktūrām piemīt augstāka simetrija, no kā seko, ka *enant*–**2**–A un *enant*–**2**–B struktūras tādējādi varētu aprakstīt ar attiecīgi centrosimetriskajām telpiskajām grupām *P*—1 un *Pbca*. Attiecīgās šķietamās telpiskās grupas ir iepriekšējo telpiskās supergrupas[34]. *Kvazi*–centrosimetrija tiek nodrošināta ar asimetriskajām vienībām (2.11. att. I), kuras sastāv no pāra skaita molekulu, kuras, savukārt, saistītas ar pseidoinversijas centru.

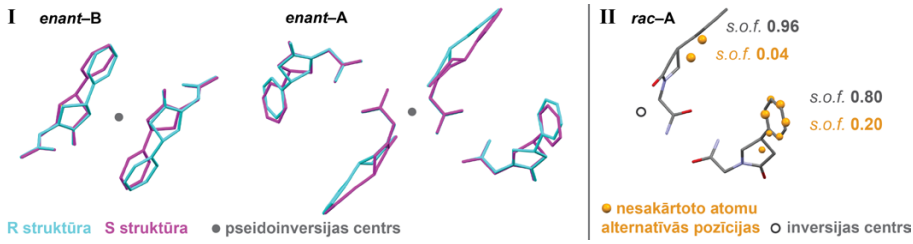

2.11. att. **I: Atbilstošo enantiomorfo struktūru superpozīcija formām *enant*–2–B (*Z*'=2) un *enant*–2–A (*Z*'=4). II: Formas *rac*–2–A (*Z*'=2) asimetriskā vienība ar attēlotu nesakārtotību.**

Molekulu konformācijas pāros atšķiras – viens no konformēriem imitē otra konformēra pretējo enantiomēru (pievērst uzmanību pretējās hiralitātes struktūrām 2.11. attētā). *Enant*–**2**–A un *rac*–**2**–A struktūras ir izostrukturālas un attēlo cietā šķīduma **2**–α robežgadījuma struktūras, attiecīgi **2**–$\alpha_{x=0}$ un **2**–$\alpha_{x=0,5}$. Attiecīgo struktūru telpiskās grupas ir *P*1 un *P*—1, *rac*–**2**–A asimetriskā vienība ir tāpēc puse no *enant*–**2**–A asimetriskās vienības un uzrāda nesakārtotību hirālā centra tuvumā (skat. 2.11. att. II). Visi četri konformēri, kas atrodami enantiotīrajā struktūrā (*enant*–**2**–A) ir sastopami arī racēmiskajā struktūrā (*rac*–**2**–A). Dažādo konformēru daudzuma attiecībai būtu jāizriet no enerģētiskā izdevīguma apstākļiem.

Cieto šķīdumu **2**–α un **2**–β kristāliskās struktūras ir ļoti atšķirīgas. Abos gadījumos fenilpiracetāma molekula veido 4 ūdeņraža saites, tomēr struktūrām ir ļoti atšķirīgs molekulu pakojums. *Enant*–**2**–A struktūrā novērojami divi dažādi N–H···O veida dimēra sintoni (skat. 2.12. att.). Abi sintoni ir *kvazi*–centrosimetriski. Līdz ar to struktūrās novērojamas ķēdes, kas veidojušās no ūdeņraža saišu motīviem, kas, savukārt, atbilst grafu kopām $R_2^2(14)$ un $R_2^2(8)$.

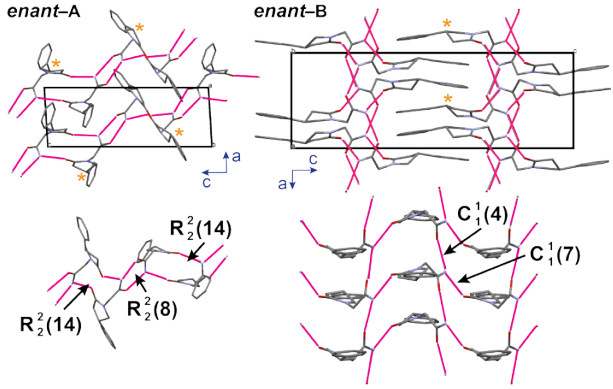

2.12. att. **Pakojuma attēlojums un ūdeņraža saišu motīvi struktūrās *enant*–2–A un *enant*–2–B (hirālais centrs atzīmēts ar zvaigznīti).**

Enant–**2**–B struktūrā novērojami cita veida ūdeņraža saišu motīvi, kas atbilst grafu kopām $C_1^1(4)$ un $C_1^1(7)$ (2.12. att.), kā rezultātā struktūrā izdalāmi molekulu slāņi. *Kvazi*–centrosimetrija šajā gadījumā novērojama starp molekulām no di-

viem dažādiem slāņiem, nevis starp ar ūdeņraža saitēm saistītām molekulām kā *enant*–**2**–A struktūrā. No aprakstītajām struktūrām izriet, ka cietā šķīduma **2**–α gadījumā struktūra veidota no kopā sapakotām ķēdēm, bet **2**–β gadījumā – no slāņiem. Ķēdes un slāņi savstarpēji turas kopā, pateicoties dispersijas mijiedarbībām. Var ievērot, ka hirālā oglekļa aizvietotāji nav tieši saistīti ar ūdeņraža saišu tīkla veidošanu, kas tādējādi var tikt saglabāts, ja molekulas konfigurācija tiek mainīta uz pretējo. Turklāt, konfigurācijas maiņa struktūrā drīzāk ietekmē tikai dispersijas mijiedarbības, kuras praktiski nav virzienspecifiskas, tāpēc sagaidāms, ka šī maiņa rezultātā dotu tikai nelielas kristāliskā režģa enerģijas izmaiņas. No tā var secināt, ka fenilpiracetāma gadījumā iespēja saglabāt enerģētiski izdevīgu ūdeņraža saišu tīklu, kā arī fakts, ka ieviestās izmaiņas kristāliskā režģa enerģijā būtu nelielas, ir enerģētiskie iemesli enantiomēru neatpazīšanai kristāliskā stāvoklī.

2.3. NAFTALIMĪDA ATVASINĀJUMU (3) ENANTIOMĒRU VEIDOTIE CIETIE ŠĶĪDUMI

No pētījumā par **3a**[32] noteiktajām struktūrām redzams, ka savienojums atbilst visiem priekšnosacījumiem II tipa cieto šķīdumu veidošanai (skatīt 2.13. att.).

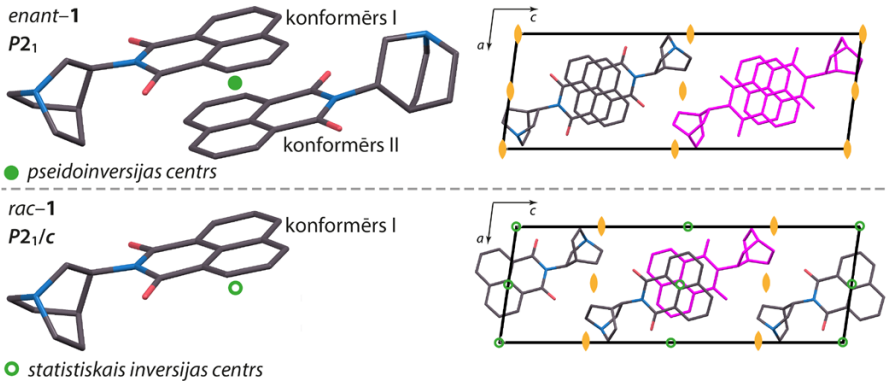

2.13. att. **Formu *enant*–3a un *rac*–3a asimetriskās vienības (pa kreisi) un pakojumu attēlojums (pa labi, asimetriskās vienības iekrāsotas purpura krāsā). Ūdeņraža atomi kā arī racēmiskās struktūras nesakārtotība nav attēlota uzskatāmības labad.**

Lai dziļāk izpētītu abu struktūru līdzības un atšķirības, tika analizētas starpmolekulārās mijiedarbības *rac*–**3a** and *enant*–**3a** struktūrās. Tā saucamie pirkstu nospiedumu grafiki Hiršfelda virsmām attēloti 2.14. attēlā.

Tā kā abi pakojumi ir izostrukturāli, un abas konformācijas atšķiras tikai nedaudz, pirkstu nospiedumu grafiki ir ļoti līdzīgi. Turklāt, nav īpaši lielu atšķirību starp abu I konformēru grafikiem, un tomēr tie nav pilnībā identiski, jo Hiršfelda virsma ir tikai un vienīgi definējama kristāliskās struktūras kontekstā, līdz ar to tā ir atkarīga no vides apkārt interesējošajai molekulai.

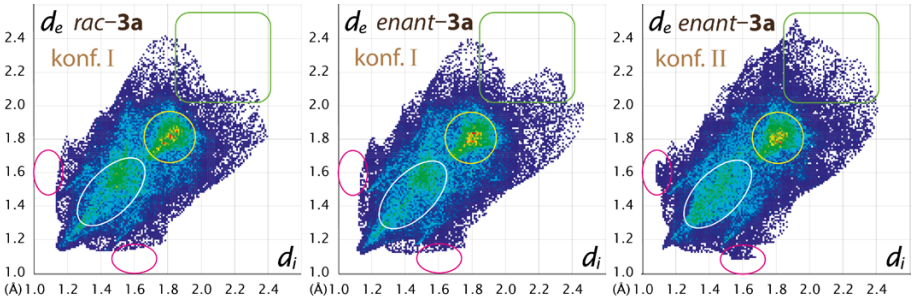

2.14. att. **Hiršfelda virsmu pirkstu nospiedumu grafiki *rac*–3a un *enant*–3a kristālisko struktūru simetriski neatkarīgajām molekulām.**

Visos trīs gadījumos visraksturīgākās mijiedarbības ir C···C kontakti (atbilstīgi naftalīna fragmenta π···π mijiedarbībām), kas 2.14. attēlā apzīmēti ar dzeltenu riņķa līniju. Šie apgabali ir ļoti līdzīgi, norādot, ka konformācijas (līdz ar to molekulas konfigurācijas) atšķirības praktiski neietekmē atbilstošās mijiedarbības. Nav novērojamas arī būtiskas atšķirības O···H kontaktiem (skatīt gaiši zilās strīpas starp atzīmētajām elipsēm). Papildu mijiedarbības blīvums parādās II konformēra pirkstu nospiedumu grafikā (skatīt elipses purpura krāsā). Šie kontakti piedēr N···H un H···H mijiedarbībām, kas pārsvarā rodas no hinuklidīna fragmenta, kura relatīvais novietojums abiem konformēriem nedaudz atšķiras. Apgabals, kas apzīmēts ar baltu elipsi (H···H kontakti) atšķirās starp konformēriem I un II tādā veidā, ka II konformēra gadījumā tas ir vienmērīgi blīvs, turpretim I konformēra gadījumā kontaktu blīvums vairāk koncentrēts elipses augšējā daļā. No tā izriet, ka *enant*–**3a** struktūras gadījumā ir skaitliski vairāk īsāku H···H kontaktu, nekā *rac*–**3a** struktūrā, turklāt, tie rodas no molekulām, kuras ieņem II konformāciju. Visbeidzot, no apgabaliem, kuri apzīmēti ar zaļu noapaļotu kvadrātu, var secināt, ka II konformēra gadījumā struktūrā *enant*–**3a** ir kontakti, kuru attālumi ir relatīvi gari. Tas liecina par ne tik efektīvi sapakotu telpu, salīdzinot ar struktūru *rac*–**3a**.

Lai pētītu kristāliskā pakojuma enerģētiskos aspektus, tika aprēķinātas *rac*–**3a** un *enant*–**3a** kristālrežģu enerģijas. Aprēķinātās enerģijas un to komponentes apkopotas 2.2. tabulā.

2.2. tabula. ***Rac*–3a un *enant*–3a struktūru kristālrežģa enerģijas un to komponentes (kJ·mol^{-1})**

	E_{Kulona}	$E_{\text{pol.}}$	$E_{\text{disp.}}$	$E_{\text{atgr.}}$	$E_{\text{kop.}}$
rac–**3a**	–35,1	–18,5	–174,3	98,9	–129,0
enant–**3a**	–36,6	–19,9	–177,4	106,9	–127,2

Kristālrežģa stabilizēšanā vislielāko ieguldījumu sniedz dispersijas enerģijas komponente, kas saistāma ar enerģētiski izdevīgām naftalīna fragmentu π···π mijiedarbībām. Tā kā struktūrās nav novērojamas ne ūdeņraža saites, ne jonu klātbūtne, Kulona mijiedarbībām ir mazsvarīga nozīme kristāliskās struktūras

stabilizēšanā. Enerģijas stabilizācijas komponentes abu struktūru gadījumos ir līdzīgas, savukārt atgrūšanās enerģijas komponentes ir ievērojami atšķirīgas (8 kJ·mol^{-1} starpība). Identisku pakojumu un vienādu (abu enantiomēru) molekulu gadījumā palielināta šīs enerģijas komponentes vērtība saistāma ar to, ka molekulu atomi kristāliskajā struktūrā ir neefektīvi tuvu viens otram. Tas sakrīt ar Hiršfelda virsmu analīzes rezultātiem, no kuriem var secināt, ka konformēra II gadījumā ir vērojams lielāks kontaktu blīvums pie mazākām d_e un d_i vērtībām (skat. iezīmētās elipses 2.14. att.), kas atbilst N···H un H···H kontaktiem.

Lai pierādītu, ka enantiomēri patiešām kristāliskā stāvoklī netiek atpazīti, tika noteiktas arī struktūras skalēmiska sastāva kristāliem. Tika noskaidrots, ka šādiem kristāliem nesakārtota ir tikai viena no abām simetriski neatkarīgo molekulu pozīcijām, turklāt, tā ir II konformēra pozīcija. Starpmolekulāro mijiedarbību analīzē jau tika noskaidrots, ka konformērs II kristāliskajā struktūrā nav izdevīgs. Tāpēc saprotams, ka, ja vien iespējams, šīs molekulu pozīcijas tiktu aizvietotas ar I konformēru. Kristāliskās struktūras dati norāda, ka, enantiotīrā struktūrā iekļaujot pretējo enantiomēru, tas ieņem I konformāciju un attiecīgajās kristalogrāfiskajās molekulu pozīcijās aizvieto konformēru II. Līdz ar to, cik vien iespējams, tiek izveidoti centrosimetriski SI–RI pāri. Šādā veidā sagaidāms, ka racēmiski kristāli būtu veidoti tikai no molekulām, kas ieņem I konformāciju, līdz ar to veidotos tā saucamais racēmiskais savienojums. Tomēr *rac*–**3a** noteiktās struktūras asimetriskajā vienībā ir viena molekula, kas ir superpozīcija no abām konformācijām I un II. Kā noskaidrots trīs dažādu monokristālu gadījumā, konformēru attiecība (I:II) ir līdzīga, bet tomēr nedaudz variē – 85:15, 87:13 un 90:10. Asimetriskās vienības un konformēru izplatība struktūrās atkarībā no enantiomēru sastāva ir attēlota 2.15. attēlā.

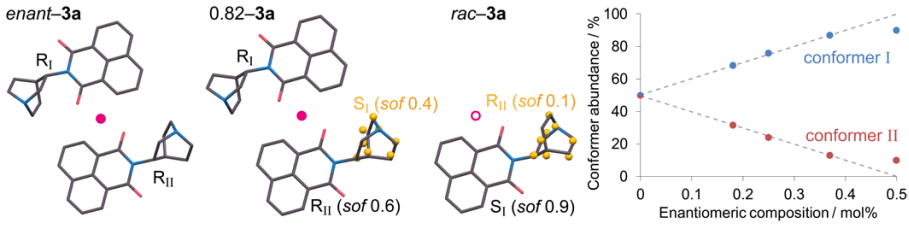

2.15. att. **Cietā šķīduma 3a struktūru asimetriskās vienības (ūdeņraža atomi netiek attēloti skaidrības labad) un konformēru izplatība kristāliskajās struktūrās atkarībā no enantiomēru sastāva.**

Konformēru izplatības novirze no lineāras sakarības varētu tikt skaidrota ar konfigurācijas entropiju. Ir ziņots, ka Bolcmaņa statistika var tikt pielietota, lai izskaidrotu nesakārtotību molekulārajos kristālos[35].

Bromaizvietotā savienojuma (**3b**) gadījumā kristāliskās struktūras noteikt nebija iespējams. Pulvera rentgendifrakcijas ainas paraugiem ar dažādu enantiomēru sastāvu ir gandrīz identiskas, nelielas atšķirības novērojamas difrakcijas refleksu pozīcijām un intensitātēm (skat. 2.16. att.), kas ir raksturīgs cietajiem šķīdumiem.

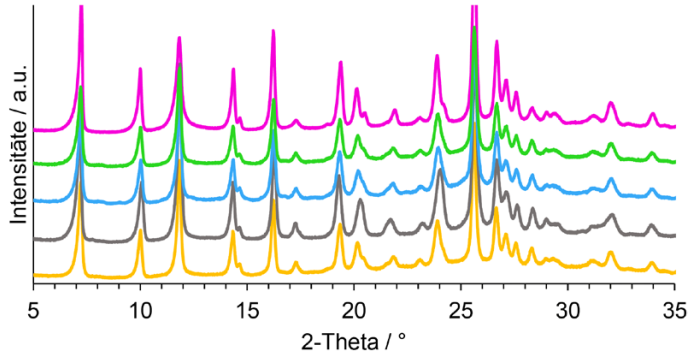

2.16. att. **Pulvera rentgendifrakcijas ainas 3b paraugiem ar dažādu enantiomēru sastāvu (no apakšas uz augšu: enantiotīrs, 0,80, 0,75, 0,60, racēmisks).**

Diemžēl, tā kā šai vielai novēro degradāciju pirms kušanas, nebija iespējams konstruēt **3b** enantiomēru divkomponentu fāžu diagrammu, kas nepārprotami pierādītu cieto šķīdumu eksistenci, balstoties uz termodinamiskiem apsvērumiem. Tomēr rentgendifrakcijas dati pārliecinoši norāda uz cietā šķīduma veidošanos visa kompozīcijas diapazona apgabalā.

No savienojumu *enant*–**3c** un *rac*–**3c** struktūrām noskaidrots, ka tie kristalizējas attiecīgi $P2_12_12_1$ (Z=8, Z'=2) un *Pccn* (Z=8, Z'=1) telpiskajās grupās. Enantiotīrajā struktūrā novērojama *kvazi*–centrosimetrija, kas norāda uz iespējamu cieto šķīdumu eksistenci. Telpiskās grupas $P2_12_12_1$ un *Pccn* gan nav tiešā subgrupas-supergrupas attiecībā, līdz ar to nav iespējama cietā šķīduma veidošanās visā kompozīcijas apgabalā. Skalēmiska sastāva monokristālu izpēte atklāja, ka tā vietā veidojas divi dažādi cietie šķīdumi – viens racēmiska sastāva apgabalā, un otrs – enantiotīra sastāva apgabalā. 0,86 un 0,70 enantiomēru sastāva kristālu struktūras ir izostrukturālas formai *enant*–**3c**, bet 0,58 enantiomēru sastāva kristāls ir izostrukturāls formai *rac*–**3c**. Neskatoties uz to, abiem cietajiem šķīdumiem novērojami identiski struktūrālie fragmenti – ar π···π mijiedarbībām saistītu molekulu bloki (skat 2.17. att.).

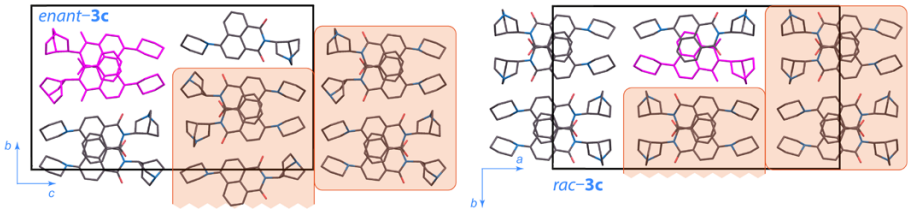

2.17. att. **Formu *enant*–3c un *rac*–3c struktūras (asimetriskās vienības iekrāsotas purpurā).**

Galvenā struktūru atšķirība novērojama starp blakusesošo molekulu bloku savstarpējo nobīdi. Enantiotīrajā struktūrā blakusesošie bloki nobīdīti savā starpā par 1/4 no elementāršūnas malas garuma, bet racēmiskajā struktūrā šī nobīde ir

1/2 (skatīt iekrāsotos laukumus 2.17. att.). No tā var secināt, ka kristāliskā struktūra ir enerģētiski izdevīgāka, ja [1,0 ; 0,70) enantiomēru sastāva bloki ir sapakoti ar 1/4 nobīdi, un (0,58 ; 0,50] sastāva bloki – ar 1/2 nobīdi.

Pretēji formas *rac*–**3a** gadījumam, *rac*–**3c** formas gadījumā nesakārtotība struktūrā netika pārliecinoši pierādīta. Lai arī struktūras risināšanas gaitā bija novērojams neliels elektronu blīvums pozīcijās, kas atbilstu superpozicionētam II konformēram, struktūras modelis bez nesakārtotības bija ar zemāku sakritības faktoru. Līdz ar to nevar viennozīmīgi apgalvot, ka savienojuma **3a** racēmiskā struktūra ir pilnībā sakārtota (atbilstīga patiesam racēmiskajam savienojumam). Šie novērojumi parāda, ka II tipa cieto šķīdumu definīcija, kuru piedāvājis Šions *et al.* un kura norāda uz pilnībā sakārotu racēmisku fāžu rašanos, ir jāpārskata. Šajā promocijas darbā parādīts, ka nesakārtotības pakāpe racēmiska sastāva kristāliem variē no savienojuma uz savienojumu, tikmēr kristalogrāfisko molekulu pozīciju enantioselektivitāte nenoliedzami tiek novērota (pretēji I tipa cietajiem šķidumiem). Nesakārtotības pakāpi varētu ietekmēt kristāla augšanas process, piemēram, kristāliskajā struktūrā ir saglabājušies kādi kinētiski artefakti, piem., no molekulu pašasociācijas šķīdumā utml. Tāpat nesakārtoti kristāli varētu reprezentēt termodinamiski līdzsvarotu sistēmu. Šajā gadījumā nesakārtotība pastāv konfigurācijas entropijas dēļ, proti, struktūru veido dažādi ekvienerģiski lokāli struktūras modeļi ar dažādu sastopamības varbūtību, kā rezultātā noteiktajā vidējā struktūrā novērojama nesakārtotība.

Ņemot vērā abu savienojuma **3c** cieto šķīdumu strukturālo līdzību, tika analizēti arī to veidošanās enerģētiskie aspekti. Tika veikti kristāliskā režģa enerģijas aprēķini, lai noskaidrotu iemeslus eksperimentālajās struktūrās novērotajiem atšķirīgi savstarpēji nobīdītajiem blokiem. Tā kā kristālrežģa enerģijas aprēķini nevar tikt veikti nesakārtotām struktūrām, tika analizētas tikai sakārtotas racēmiskas un enantiotīras fāzes. Turklāt, bez eksperimentālajām struktūrām tika analizētas arī līdzīgas hipotētiskas struktūras (racēmiskas un enantiotīras ar dažādām savstarpējajām nobīdēm starp blokiem). 2.18. attēlā attēlotas visas izveidotās kombinācijas.

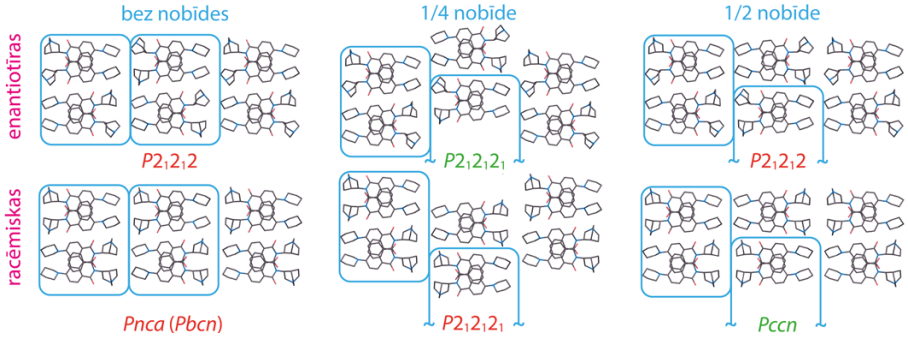

2.18. att. **Savienojuma 3c eksperimentālās (telpiskās grupas zaļā krāsā) un hipotētiskās (telpiskās grupas sarkanā krāsā) struktūras.**

Racēmiskās struktūras tika konstruētas gan ar I, gan ar II konformēru asi-

metriskajā vienībā. Kristālrežģa enerģijas (un to komponentes) relaksētām struktūrām uzskaitītas 2.3. tabulā. Aprēķini uzrāda, ka enerģētiski izdevīgākās struktūras rodas, ja racēmiski molekulu bloki ir sapakoti ar svstarpējo nobīdi 1/2, bet enantiotīri molekulu bloki ar nobīdi 1/4, kas pilnībā atbilst novērotajām eksperimentālajām struktūrām. Tāpat var novērot, ka pretēji racēmiskās struktūras gadījumam enantiotīrā struktūra ar nobīdi 1/2 ir mazāk stabila par struktūru ar nobīdi 1/4, kas ir galvenokārt mazāk izdevīgu dispersijas un Kulona mijiedarbību dēļ.

2.3. tabula. **Kristālrežģa enerģijas un to komponentes (kJ·mol^{-1}) eksperimentālajām un hipotētiskajām *rac*–3c un *enant*–3c formām**

	Strukt.	Nobīde	E_{Kulona}	$E_{\text{pol.}}$	$E_{\text{disp.}}$	$E_{\text{atgr.}}$	$E_{\text{kop.}}$
rac	*Pccn* I *	1/2	−96,1	−51,8	−286,8	286,2	−148,5
	$P2_12_12_1$ †	1/4	−100,2	−56,4	−295,2	311,6	−140,1
	Pccn II	1/2	−92,1	−54,0	−278,7	286,4	−138,4
	Pnca I	0	−90,6	−48,7	−269,9	271,2	−138,0
	Pnca II	0	−98,9	−56,4	−293,8	312,1	−137,1
enant	$P2_12_12_1$ *	1/4	−97,3	−50,6	−288,6	291,0	−145,6
	$P2_12_12$	1/2	−94,5	−50,7	−281,6	286,0	−140,8
	$P2_12_12$	0			§		

* – eksperimentālās struktūras; † – struktūras relaksāciju laikā atšķirība starp konformēriem I un II zudusi, § – struktūras relaksācijas laikā iegūta *P*1 (*Z*'=8) struktūra, kas atgādina $P2_12_12$ struktūru, bet kurai nav pilnīgas simetrijas (konkrētie enerģijas aprēķini iespējami tikai struktūrām, kur *Z*'<3).

Racēmiskā sastāva gadījumā turpretim fāze ar nobīdi 1/4 zaudē fāzei ar nobīdi 1/2 īpaši palielinātās atgrūšanās enerģijas komponentes dēļ, lai gan enerģijas stabilizācijas komponenti 1/4 nobīdes fāzes gadījumā kopumā ir zemāki. Kristālrežģa enerģijas aprēķini atbilst eksperimentālajiem novērojumiem. Turklāt, tie izskaidro, kāpēc veidojas divi strukturāli atšķirīgi cietie šķīdumi – viens racēmiskā sastāva, otrs – enantiotīrā sastāva apgabalā.

SECINĀJUMI

1. Pētīto savienojumu enantiomēru cieto šķīdumu veidošanās ir iespējama, jo hirālā oglekļa aizvietotāji nav tieši iesaistīti kristālisko struktūru stabilizējošās mijiedarbībās. Pimobendāna un fenilpiracetāma gadījumā neatkarīgi no hirālā oglekļa konfigurācijas tiek saglabāts ūdeņraža saišu tīkls, naftalimīda atvasinājumu kristālisko struktūru stabilitāti nosaka stereonespecifiskas π···π mijiedarbības.

2. Pimobendāna enantiomēri ir grūti atšķirami kristāliskajā stāvoklī, jo papildus tam, ka hirālā oglekļa aizvietotāji nav ne ūdeņraža saišu donori, ne akceptori, hirālais centrs ir iekļauts heterociklā, bet tā atlikušie aizvietotāji ir ūdeņraža atoms un metilgrupa, kas pēc izmēra ir relatīvi mazi, tādējādi iespējamā stēriskā un enerģētiskā ietekme uz apkārtējām molekulām ir samazināta.

3. Vairumā gadījumu strukturāli atšķirīgu cieto šķīdumu veidošanās racēmiskā un enantiotīrā sastāva apgabalā līdz galam nav pilnībā izprasta. It sevišķi pimobendāna gadījumā nav skaidrs, kāpēc neviens no cietajiem šķīdumiem nav nepārtraukts, bet tā vietā racēmiskajā un enantiotīrajā apgabalā veidojas atšķirīgas cieto šķīdumu struktūras. Tas norāda, ka robežkoncentrācijām tuvas sistēmas tomēr tiek atšķirtas, lai arī nepieredzēti lielā cieto šķīdumu daudzveidība pimobendāna gadījumā pirmām kārtām skaidrojama ar abu enantiomēru niecīgajām molekulāro struktūru atšķirībām.

4. Pretēji tam, kas norādīts Šiona *et al.* definīcijā (tādējādi novedot pie nepareizas enantiomēru cieto šķīdumu klasifikācijas dažos literatūras avotos), II tipa cietajiem šķīdumiem (ar strukturālu enantioselektivitāti) racēmiska sastāva gadījumā nav jābūt pilnībā sakārtotiem. Nesakārtotības pakāpe šādos gadījumos saistāma ar konfigurācijas entropiju vai kinētiskiem aspektiem kristāla augšanas procesā.

5. Četras no sešām noteiktajām enantiotīrās robežkoncentrācijas cieto šķīdumu struktūrām tikai formāli kristalizējas Zonkes telpiskajās grupās. Struktūrās novērojama šķietama centrosimetrija un, neievērojot dažus atomus, struktūras var aprakstīt ar noteikto telpisko grupu atbilstošajām centrosimetriskajām supergrupām. Tas pierāda, ka centrosimetrija molekulāros kristālos ir patiešām dominējoša, un norāda uz iespējamo iemeslu, kāpēc tik lielā pārsvarā (90%) patvaļīgi veidojas racēmiskie savienojumi.

6. Trīs dažādu II tipa cieto šķīdumu skalēmiska sastāva kristālu pētījumi parāda, ka patiesi centrosimetriski molekulu pāri dominē pār *kvazi*–centrosimetriskiem molekulu pāriem. Pēdējie drīzāk veidojas kompromisa starp enantiomēru sastāvu un mērķa kristālisko struktūru dēļ. Šie novērojumi demonstrē kristalogrāfisko molekulu pozīciju enantioselektivitātes izcelsmi. Vienā cieto šķīdumu gadījumā tika atrasts, ka *kvazi*–centrosimetriskā enantiotīrā struktūrā novērojams neefektīvāks pakojums un neefektīvi tuvāki atomu savstarpējie kontakti, salīdzinot ar centrosimetrisko racēmisko struktūru. Enantiotīrā struktūra veidojas uz joprojām efektīvu dispersijas mijiedarbību noteiktās kristālrežģa enerģijas palielināšanās rēķina.

7. Ņemot vērā cieto šķīdumu strukturālos aspektus (molekulu konformacionālā brīvība; hirālā centra aizvietotāju starpmolekulāro mijiedarbību nespecifiskums u.c.), ir iespējams mērķtiecīgi sintezēt savienojumus, kuri šādus cietos šķīdumus veido.

LITERATŪRAS SARAKSTS

1. Carey, F. A.; Sundberg, R. J. *Advanced Organic Chemistry* **2007**, Springer.
2. Rouhi, A. M. *Chem. Eng. News* **2003**, *81*, 45–61.
3. Guo-Qiang, L.; Qi-Dong, Y.; Jie-Fei, C. *Chiral Drugs* **2011**, John Wiley & Sons.
4. Lorenz, H.; Seidel-Morgenstern, *A. Angew. Chemie Int. Ed.* **2014**, *53*, 1218–1250.
5. Sato, O. *Nat. Chem.* **2016**, *8*, 644–656.
6. Jacques, J.; Collet, A.; Wilen, S. H. *Enantiomers, racemates, and resolutions* **1981**, Wiley.
7. Vogt, F. G.; Copley, R. C. B.; Mueller, R. L.; Spoors, G. P.; Cacchio, T. N.; Carlton, R. A.; Katrincic, L. M.; Kennady, J. M.; Parsons, S.; Chetina, O. V. *Cryst. Growth Des.* **2010**, *10*, 2713–2733.
8. Bredikhin, A. A.; Bredikhina, Z. A.; Zakharychev, D. V.; Gubaidullin, A. T.; Fayzullin, R. R. *CrystEngComm* **2012**, *14*, 648–655.
9. Esteves de Castro, R.; Canotilho, J.; Barbosa, R. M.; Silva, M. R.; Beja, A. M.; Paixão, J. A.; Redinha, J. S. *Cryst. Growth Des.* **2007**, *7*, 496–500.
10. de Diego, H. L., Bond, A. D.; Dancer, R. J. *Chirality* **2011**, 23, 408–416.
11. Huang, J.; Chen, S.; Guzei, I. A.; Yu, L. *J. Am. Chem. Soc.* **2006**, *128*, 11985–11992.
12. Chion, B.; Lajzerowicz, J.; Bordeaux, D.; Collet, A.; Jacques, J. *J. Phys. Chem.* **1978**, *82*, 2682–2688.
13. Kitaigorodsky, A. I. *Mixed Crystals* **1984**, Springer.
14. Kaemmerer, H.; Lorenz, H.; Black, S. N.; Seidel-Morgenstern, A. *Cryst. Growth Des.* **2009**, *9*, 1851–1862.
15. Taratin, N. V.; Lorenz, H.; Kotelnikova, E. N.; Glikin, A. E.; Galland, A.; Dupray, V.; Coquerel, G.; Seidel-Morgenstern, A. *Cryst. Growth Des.* **2012**, *12*, 5882–5888.
16. Wermester, N.; Aubin, E.; Pauchet, M.; Coste, S.; Coquerel, G. *Tetrahedron: Asymmetr.* **2007**, *18*, 821–831.
17. Bredikhin, A. A.; Bredikhina, Z. A.; Zakharychev, D. V. *Mendeleev Commun.* **2012**, *22*, 171–180.
18. Gallis, H. E.; Bougrioua, F.; Oonk, H. A. J.; van Ekeren, P. J.; van Miltenburg, J. C. *Thermochim. Acta* **1996**, *274*, 231–242.
19. Oonk, H. A. J.; Tjoa, K. H.; Brants, F. E.; Kroon, J. *Thermochim. Acta* **1977**, *19*, 161–171.
20. Flack, H. D. *Helv. Chim. Acta* **2003**, *86*, 905–921.

21. Gordon, S. G.; Miller, M. W.; Saunders, A. B. *J. Am. Anim. Hosp. Assoc.* **2006**, *42*, 90–93.
22. Chu, K. M.; Shieh, S. M.; Hu, O. Y. Clin. *Pharmacol. Ther.* **1995**, *57*, 610–621.
23. Bell, E. T.; Devi, J. L.; Chiu, S.; Zahra, P.; Whittem, T. J. *Vet. Pharmacol. Ther.* **2015**, *38*, 1–8.
24. Boeren, M. M. M.; Paridaans, R. J.; Petkune, S.; Lusis, V.; Muceniece, D. *Crystalline pimobendan, process for the preparation thereof, pharmaceutical composition and use* European Patent, **2014**.
25. Zvirgzdins, A.; Delina, M.; Mishnev, A.; Actins, A. *Acta Crystallogr. Sect. E Struct. Reports Online* **2013**, *69*, 1677–1677.
26. Malykh, A. G.; Sadaie, M. R. *Drugs* **2010**, *70*, 287–312.
27. Zvejniece, L. Svalbe, B.; Veinberg, G.; Grinberga, S.; Vorona, M.; Kalvinsh, I.; Dambrova, M. *Basic Clin. Pharmacol. Toxicol.* **2011**, *109*, 407–412.
28. Veinberg, G.; Vavers, E.; Orlova, N.; Kuznecovs, J.; Domracheva, I.; Vorona, M.; Zvejniece, L.; Dambrova, M. *Chem. Heterocycl. Compd.* **2015**, *51*, 601–606.
29. Merz Pharma GmbH & Co. KGaA. *Use of (R)-phenylpiracetam for the treatment of sleep disorders* European Patent, **2015**.
30. Zvejniece, L.; Svalbe, B.; Vavers, E; Makrecka-Kuka, M.; Makarova, E.; Liepins, V.; Kalvinsh, I.; Liepinsh, E.; Dambrova M. *Pharmacol. Biochem. Behav.* **2017**, *160*, 21–29.
31. Ksenafontov, D. N.; Moiseeva, N. F.; Rykov, A. N.; Shishkov, I. F.; Oberhammer, H. *Struct. Chem.* **2013**, *24*, 171–179.
32. d'Agostino, S.; Braga, D.; Grepioni, F.; Taddei, P. *Cryst. Growth Des.* **2014**, *14*, 821–829.
33. Hilfiker, R. *Polymorphism: In the Pharmaceutical Industry* **2006**, Wiley.
34. Ivantchev, S.; Kroumova, E.; Madariaga, G.; Pérez-Mato, J. M.; Aroyo, M. I. *J. Appl. Crystallogr.* **2000**, *33*, 1190–1191.
35. Teteruk, J. L.; Glinnemann J.; Heyse W.; Johansson K. E.; van de Streek J.; Schmidt M. U. *Acta Crystallogr. Sect. B Struct. Sci. Cryst. Eng. Mater.* **2016**, *72*, 416–433.

UNIVERSITY OF LATVIA
FACULTY OF CHEMISTRY

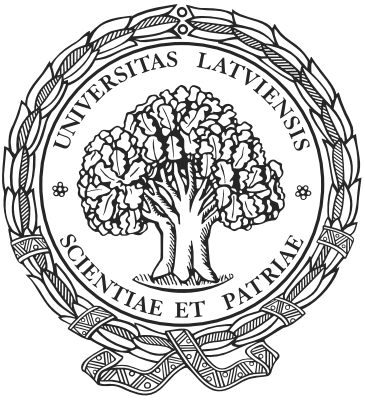

Toms Rēķis

Enantiomer recognition in molecular crystals: structural and thermodynamic aspects of enantiomer solid solutions of selected small organic molecules

DOCTORAL THESIS

Submitted for the Degree of Doctor of Chemistry
Subfield of Physical Chemistry

Riga, 2018

I call any geometrical figure, or group of points, 'chiral', and say that it has chirality if its image in a plane mirror, ideally realized, cannot be brought to coincide with itself.

Sir William Thomson Lord Kelvin, 1894

The Doctoral Thesis was carried out at the Chair of Physical Chemistry, Faculty of Chemistry, University of Latvia, Riga, Latvia; Laboratory of Physical and Chemical Foundations of Process Engineering, Max Planck Institute for Dynamics of Complex Technical Systems, Magdeburg, Germany; Molecular Crystal Engineering Group, University of Bologna, Bologna, Italy, from 2014 to 2017.

The Thesis contains the Summary in Latvian and English, 4 scientific articles. Form of the Thesis: collection of scientific articles in Chemistry, Physical Chemistry.

Supervisor:	Senior researcher, *Dr.chem.* Liāna Orola
Scientific advisors:	Senior researcher, *Dr.chem.* Agris Bērziņš
	Prof., *Dr.chem.* Andris Actiņš
	apl. Prof., *Dr.rer.nat.* Heike Lorenz
	Prof., *Dr.* Fabrizia Grepioni

Reviewers:

Dr.phys. Anatolijs Mišņovs (Latvian Institute of Organic Synthesis)
Prof., *Dr.chem.* Māris Turks (Riga Technical University)
Asoc. prof., *Dr.chem.* Pēteris Mekšs (University of Latvia)

The Thesis will be defended in a public session of the Promotional Committee of Chemistry, University of Latvia, at 14.00 on May 10, 2018 at the University of Latvia, Academic Center for Natural Sciences, Jelgavas 1, Riga, room 701.

The summary of the Thesis is available at the Library of the University of Latvia, Riaņa bulv. 19.

ISBN 978-9934-556-33-3

ABSTRACT

Several systems of enantiomer solid solutions have been studied. Solid phase diversity, including polymorphism and solvatomorphism, of racemic and enantiopure forms of the studied compounds has been explored. The enantiomer systems have been characterized by melt phase diagrams showing stable and metastable solid solutions in full and limited composition regions. Furthermore, crystal structures have been determined revealing existence of solid solutions with enantioselective and non-stereospecific crystallographic molecular positions. The definition of structural aspects of one type of solid solutions (showing enantioselectivity) has been revised based on the analysis of the experimental findings and literature. The structural origin of the lack of enantiomer recognition in the studied systems has been determined, illustrating either the role of chiral centre configuration-independent hydrogen bonding or non-stereospecific π···π stacking. Finally, two novel compounds were synthesized to form enantiomer solid solutions, thus, showing that such extremely rarely occurring phases could be intentionally designed.

Solid solutions of enantiomers, Enantiomer recognition in the solid state, Melt phase diagrams, *Quasi*–centrosymmetric structures, Disordered structures

INTRODUCTION

Chirality plays a significant role in many divisions of science. Enantiomers of a chiral compound are indistinguishable with respect to an achiral media[1]; however, due to crucial differences of the mutual interactions, it is not the case, when other species possessing handedness are introduced in the system. It also applies when a mixture of both enantiomers is considered over a single enantiomer. Phenomenon of chirality is therefore especially crucial when optically active compounds are intended to interact with biological systems. Very often in pharmacy, agrochemistry, or food industry a single enantiomer is preferred[2,3] over a mixture of enantiomers or diastereomers due to harmful, potentially harmful, or unnecessary intake or use of the related optical isomers. However, most often it is exceptionally more feasible to synthesize equimolar (racemic) mixtures of enantiomers rather than molecules in their enantiopure form. The process of producing single enantiomers has therefore challenged organic and physical chemists ever since[4].

Over past decades a considerable progress has been made developing enantioselective or stereospecific synthetic methods. However, historically single enantiomers have been obtained from racemic mixtures using separation methods. Enantioseparation by crystallization is still highly preferred in industry as it is very robust and considerably cheaper method. Crystallization based resolution of enantiomers can be achieved *via* diastereomeric adduct (salt, co-crystal, or even covalent) formation or rarely directly from the racemic mixture[4]. Fundamental studies of stereoselectivity and stereospecificity in the solid state are therefore important to systemize and rationalize aspects of different crystalline phase formation. Furthermore, as there is an increasing research conducted on molecular crystals for their potential applications in molecular devices[5], fundamental knowledge on aspects governing enantioselectivity and enantiospecificity in the solid state is appealing from a crystal engineering point of view. Although both enantiomers are symmetrical to each other, they are not congruent objects and therefore represent different building blocks when it comes to the formation of a crystal structure. Accordingly, there is a larger diversity of phases possible concerning two different (but essentially the same) molecules, being the two enantiomers of a chiral compound.

When crystallizing racemic mixtures three possible outcomes can be expected: 1) racemic compounds (~90%); 2) conglomerates (~10%); 3) solid solutions of enantiomers (<1%)[6]. Racemic compounds are single phases consisting of both enantiomers, in principle, 'racemic compound' can be regarded as a term for a 1:1 molecular compound formed by both enantiomers in equimolar ratio. Rarely, however, no stable racemic compound forms and each of the enantiomers crystallizes in a distinct crystal structure. Both structures are mirror phases with respect to each other. Very seldom formation of enantiomer solid solutions occurs.

Estimated probability of occurrence of the three mentioned cases indicates

that usually the crystallographic molecular positions are strictly stereospecific. Racemic compounds *per se* have strict order of enantiomers in the crystal structure and in case of conglomerates each one of the structures comprises a single enantiomer. Enantiomer solid solutions therefore is a very rare example, where two components (enantiomers) are not recognized in the solid state, which is not typical for crystals usually comprehended as systems possessing, in particular, three-dimensional translation symmetry.

Since solid solutions of enantiomers are only an occasionally occurring matter, they are not so widely studied. However, they hide answers on how stereoselectivity and stereospecificity are governed in the solid state. In early studies enantiomer solid solutions were rather identified and characterized by binary melt phase diagrams[6]. Due to development of higher resolution diffractometers and data processing software, an accurate characterization of several structures has been possible clearly showing the disordered nature of such systems[7–11] and allowing to analyse structural aspects of solid solutions of enantiomers, which generally have been described already decades ago by the pioneering works of Chion *et al.* and Kitaigorodsky[12,13].

Up to date no rigorous approach has been elucidated, that would allow one to foresee enantioselectivity and enantiospecificity issues in the solid state, which would eventually aid stereospecific crystallization design avoiding exhaustive experimental (trial and error) work. It is therefore also not possible to predict formation of solid solutions of enantiomers or intentionally design chiral molecules possible to form such mixed crystal phases. Such solid solutions of enantiomers, however, might be interesting for applications in molecular devices as single phase crystalline materials could be obtained with finely tuneable (composition dependent) properties, *e.g.*, non-linear optical properties.

The **aim** of this research was to investigate multi-component systems of chiral small organic molecules showing lack of enantiomer recognition in the crystalline state in order to rationalize structural and thermodynamic aspects of enantiomer solid solution formation.

TASKS

1. Characterizing phenylpiracetam enantiomer system by means of melt phase diagram and detailed structural study.
2. Characterizing pimobendan enantiomer system by means of melt phase diagram.
3. Characterizing the extensive solvate system of pimobendan enantiomers by means of powder X-ray diffraction and thermal methods of analysis.
4. Performing a structural study of enantiopure and racemic pimobendan phases.
5. Exploring enantiomer system of a naphthalimide derivative suspected to form solid solutions by means of detailed structural study of racemic and non-racemic composition crystals.

6. Synthesizing novel chiral naphthalimide derivatives lacking enantiomer recognition in the solid state.

SCIENTIFIC NOVELTY

1. In total 9 novel structures of phases showing lack of enantiomer recognition have been determined, which is around the same number as reported in total prior this study, thus, allowing to rationalize structural aspects of solid solution formation in more detail.
2. Two melt phase diagrams have been construed illustrating thermodynamic aspects of enantiomer solid solutions studied, as well as showing the complicated nature of such systems (involving enantiotropic relationship between polymorphs and several metastable solid solutions).
3. Extensive pimobendan enantiomer solid solution system has been explored involving not only non-solvated but also solvated phases. Thus, it is the first case reported showing that enantiomer solid solution formation can be tracked down to the molecular level and it is not necessarily always an interplay between the molecular structure and specific features of the crystal structure.
4. Detailed structural study of several scalemic composition crystals of two enantiomer solid solutions has been performed, which is considered rare as previously rather only the enantiopure and racemic limiting cases have been structurally studied. Findings justify aspects of type II solid solutions (showing enantioselectivity of the crystallographic molecular positions), thus, proving that some of the solid solutions classified as Type I in some literature sources are in fact Type II solid solutions.
5. Two novel compounds have been synthesised and proven to exist as solid solutions. Such solid phases showing lack of enantiomer recognition have not been intentionally designed prior this study.

PRACTICAL SIGNIFICANCE

1. Study on pimobendan (produced by JSC *Grindeks*) solid solutions aided resolving of the quality control issues regarding racemic pimobendan form A.
2. Study on phenylpiracetam (produced by JSC *Olainfarm*) solid solutions aided resolving of the patenting issues regarding enantiopure phenylpiracetam.
3. Structural aspects of enantiomer solid solution formation have been justified, thus, opening an access to appealing molecular crystal materials with finely tuneable (enantiomer composition-dependent) properties in a crystal engineering manner.

RESULTS PUBLISHED

Publications, proceedings and patents

1. Rekis, T., Bērziņš, A., Sarceviča, I., Kons, A., Balodis, M., Orola, L., Lorenz, H., Actiņš, A., A maze of solid solutions of pimobendan enantiomers: an extraordinary case of polymorph and solvate diversity. *Cryst. Growth Des.* **2018**, 18(1), 264–273.

   T. Rēķis carried out 40% of the experimental work, developed the concept and wrote the article, prepared the experimental results according to the journal guidlines, as well as prepared the answers to the questions and remarks given by the rewievers.

2. Rekis, T., d'Agostino, S., Braga, D., Grepioni, F., Designing solid solutions of enantiomers: lack of enantioselectivity of chiral naphthalimide derivatives in the solid state. *Cryst. Growth Des.* **2017**, 17(12), 6477–6485.

   T. Rēķis carried out 70% of the experimental work, developed the concept and wrote the article, prepared the experimental results according to the journal guidlines, as well as prepared the answers to the questions and remarks given by the rewievers.

3. Rekis, T., Bērziņš, A., Džabijeva, D., Nakurte, I., Orola, L., Actiņš, A., Structure and Stability of Racemic and Enantiopure Pimobendan Monohydrates: On the Phenomenon of Unusually High Stability. *Cryst. Growth Des.* **2017**, 17(4), 1814–1823.

   T. Rēķis carried out 70% of the experimental work, contributed to writing the article (80%), prepared the experimental results according to the journal guidlines, as well as contributed in answering the questions and remarks given by the rewievers.

4. Rekis, T., Bērziņš, A., Orola, L., Holczbauer, T., Actiņš, A., Seidel-Morgenstern, A., Lorenz, H., Single Enantiomer's Urge to Crystallize in Centrosymmetric Space Groups: Solid Solutions of Phenylpiracetam. *Cryst. Growth Des.* **2017**, 17(3), 1411–1418.

   T. Rēķis carried out 90% of the experimental work, developed the concept and wrote the article, prepared the experimental results according to the journal

guidlines, as well as prepared the answers to the questions and remarks given by the rewievers.

5. Rekis, T., Bērziņš, A., Orola, L., Actiņš, A., Seidel-Morgenstern, A., Lorenz, H., On the formation of phenylpiracetam solid solutions: thermodynamic and structural considerations. *Proceedings 23rd Int Workshop on Industrial Crystallization (BIWIC 2016)* **2016**, 106-111.

6. Rekis, T., Oša, G., Bērziņš, A., Actiņš, A. *Process of Preparation of Crystalline Form A of Pimobendan.* Patent A61K31/501, **2013**

Conferences

1. T. Rekis, A. Bērziņš, L. Orola, A. Actiņš, A. Seidel-Morgenstern, H. Lorenz, On the formation of phenylpiracetam solid solutions: thermodynamic and structural considerations. *23rd International Workshop on Industrial Crystallization (BIWIC 2016)*, Magdeburg, Germany, **2016**

2. T. Rekis, G. Oša, A. Bērziņš, L. Orola, I. Sarceviča, A. Actiņš, H. Lorenz, The chaos in a solid solution decreased in the presence of a solvent: the case of racemic pimobendan. *14th European Powder Diffraction Conference (EPDIC 2016)*, Bari, Italy, **2016**

3. T. Rekis, A. Bērziņš, L. Orola, I. Sarceviča, G. Oša, I. Heinmaa, R. Prekup, A. Actiņš The chaos in a solid solution decreased in the presence of a solvent: the case of racemic pimobendan. *8th Crystal Forms @ Bologna*, Bologna, Italy, **2015**

4. T. Rēķis, G. Oša, A. Bērziņš, L. Orola, I. Sarceviča, A. Actiņš Time dependent systematic unit cell parameter change of pimobendan polymorph. *7th Crystal Forms @ Bologna*, Bologna, Italy, **2013**

5. T. Rēķis, L. Orola, O. Sežanova, A. Bērziņš, A. Actiņš. Polymorphic and solvatomorphic forms of pimobendan. *University of Latvia 70th conference*, Riga, Latvia, **2012**

CHAPTER 1
RESEARCH BACKGROUND

1.1. THERMODYNAMIC CHARACTERIZATION OF SOLID SOLUTIONS OF ENANTIOMERS

Solid solutions are isostructural single phases consisting of at least two components with variable compositions. Construction of a melt phase diagram of an enantiomer system reveals formation of solid solutions (if any) as well as allows to characterize them by, *e.g.*, assessing thermodynamic stability and miscibility limits. Figure 1.1. shows principal types of phase diagrams involving solid solutions.

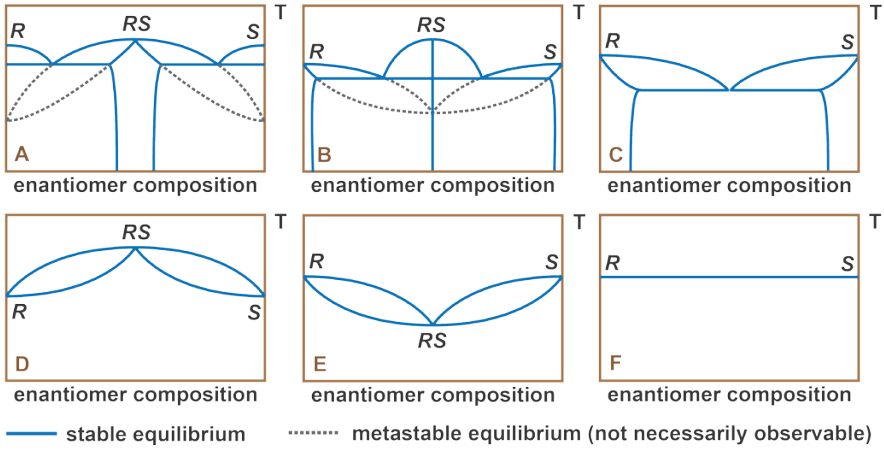

Figure 1.1. **Melt phase diagrams of enantiomer systems involving solid solution formation (A–C partial and D–F full miscibility in solid state).**

Miscibility around the racemic composition[14], near the pure enantiomer region[12,15,16] or covering the whole composition range[7,8,10,11,17–19] have been reported for particular compounds. The phase diagram obtained for a certain compound is governed by the thermodynamics of the respective solid phases. For example in case of miscibility around the racemic composition (Figure 1.1. A) there is a racemic phase RS that must have a structural feature which allows exchange of the enantiomers with their opposite counterparts, therefore forming solid solutions with scalemic compositions. However, the miscibility region is not covering the whole composition range due to the existence of a stable structurally different enantiomerically pure solid phase S (or R). The miscibility region width and other quantitative phase diagram properties are determined by properties of the solid phases RS and S (or R), namely the enthalpies of melting and melting temperatures. In case of miscibility close to the pure enantiomer region (Figure 1.1 B and C) there

is a solid phase S (or R) with a structural ability to form solid solutions. For case B a stable racemic compound RS emerges. Depicted metastable equilibria are not necessarily observable. For case C, however, limited miscibility arises because the solid solution at a certain composition is no longer thermodynamically stable and a mixture of two phases with the limiting compositions forms instead. Cases D, E, and F represent miscibility in the whole composition range for non-ideal solid solutions with maximum, and minimum melting temperature at the racemic composition, and ideal solid solutions, respectively. The solid phases RS and S (or R) in those cases are isostructural.

1.2. STRUCTURAL ASPECTS OF SOLID SOLUTIONS OF ENANTIOMERS

From a structural point of view two cases can be distinguished regarding enantiomer recognition in the solid solutions: 1) non-enantiospecific (Type I); 2) enantioselective (Type II). Type I has been defined as follows: within a crystal containing x mole R molecules and $(1-x)$ mole S molecules the probability of finding an R molecule on a given site is proportional to x, and the probability of finding an S molecule is proportional to $(1-x)$[12].

Type II in the present study is left for structures showing a certain degree of enantioselectivity, which arises from reasonable structural aspects. In the original definition by Chion *et al.* continuous miscibility has been reported to affect only a part of the crystallographic positions eventually giving completely ordered racemic compound at the racemic composition. However, as it can be observed in several structures reported in the literature[7–11] for which the enantioselectivity is evidently present, not necessarily completely ordered racemic compound is obtained at the racemic composition, but rather the structures only tend to enantiospecific limiting cases. The definition of Type II has been therefore slightly revised compared to that introduced decades ago in the pioneering study of structural aspects of solid solutions of enantiomers[12]. The definition originally given, rather describes an idealized case of the enantioselective (Type II) solid solutions.

While in Type I solid solutions there is simply no recognition of the enantiomers at all, structural aspects of Type II solid solutions deserve a discussion in more detail. Due to physical and chemical considerations a single enantiomer can only crystallize in one of the 65 Sohncke space groups (without any symmetry element of the second kind – generating the opposite enantiomer, namely, inversion centres, rotoinversion axes, mirror or glide planes)[20]. However, usually in crystal structures of Type II solid solutions apparent centrosymmetry is observed: molecules with identical configuration occupy different conformations, which are approximate mirror images to each other. The mentioned structural aspects describing the formation of solid solutions are illustrated in the Figure 1.2.

The enantiopure sample crystallizes in a *quasi*–centrosymmetric structure so that the absent enantiomer is mimicked by adjusting the conformation of the present enantiomer. Scalemic structures locally would contain some genuine in-

version centres (or other loci of symmetry operations of the second kind).

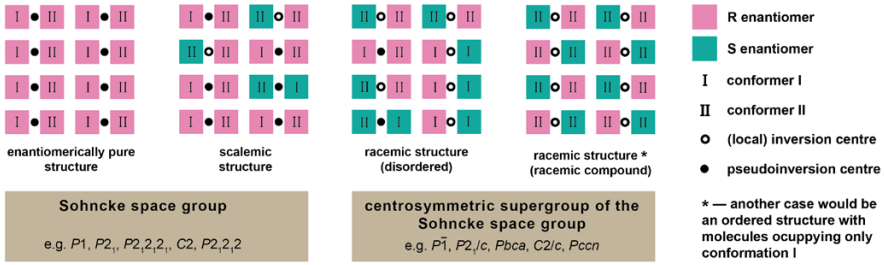

Figure 1.2. **Graphical representation of the Type II solid solution formation from two enantiomers.**

Two cases are depicted for racemic composition crystals – a completely ordered structure (only genuine inversion centres are present, thus all the molecules occupy only one of the conformations), and a disordered structure. Note that in such disordered structures only conformer pairs RI – SII and RI – SI are present if the locus of symmetry for the pair of two crystallographic positions is of the second kind (changing the handedness (see Figure 1.2)). This structural restriction, in fact, distinguishes the Type II from Type I. Regardless of the presence of disorder, the space group of the racemic composition crystal in such Type II structures changes to a centrosymmetric supergroup of the Sohncke space group. However, in case of disordered phases the centrosymmetric space group is only due to statistical reasons. In practice the asymmetric unit of disordered racemic crystal appears to be a superimposition of a pair of molecules, e.g., RI – SII. Thus, with a certain probability either one or another conformation (and enantiomer) is observed in every molecular site. Enantiomerically pure samples, on contrary, are never disordered (as long as any static disorder does not arise from other reasons), therefore their asymmetric unit contains even number of molecules occupying different conformations – those superimposed in the racemic structure.

1.3. OBJECTS OF INVESTIGATION

In total five compounds were studied (chemical schemes are given in Figure 1.3.).

Pimobendan (**1**) (4,5–dihydro–6–[2–(*p*–methoxyphenyl)–5–benzimidazolyl]–5–methyl–3(2H)–pyridazinone) is an active pharmaceutical ingredient used as positive ionotrop and vasodilator mainly to treat heart failure either in veterinary or human medicine[21,22]. The molecule is marketed as a racemate. As observed for enantiomers of many other chiral compounds, the pharmacokinetics and pharmacodynamics of pimobendan enantiomers differ[22,23]. Prior this work solid forms of racemic pimobendan have been reported in a patent[24], including a number of polymorphs and solvates (1,4–dioxane, methanol, water). Furthermore, solid form diversity of pimobendan have been extensively explored by co-workers of the author and the information has been available as unpublished data within

the Department of Physical Chemistry, Faculty of Chemistry. The structure of pimobendan polymorph B have been reported solved from the PXRD data[25].

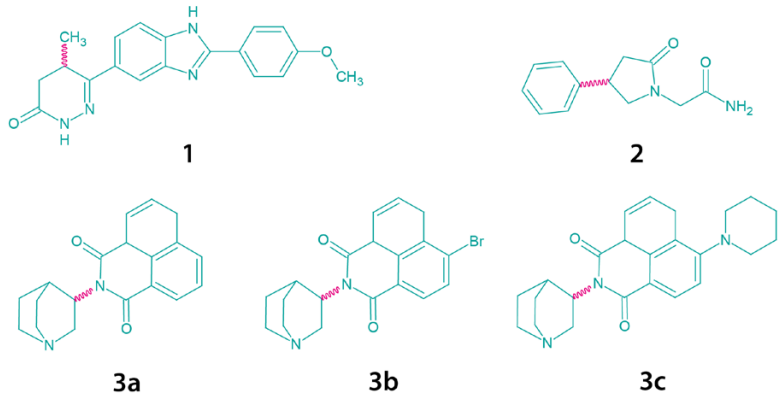

Figure 1.3. **Chemical schemes of the compounds studied (1 – pimobendan; 2 – phenylpiracetam; 3 – naphthalimide derivatives).**

Phenylpiracetam (**2**) (2–(2–oxo–4–phenylpyrrolidin–1–yl)–acetamide) is a mild nootropic drug that may have anti-amnesic, antidepressant, anticonvulsant, anxiolytic, and memory enhancement effects[26–28]. Its R enantiomer has been reported to be used to treat sleep disorders[29]. Its S enantiomer has been reported to reduce body weight gain[30]. Phenylpiracetam molecular structure has been studied by gas electron diffraction and quantum chemical calculations[31]. Information on the solid form diversity studies of racemic and enantiopure compound has been available as unpublished data within the Department of Physical Chemistry, Faculty of Chemistry.

Finally, three model compounds were studied: 2–(quinuclidin–3–yl)–1,8–naphthalimide (**3a**), 4–bromo–*N*–(quinuclidin–3–yl)–1,8–naphthalimide (**3b**), and 4–(piperidin–1–yl)–*N*–(quinuclidin–3–yl)–1,8–naphthalimide (**3c**). For naphthalimide derivative **3a** racemic and enantiopure structures have been reported[32]. Based on the structural data it was suspected that **3a** represents a system of solid solutions[32]. Racemic and enantiopure forms of **3a** were synthesised to explore this enantiomer system. Furthermore, both remaining compounds (**3b** and **3c**) were synthesised in their racemic and enantiopure forms in order to try to intentionally design solid solutions of enantiomers.

CHAPTER 2
RESULTS AND DISCUSSION

2.1. SOLID SOLUTIONS OF PIMOBENDAN (1) ENANTIOMERS

There are several polymorphs of enantiopure and racemic pimobendan: *rac*–**1**–A, *rac*–**1**–B, *rac*–**1**–C, *enant*–**1**–D, *enant*–**1**–E, *enant*–**1**–F, and *rac*–**1**–Gd (isostructural desolvate of an isostructural solvate family *rac*–**1**–G). Furthermore, there are five hydrates: *rac*–**1**–H1 (a monohydrate), *rac*–**1**–H2 (a monohydrate), *rac*–**1**–H3 (a hemihydrate), *rac*–**1**–H4 (a trihydrate), and *enant*–**1**–H5 (a monohydrate), and finally, plenty of solvates: *rac*–**1**–MS1 (a methanol monosolvate), *rac*–**1**–MS2 (a methanol hemisolvate), *rac*–**1**–DS1 (a 1,4–dioxane monosolvate), *enant*–**1**–DS2 (a 1,4–dioxane monosolvate), and *rac*–**1**–G (an isostructural solvate family with at least 12 different solvents). The PXRD patterns of polymorphs and solvates of pimobendan are depicted in Figure 2.1.

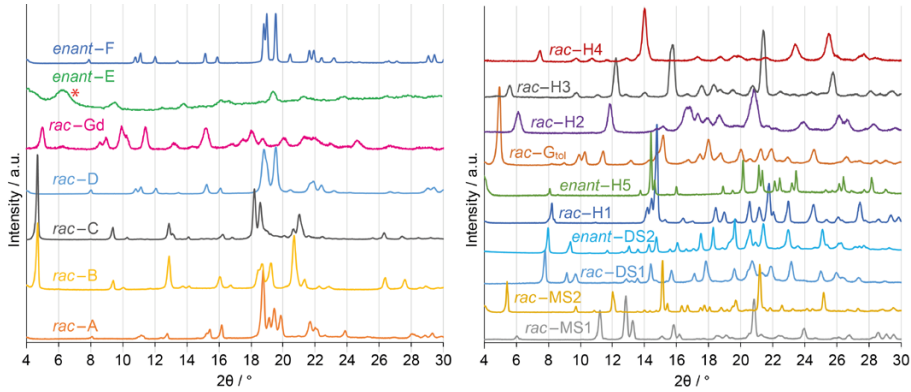

Figure 2.1. **PXRD patterns of non-solvated (left) and solvated (right) pimobendan crystal forms (* – the broad peak observed at 6.3° 2θ for *enant*–E arises from the film of the variable temperature chamber).**

Non-solvated forms of pimobendan were studied to show existence of a complicated solid solution system. The melt phase diagram characterizing non-solvated phases is given in Figure 2.2. Pimobendan enantiomers form a eutectic system of two solid solutions, thus, there is a miscibility of the enantiomers in the solid state around the racemic and near the enantiopure composition regions. There are also two metastable solid solutions **1**–δ and **1**–γ around the racemic composition.

Scalemic samples of pimobendan were studied in order to explore enantiomer recognition aspects of known racemic and enantiopure solvates. Surprisingly, all solvates that were experimentally accessible in a reasonable manner, were found to be solid solutions. Preparing the methanol hemisolvate from different enantiomeric composition samples, the products show very similar PXRD pat-

terns, which is typical for solid solutions. TG/DSC analysis of 30% and racemic composition samples show identical behaviour and the same weight loss corresponding to hemimethanolate stoichiometry (see Figure 2.3.). Upon desolvation form **1**–C (solid solution **1**–γ) is obtained.

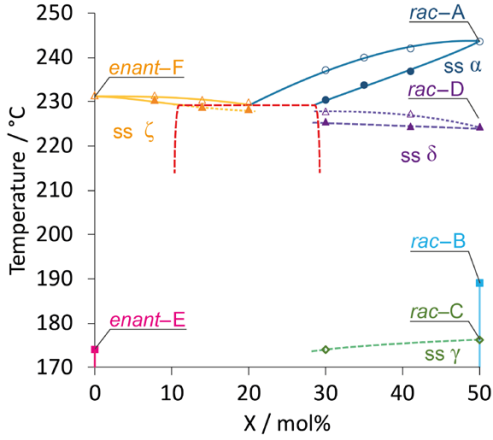

Figure 2.2. **Melt phase diagram of pimobendan enantiomers (closed markers – solidus; open markers – liquidus; lines are guides for the eyes; only half of the phase diagram is shown).**

In a similar manner several other pimobendan solvates were proven to lack enantiomer recognition, accordingly forming solid solutions (methanol solvate **1**–MS1; hydrates **1**–H1, **1**–H3, **1**–H5; dioxane solvates **1**–DS1 and **1**–DS2; isostructural solvate **1**–G). Interestingly, monohydrates *rac*–**1**–H1 and *enant*–**1**–H5 do not represent limiting cases of the same solid solution, instead solid solution **1**–H1 is stable around the racemic and **1**–H5 near the pure enantiomer region. Furthermore, also 1,4–dioxane monosolvates *rac*–**1**–DS1 and *enant*–**1**–DS2 are not isostructural, but represent two different solid solutions.

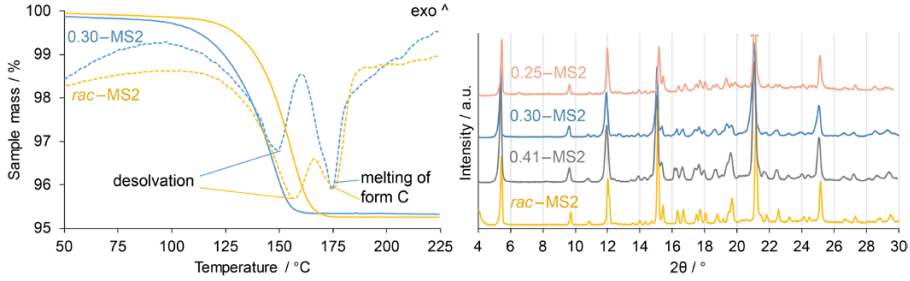

Figure 2.3. **TG (solid lines) and DSC (dashed lines) curves; PXRD patterns of racemic and scalemic composition samples of pimobendan methanol hemisolvate 1–MS2.**

Due to inability to grow single crystals in most of the cases, the structures were determined only for a few pimobendan phases. Form *rac*–**1**–A was found

to crystallize in the monoclinic crystal system *C*2/*c* space group (*Z*=8, *Z*'=1). The structure was disordered as the asymmetric unit was refined as superimposition of two conformers with occupancy factor ratio of around 3:1. Thus, pimobendan solid solution **1**–α corresponds to a Type II solid solution showing enantioselectivity of the crystallographic molecular positions.

The structure of the thermodynamically most stable enantiopure polymorph of pimobendan (*enant*–**1**–F) was solved from the PXRD data with the aid of ^{13}C solid-state NMR spectroscopy measurements. It was found to crystallize in the trigonal crystal system $P3_121$ (and $P3_221$) space group (*Z*=6, *Z*'=1). From the molecule count in the asymmetric unit it follows that the corresponding solid solution **1**–ζ (see Figure 2.2.) must be of a Type I – as there are no at least 2 symmetrically independent molecules present. The structures of *rac*–**1**–A and *enant*–**1**–F possess identical hydrogen bond networks represented by $R_2^2(16)$ rings and $C_1^1(11)$ chains (see Figure 2.4.).

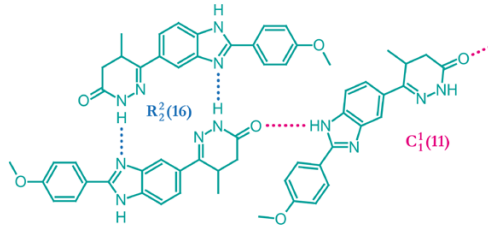

Figure 2.4. **Representation of hydrogen bond network in the structures of *rac*–1–A and *enant*–1–F.**

The differences between the structures are found in molecule conformations and packing of the molecules. In the structure of *rac*–**1**–A the infinite $C_1^1(11)$ chains stacked parallel are forming layers which are interconnected *via* centrosymmetric $R_2^2(20)$ hydrogen bonded moieties. In *enant*–**1**–F the $C_1^1(11)$ chains form rods which have 3-fold screw axis symmetry. The rods are interconnected via $R_2^2(20)$ hydrogen bonds (see Figure 2.5.).

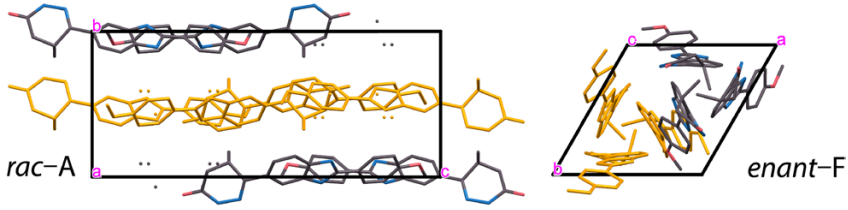

Figure 2.5. **Packing representation of *rac*–1–A and *enant*–1–F along the crystallographic *a* and *c*–axis, respectively. Layers and rods formed *via* $C_1^1(11)$ hydrogen bonds are shown in orange.**

Furthermore, the structures of racemic and enantiopure pimobendan monohydrates (*rac*–**1**–H1 and *enant*–**1**–H5, respectively) were determined from single crystal diffraction data. Racemic pimobendan monohydrate was found to

crystallize in the monoclinic crystal system, $P2_1/c$ (Z=4, Z'=1) space group. Enantiopure pimobendan hydrate, however, crystallizes in the orthorhombic crystal system, $P2_12_12_1$ space group (Z=4, Z'=1). Both hydrates contain one pimobendan and one water molecule in the asymmetric unit. The unit cell parameters of the studied monohydrates are very similar and the geometries of the pimobendan molecules in the asymmetric units of *rac*–**1**–H1 and *enant*–**1**–H5 are nearly identical (see Figure 2.6.).

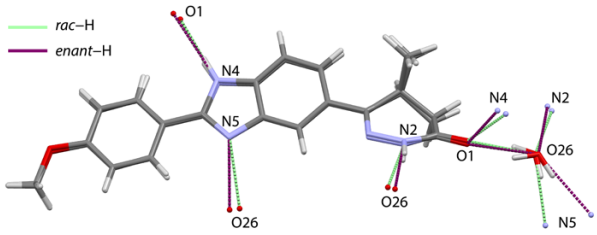

Figure 2.6. **Representation of the asymmetric units of *rac*–1–H1 and *enant*–1–H5 pimobendan showing hydrogen bonds.**

In both crystal structures there are the same $C_1^1(11)$ chains present as in pimobendan *rac*–**1**–A and *enant*–**1**–F (see Figure 2.4.). Furthermore, the remaining unprotonated nitrogen atom of the benzimidazole moiety (N5) similarly is linked to the protonated nitrogen atom of the pyridazinone cycle (N2), however, not *via* a direct hydrogen bond, but *via* water molecule bridges. In *rac*–**1**–H1 therefore (similarly to *rac*–**1**–A) centrosymmetric rings form (two water-linked pimobendan molecules form $R_4^4(20)$ rings). In *enant*–**1**–H5 no rings are present, as for every pimobendan molecule the water bridges link two different pimobendan molecules. There are isostructural layers present in both structures parallel to (004). In *rac*–**1**–H1 alternating R/S layers are stacked together, while in *enant*–**1**–H5 every second layer is a mirror image of that in *rac*–**1**–H1 (see Figure 2.7.).

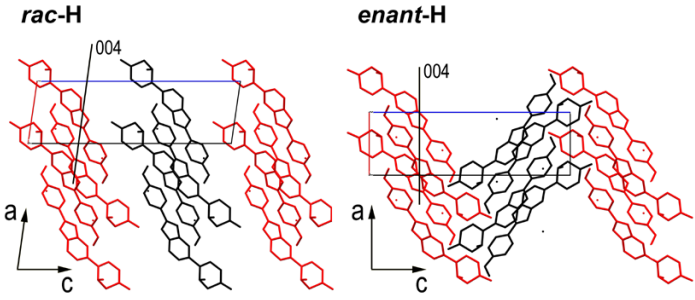

Figure 2.7. **Molecular packing representation of *rac*–1–H1 and *enant*–1–H5 pimobendan viewed along the crystallographic *b*-axis (red coloured moieties are isostructural, the black ones are mirror images).**

Of all four determined structures clear structural origin of solid solution existence is found only in *rac*–**1**–A (superimposition of two conformers as typical

for Type II (see Figure 1.2.)). However, PXRD and TG/DSC analysis have shown that the remaining three structures are also enantiopure or racemic limiting cases of solid solutions. For both enantiopure structures there are no *quasi*–centrosymmetry present typical for Type II, moreover, as $Z'=1$, it follows that no partial enantiomer recognition can be present and solid solutions **1**–F (**1**–ζ) and **1**–H5 are of Type I. Solid solution **1**–H1 rather represent a Type II solid solution with completely ordered structure at the racemic composition (see Figure 1.2.), or experimentally inaccessible disorder in a minor extent might as well be present. It must be mentioned that during a conventional SCXRD analysis site occupancy factors of, *e.g.*, carbon atoms below 10% is hard to refine as the electron density to detect in that case is small (roughly the same as of hydrogen atoms).

The surprising count of solid solutions found for pimobendan leads to conclude that in this case the structural aspects of their formation can be tracked down to the molecular level. As the chiral centre is fixed in a heterocycle with the remaining two substituents being a hydrogen atom and a methyl group, it is assumed that the lack of enantiomer recognition occurrs as follows: the changes introduced by placing one or another enantiomer in a crystallographic molecular position are not crucial, because in terms of intermolecular interactions: 1) no steric effect hindrance is expected because of comparable sizes of the non-ring chiral centre substituents; 2) only the dispersion energy term is affected by the change, which obviously has a minor importance determining the lattice energy as an efficient hydrogen bond network can be expected. The mentioned reasons are in agreement with the determined crystal structures.

2.2. SOLID SOLUTIONS OF PHENYLPIRACETAM (2) ENANTIOMERS

Investigation of racemic and enantiomerically pure phenylpiracetam (**2**) reveals that the racemic mixture crystallizes in one form (*rac*–**2**–A), however, two different crystal forms *enant*–**2**–A and *enant*–**2**–B can be obtained for an enantiomerically pure sample. PXRD patterns of all three crystalline phases are given in Figure 2.8.

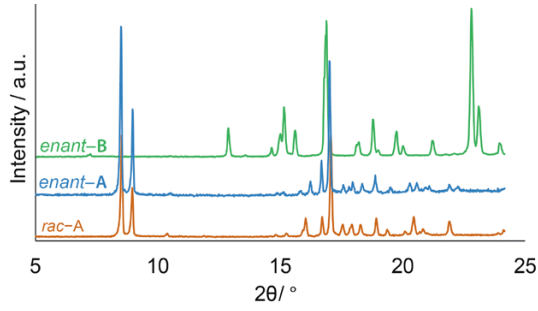

Figure 2.8. **PXRD patterns of racemic and enantiomerically pure phenylpiracetam (2) crystalline phases.**

Nearly identical PXRD patterns of *rac*–**2**–A and *enant*–**2**–A indicate very

high structural similarity of those crystalline phases and yet, because of noticeable differences, conglomerate formation is disregarded in this case. Therefore, it is suggested and further confirmed by the phase diagram that both phases are extreme cases of a solid solution. The DSC study (Figure 2.9.) shows that the melting of *enant*–**2**–A is accompanied by a subsequent crystallization of *enant*–**2**–B, which is observed as an exothermic peak.

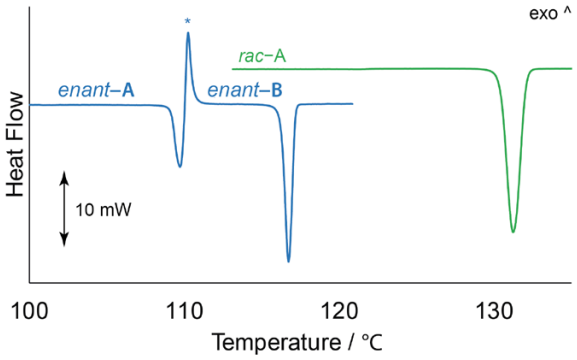

Figure 2.9. **DSC curves of phenylpiracetam (2) crystal forms (crystallization event marked with an asterisk).**

Melting points and enthalpies of melting are listed in Table 2.1. Melting enthalpy of *enant*–**2**–A was calculated taking into account that the overlapping exothermic peak must be of the same area as the peak of *enant*–**2**–B melting.

Table 2.1. **Melting points and enthalpies of melting of phenylpiracetam crystal forms**

Form	Melting point / °C	ΔH^f / kJ·mol^{-1}
rac–**2**–A	130.4	30.0(3)
enant–**2**–A	109.2	25.1(6)
enant–**2**–B	116.3	22.4(3)

As there are two single component phases (*enant*–**2**–A and *enant*–**2**–B) in the scope of studied system, the question arises, whether there is a monotropic or an enantiotropic relationship between them. This was determined using the heat of fusion rule[33] and also confirmed *via* slurrying experiments founding that *enant*–**2**–A and *enant*–**2**–B are enantiotropically related. The transition point was determined based on a purely thermodynamic approach by calculating the Gibbs free energy difference of *enant*–**2**–A and *enant*–**2**–B as a function of temperature using isobaric heat capacity measurements and the determined melting temperatures and enthalpies of melting. The transition point for *enant*–**2**–A and *enant*–**2**–B transition is 70(7) °C.

To clearly identify that *enant*–**2**–A and *rac*–**2**–A are limiting cases of a solid solution (**2**–$\alpha_{x=0}$ and **2**–$\alpha_{x=0.5}$, respectively), the melting behaviour of samples

with different composition was studied and the melt phase diagram was constructed (Figure 2.10.). Furthermore, it was found that also *enant*–**2**–B is a limiting case of another solid solution **2**–$\beta_{x=0}$). There is a relatively narrow miscibility gap of phenylpiracetam enantiomer solid solutions **2**–α and **2**–β. Close to the eutectic temperature the biphasic region exists in enantiomeric composition range between 2 and 9%. This is because there is a large difference in melting points of the racemic composition phase and the enantiomerically pure phenylpiracetam *enant*–**2**–B. Therefore, it follows that the liquidus lines intersect far from the racemic composition. The eutectic invariant is observed at 114.4 °C and around enantiomeric composition 3:97. Due to the narrow miscibility gap and the position of the eutectic point it is not possible to determine the eutectic composition more accurately using the Tamman plot.

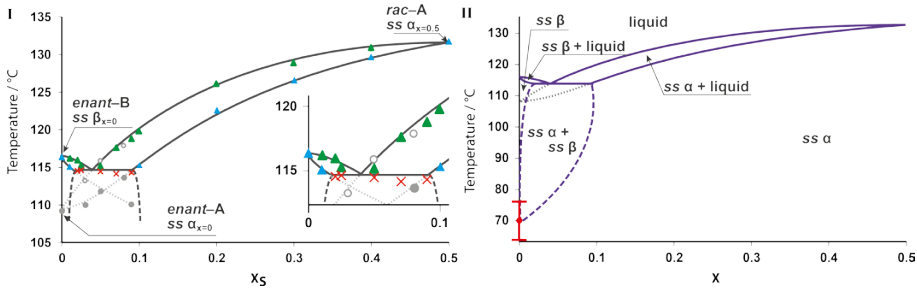

Figure 2.10. **Two component phase diagram of the phenylpiracetam enantiomer system. I: Showing experimental data points from DSC measurements (green triangles – liquidus of the stable equilibrium, blue triangles – solidus of the stable equilibrium, red crosses – eutectics, grey open circles – liquidus of the metastable equilibrium, grey circles – solidus of the metastable equilibrium; the lines are guides for the eyes). II: Proposed general shape of the phase diagram taking into account the enantiotropic transition (red circle – transition temperature).**

The metastable equilibrium of solid solution **2**–α can also be observed. As the enantiotropic relationship holds, samples where the mole fraction of the opposite enantiomer is below 0.1 (metastable region of **2**–α) crystallized at room temperature show absence of the eutectic melting. Continuation of the solidus and liquidus of the solid solution **2**–α reaching single enantiomer composition is therefore easily experimentally accessible. At temperatures below the enantiotropic phase transition point phenylpiracetam enantiomers show complete miscibility in the solid state. Existence of the solid solution **2**–β may seem arguable as it is shown to exist in such a narrow composition region, however, **2**–β with a metastable composition can be accessed experimentally by seeding melts of different enantiomer compositions with *enant*–**2**–B.

To explore the structural aspects of solid solutions formed by the phenylpiracetam enantiomers structures of *enant*–**2**–A, *enant*–**2**–B, and *rac*–**2**–A were determined. *Enant*–**2**–A crystallizes in the triclinic crystal system *P*1 space

group (Z=4, Z'=4), while *enant*–**2**–B crystallizes in the orthorhombic crystal system $P2_12_12_1$ space group (Z=8, Z'=2). Both space groups as restricted by chemical composition are Sohncke space groups[20]. However, ignoring the positions of chiral carbons and a few surrounding atoms in the unit cell, both enantiomerically pure structures possess higher symmetry resulting in description of *enant*–**2**–A and *enant*–**2**–B structures with centrosymmetric space groups $P\bar{1}$ and *Pbca*, respectively. The respective apparent space groups are supergroups of the former ones[34]. *Quasi*–centrosymmetry is ensured by asymmetric units (Figure 2.11. I) containing even number of molecules related by pseudoinversion centre.

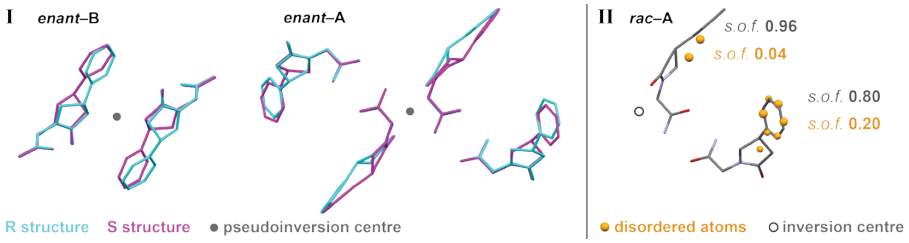

Figure 2.11. **I: Superimposition of the asymmetric units of the enantiomorphic structures of *enant*–2–B (Z'=2) and *enant*–2–A (Z'=4). II: Asymmetric unit of *rac*–2–A (Z'=2) showing disorder.**

Obviously, conformations of the molecules in these pairs differ – one of the conformers is mimicking the opposite enantiomer of the former conformer (pay attention to the overlay of the structures of opposite chirality). Furthermore, the structures of *enant*–**2**–A and *rac*–**2**–A are isostructural and represent limiting cases of solid solution α as **2**–$\alpha_{x=0}$ and **2**–$\alpha_{x=0.5}$, respectively. The space groups of the corresponding structures are $P1$ and $P\bar{1}$, the asymmetric unit of *rac*–**2**–A is therefore half of that of *enant*–**2**–A and shows disorder around the chiral carbon (Figure 2.11. II). All four conformers found in the enantiomerically pure structure (*enant*–**2**–A) are present in the racemic one (*rac*–**2**–A). The observed conformer abundance must be related to energetic reasons.

The crystal structures of solid solutions **2**–α and **2**–β are very different. In both cases each phenylpiracetam molecule forms 4 hydrogen bonds, however, the structures possess very different molecular packings. In *enant*–**2**–A there are two types of simple NH···O dimer synthons present (see Figure 2.12.). The synthons are *quasi*–centrosymmetric. Consequently, chains linked with hydrogen bonding motifs represented by $R_2^2(14)$ and $R_2^2(8)$ graph sets are observed.

Different hydrogen bonding motifs represented by $C_1^1(4)$ and $C_1^1(7)$ graph sets have formed in *enant*–**2**–B, (Figure 2.12.) resulting in formation of layers. *Quasi*–centrosymmetry is present between the molecules of two adjacent layers instead of hydrogen-bonded molecules like in *enant*–**2**–A.

Therefore, the overall structures of phenylpiracetam crystal forms can be considered to be built by packing together chains in case of **2**–α and layers in case of **2**–β. The chains and layers are held together *via* dispersion interactions. It is worth to notice that the substituents of the chiral carbons are not directly involved

in the hydrogen bond network which therefore can be preserved if the configuration of the molecule is inverted.

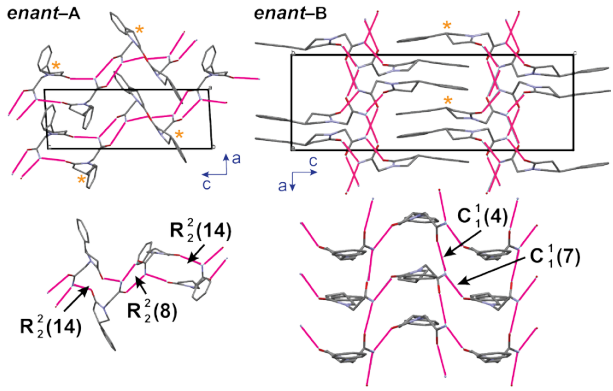

Figure 2.12. **Packing representation and hydrogen bonding motifs of *enant*–2–A and *enant*–2–B structures (chiral centres marked with an asterisk).**

Furthermore, the inversion would rather affect dispersion interactions, which are significantly less directional and therefore probably would result in only minor changes in the lattice energy. It can be concluded that in the case of phenylpiracetam the ability to preserve an efficient hydrogen bonding network and limited changes introduced to the overall lattice energy are the energetic reasons for the lack of recognition of the enantiomers in the solid state.

2.3. SOLID SOLUTIONS OF NAPHTHALIMIDE DERIVATIVE (3) ENANTIOMERS

The study of **3a**[32] has shown that all the structural prerequisites for Type II solid solution existence in a full composition range are present (see Figure 2.13.).

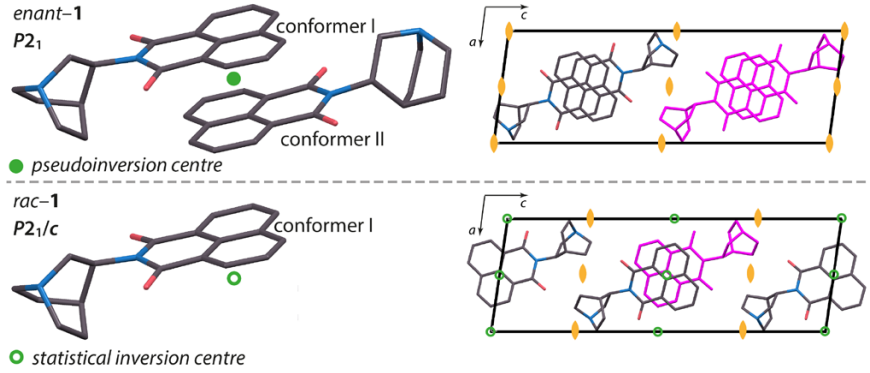

Figure 2.13. **Asymmetric units (left) and packing representation (right, asymmetric units coloured in magenta) of *enant*–3a and *rac*–3a (hydrogen atoms omitted and disorder of the racemic structure not shown at this point for the sake of clarity).**

The intermolecular interactions were analysed in the crystal structures of *rac*–**3a** and *enant*–**3a** to further explore similarities and differences of those structures. Fingerprint plots of the Hirshfeld surfaces are given in the Figure 2.14. The general shape of all three fingerprint plots is very similar since the packings are isostructural and the conformations do not differ much. Furthermore, no significant differences are observed in the plots of conformers I, however, they are not completely identical as the Hirshfeld surface is solely a property in the context of a crystal structure, thus being dependent on the environment around the molecule of interest.

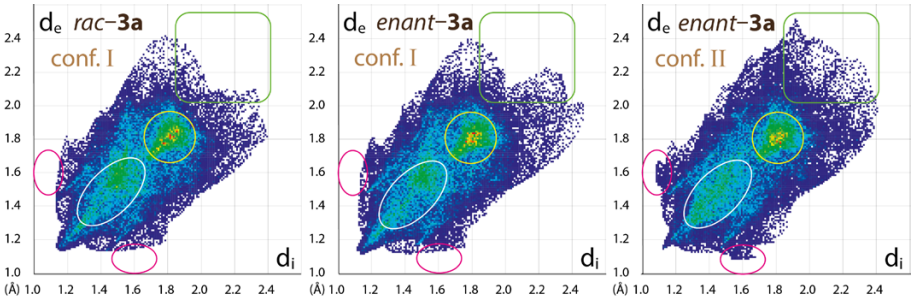

Figure 2.14. **Fingerprint plots of the Hirshfeld surfaces of symmetrically independent molecules in the crystal structures of *rac*–3a and *enant*–3a.**

Most characteristic contacts of all three molecules are C···C contacts (corresponding to π···π stacking of the naphthalene moieties) denoted with a yellow circle. The regions are very similar indicating that conformational (hence molecule configuration) differences do not affect these contacts. No significant differences of the minor O···H contacts are observed (see pairs of the light blue stripes between the depicted ellipses characteristic for the respective contacts). Additional contact density appears in the fingerprint plot of conformer II (compare the ellipses in magenta). Those contacts correspond to N···H and H···H interactions arising from a different position of the quinuclidine moiety. The region denoted with a white ellipse (H···H contacts) differs for conformer II in a way that it is approximately equally dense in the whole area, on contrary in the plots of conformer I the contact density is more concentrated in the upper part of the given range in the ellipse. Thus, in case of *enant*–**3a** there is a larger number of short H···H contacts present (compared to those in *rac*–**3a**) originating from the molecules of conformer II. Finally, the region depicted in the rounded rectangle in green shows that in the case of conformer II there are some contacts present in the structure of *enant*–**3a** being relatively long. That indicates for the existence of a space in the unit cell, which is not as efficiently packed as in the structure of *rac*–**3a**.

To explore the energetic aspects of crystal packings, lattice energies were calculated for *rac*–**3a** and *enant*–**3a**. The lattice energy values and their breakdown are summarized in Table 2.2. The main stabilizing forces in both crystal structures are dispersion interactions arising from efficient π···π stacking of naphthalene moieties.

Table 2.2. **Lattice energy values and their components of the crystal structures of *rac*–3a and *enant*–3a**

	$E_{Coulombic}$	E_{Pol}	E_{Disp}	E_{Rep}	E_{Tot}
rac–**3a**	−35.1	−18.5	−174.3	98.9	−129.0
enant–**3a**	−36.6	−19.9	−177.4	106.9	−127.2

As there are no hydrogen bonds present and no ions are involved, the Coulombic interactions are of a minor importance in determining the stability of the lattices. The energy stabilizing terms are roughly the same in both cases, however, the repulsion energy terms are considerably different (8 kJ·mol^{-1} difference). When identical packings and the same molecules comprising the crystal structures are considered, the higher repulsion energy term can be associated with atoms of the neighbouring molecules being inefficiently too close to each other. It is compatible with the analysis of the Hirshfeld surfaces showing that conformer II has higher contact density at lower d_e and d_i values (see the ellipses in white and magenta in the Figure 2.14.) corresponding to N···H and H···H contacts.

To prove that there is a lack of enantiomer recognition in the solid state the structures were determined also for scalemic crystals. For scalemic crystals disorder of only one of the molecular sites in the asymmetric units is present, furthermore, the disordered site corresponds to conformer II. Intermolecular interaction analysis already showed that the conformer II is not favoured in the overall crystal structure. It is therefore comprehensible that those sites would be occupied by conformer I, if possible. The crystallographic data indeed show that when the opposite enantiomer is introduced into the enantiopure structure it adopts conformation I and therefore substitutes conformer II molecules. As a result as many as possible genuine centrosymmetric pairs SI–RI are formed in the structures. It would be expected that racemic crystals only contain molecules occupying conformation I giving a genuine racemic compound. However, the asymmetric unit of *rac*–**3a** contains one molecule, which is in fact disordered occupying conformation I and II. As found in three different single crystals the conformer ratio (I:II) varies – 85:15, 87:13, and 90:10. Asymmetric units and conformer abundance as a function of enantiomeric composition is depicted in Figure 2.15.

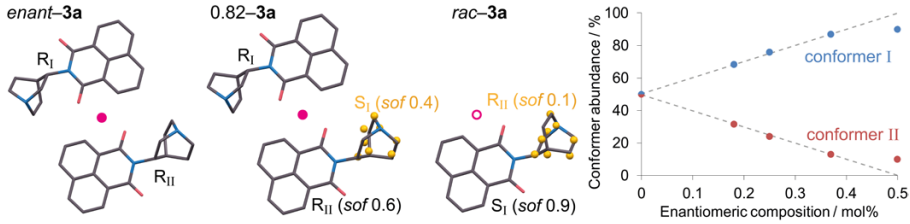

Figure 2.15. **Asymmetric units of studied solid solutions of 3a (hydrogen atoms omitted for the sake of clarity) and conformer abundance in the crystal structure as a function of enantiomeric composition.**

Deviation of the conformer abundance from a straight line may be explained by the contribution of the configurational entropy, as it has been shown that Boltzmann statistics can be applied, when explaining the disorder in molecular crystals[35].

In the case of the bromine substituted compound (**3b**) no reliable structure determination was possible. The PXRD patterns of different enantiomeric composition samples are nearly identical with only minor differences of some peak positions and intensities (see Figure 2.16.) which is typical in case of solid solutions.

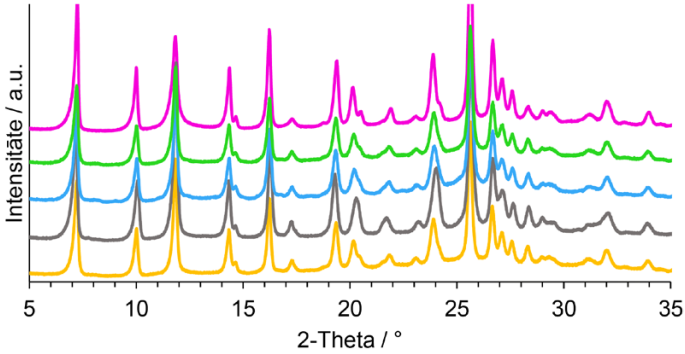

Figure 2.16. **PXRD patterns of different enantiomeric composition samples of 3b (from bottom to top: enantiopure, 0.80, 0.75, 0.60, racemic).**

Unfortunately, due to compound degradation prior to melting it was not possible to construct a melt phase diagram for the system of interest, which would prove solid solution existence from a thermodynamic point of view. However, the PXRD data convincingly suggest that the compound **3b** forms solid solutions in the whole composition range.

Compounds *enant*–**3c** and *rac*–**3c** were found to crystallize in $P2_12_12_1$ space group (Z=8, Z'=2) and *Pccn* space group (Z=8, Z'=1), respectively. In the enantiopure structure there is a *quasi*-centrosymmetry present indicating existence of solid solutions. However, the space groups $P2_12_12_1$ and *Pccn* are not in a direct group-subgroup relation, thus, no continuous miscibility of the enantiomers in the solid state is possible. Study of the scalemic structures revealed that instead two distinct solid solutions form – around the racemic and the enantiopure composition region as 0.86 and 0.70 enantiomeric composition sample structures were isostructural to that of *enant*–**3c**, but 0.58 composition sample was isostructural to that of *rac*–**3c**. Nevertheless, both solid solutions have identical structural constructs in common, namely, π···π stacked blocks (see Figure 2.17.).

Both structures in general differ by the shift between the adjacent blocks – 1/4 shift of the cell edge in the enantiopure structure and 1/2 in the racemic one (see the rounded rectangles in Figure 2.17.). It apparently indicates that a crystal structure is more stable if [1.0;0.70) enantiomer composition blocks are packed with 1/4 shift and (0.58;0.50] composition ones – with 1/2 shift.

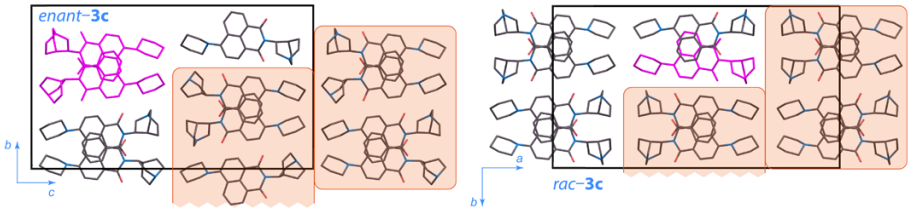

Figure 2.17. **Structures of *enant*–3c and *rac*–3c (asymmetric units coloured in magenta).**

Unlike in case of *rac*–**3a**, no disorder of the asymmetric unit of *rac*–**3c** could be successfully refined. Although, there was some electron density in the positions corresponding to the atoms belonging to conformer II, the final structure model was better without any disorder. No strong statement thus can be made that the racemic crystal is indeed completely ordered (corresponding to a genuine racemic compound) as there could be conformer II present in the crystal structure. Those findings illustrate that the original definition of Type II solid solutions by Chion *et al.* dealing with cases giving complete ordered racemic structure should be revised as the extent of the disorder at the racemic composition, in fact, has been shown to vary from compound to compound, meanwhile, the enantioselectivity of the crystallographic molecular positions is undeniably present (contrary to Type I). The extent of disorder might originate from a manner of crystal growth, specifically: are there any kinetic effects, like molecule pre-association in the solution, preserved in the crystal structure, or, on contrary, the crystal may represent the thermodynamically equilibrated state. In the latter case the disorder originates due to the configuration entropy as local equienergic structure models with a different occurence probability result in an averagely disordered structure.

Concerning the structural similarities of both solid solutions of **3c**, it was intriguing to explore the energetic aspects of their formation. Lattice energy calculations were performed to shed a light on the aspects governing the reasons of differently shifted blocks in the experimental crystal structures.

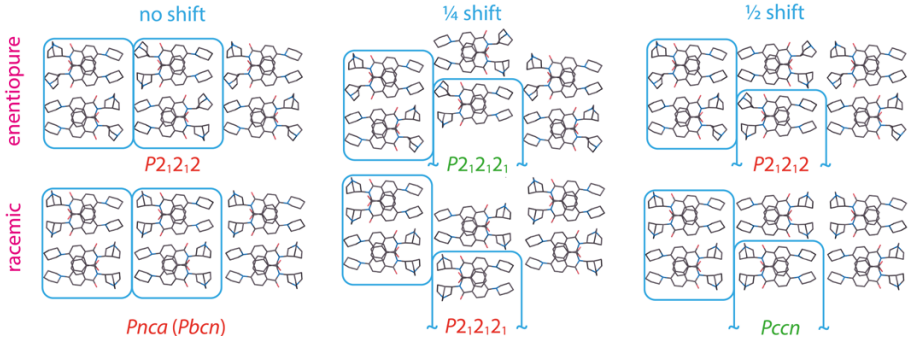

Figure 2.18. **Experimental (space groups in green) and hypothetical (space groups in red) structures of compound 3c.**

As lattice energy calculations cannot be directly carried out on disordered structures, only ordered phases were considered – enantiopure and racemic structures. Furthermore, hypothetical but similar structures than those obtained experimentally (with different shifts of the blocks and blocks being either enantiopure of racemic) were also construed. In Figure 2.18. all the variations of the structures are shown.

The racemic structures were generated either with conformer I or conformer II in the asymmetric unit. The lattice energy values (and their breakdown) of the relaxed structures are shown in Table 2.3. The lattice energy calculations show that the most favourable packings are formed when racemic blocks are packed with 1/2 shift and enantiopure ones with 1/4 shift, which corresponds to experimentally obtained structures. It can also be seen that unlike in racemic case the enantiopure structure with 1/2 shift is less stable than 1/4 shift phase, which is mostly due to less efficient dispersion and Coulombic interactions.

Table 2.3. **Lattice energy values and their components (kJ·mol^{-1}) of the experimental and hypothetical crystal structures of *rac*–3c and *enant*–3c**

	Struct.	Shift	$E_{Coulombic}$	E_{Pol}	E_{Disp}	E_{Rep}	E_{Tot}
rac	*Pccn* I *	1/2	−96.1	−51.8	−286.8	286.2	−148.5
	$P2_12_12_1$ †	1/4	−100.2	−56.4	−295.2	311.6	−140.1
	Pccn II	1/2	−92.1	−54.0	−278.7	286.4	−138.4
	Pnca I	0	−90.6	−48.7	−269.9	271.2	−138.0
	Pnca II	0	−98.9	−56.4	−293.8	312.1	−137.1
enant	$P2_12_12_1$ *	1/4	−97.3	−50.6	−288.6	291.0	−145.6
	$P2_12_12$	1/2	−94.5	−50.7	−281.6	286.0	−140.8
	$P2_12_12$	0			§		

* – experimental structures; † – distinction between the conformers I and II lost upon the relaxation of the structure, § – in case of the enantiopure hypothetical structure $P2_12_12$ with no shift between the layers the relaxation of the atomic positions lead to a $P1$ structure with Z'=8 (resembling $P2_12_12$ packing but not possessing complete symmetry).

For the racemic composition, however, the 1/4 shift phase loses to the 1/2 shift phase due to far more inefficient repulsion energy term, although the lattice energy stabilising terms are in fact lower than those of the 1/2 shift phase. The lattice energy calculations are consistent with the experimentally determined structures. Furthermore, the calculations explain why two structurally distinct solid solutions form – one around the racemic composition and the other one near the enantiopure composition region.

CONCLUSIONS

1. Formation of the solid solutions of the studied compound enantiomers is possible due to the substituents of the chiral carbon not being directly involved in the interactions stabilizing the crystal structure. In case of pimobendan and phenylpiracetam the hydrogen bond network is preserved in the respective structures regardless of the configuration of the chiral carbon; in the structures of the studied naphthalimide derivatives non-stereospecific π···π interactions determine the stability of the corresponding crystal forms.

2. Pimobendan enantiomers appear to be hardly distinguishable in the solid state as, in addition to the chiral carbon substituents not being hydrogen bond donors nor acceptors, the chiral carbon is fixed in a heterocycle with the remaining substituents being a hydrogen atom and a methyl group, which are small, thus, minimizing possible steric and thus energetic disturbance of the neighbouring molecules.

3. It is not yet fully understood, why in most of the studied cases distinct solid solutions form near the enantiopure and around the racemic composition. The pimobendan case in particular rises questions for further research as none of the solid solutions is continuous, but instead different solid solution structures form near and around the enantiopure and racemic compositions, respectively. It indicates that there is a discrimination of close-to-limiting composition systems, although the large variety of solid solutions in this system is primarily associated with the minor differences of the molecular structures of both enantiomers.

4. Unlike stated in the original definition by Chion *et al.*, thus resulting in wrong classification of enantiomer solid solutions in some literature sources, the Type II solid solutions (showing structural enantioselectivity) must not necessarily be completely ordered at the racemic composition. The extent of the disorder should be related to the configuration entropy or kinetic aspects during the crystal growth.

5. Four out of six determined crystal structures of specifically enantiopure limiting cases of solid solutions only formally crystallize in Sohncke space groups, as apparent centrosymmetry is present resulting in description of the structures with the corresponding centrosymmetric supergroups, if a few atoms are ommited. This indicates that the preference of centrosymmetry in molecular crystals is indeed prevailing and also suggests the underlying reason for spontaneous formation of stable racemic compounds

in such a vast majority (90%).

6. Structural study on scalemic crystals of three different Type II solid solutions reveals that genuinely centrosymmetric pairs in scalemic composition crystals are strongly preferred over the *quasi*–centrosymmetric pairs, which are rather formed due to a compromise between the composition given and the target crystal structure. Thus, this is the origin of the enantioselectivity of the crystallographic molecular positions. In one of the cases the analysis of the intermolecular interactions showed in particular that the *quasi*–centrosymmetric enantiopure structure possesses both slightly more ineffective packing and ineffective close contacts compared to genuinely centrosymmetric racemic structure, however, it is formed at the expense of the increase of the lattice energy, which is determined mainly by efficient dispersion interactions.

7. The study shows that taking into account the structural aspects of solid solutions (conformational freedom of the molecule; non-specificity of the intermolecular interactions of the chiral centre substituents; etc.) it is possible to intentionally design molecules that form such solid solutions.

REFERENCES

1. Carey, F. A.; Sundberg, R. J. *Advanced Organic Chemistry* **2007**, Springer.
2. Rouhi, A. M. *Chem. Eng. News* **2003**, *81*, 45–61.
3. Guo-Qiang, L.; Qi-Dong, Y.; Jie-Fei, C. *Chiral Drugs* **2011**, John Wiley & Sons.
4. Lorenz, H.; Seidel-Morgenstern, *A. Angew. Chemie Int. Ed.* **2014**, *53*, 1218–1250.
5. Sato, O. *Nat. Chem.* **2016**, *8*, 644–656.
6. Jacques, J.; Collet, A.; Wilen, S. H. *Enantiomers, racemates, and resolutions* **1981**, Wiley.
7. Vogt, F. G.; Copley, R. C. B.; Mueller, R. L.; Spoors, G. P.; Cacchio, T. N.; Carlton, R. A.; Katrincic, L. M.; Kennady, J. M.; Parsons, S.; Chetina, O. V. *Cryst. Growth Des.* **2010**, *10*, 2713–2733.
8. Bredikhin, A. A.; Bredikhina, Z. A.; Zakharychev, D. V.; Gubaidullin, A. T.; Fayzullin, R. R. *CrystEngComm* **2012**, *14*, 648–655.
9. Esteves de Castro, R.; Canotilho, J.; Barbosa, R. M.; Silva, M. R.; Beja, A. M.; Paixão, J. A.; Redinha, J. S. *Cryst. Growth Des.* **2007**, *7*, 496–500.
10. de Diego, H. L., Bond, A. D.; Dancer, R. J. *Chirality* **2011**, 23, 408–416.
11. Huang, J.; Chen, S.; Guzei, I. A.; Yu, L. *J. Am. Chem. Soc.* **2006**, *128*, 11985–11992.
12. Chion, B.; Lajzerowicz, J.; Bordeaux, D.; Collet, A.; Jacques, J. *J. Phys. Chem.* **1978**, *82*, 2682–2688.
13. Kitaigorodsky, A. I. *Mixed Crystals* **1984**, Springer.
14. Kaemmerer, H.; Lorenz, H.; Black, S. N.; Seidel-Morgenstern, A. *Cryst. Growth Des.* **2009**, *9*, 1851–1862.
15. Taratin, N. V.; Lorenz, H.; Kotelnikova, E. N.; Glikin, A. E.; Galland, A.; Dupray, V.; Coquerel, G.; Seidel-Morgenstern, A. *Cryst. Growth Des.* **2012**, *12*, 5882–5888.
16. Wermester, N.; Aubin, E.; Pauchet, M.; Coste, S.; Coquerel, G. *Tetrahedron: Asymmetr.* **2007**, *18*, 821–831.
17. Bredikhin, A. A.; Bredikhina, Z. A.; Zakharychev, D. V. *Mendeleev Commun.* **2012**, *22*, 171–180.
18. Gallis, H. E.; Bougrioua, F.; Oonk, H. A. J.; van Ekeren, P. J.; van Miltenburg, J. C. *Thermochim. Acta* **1996**, *274*, 231–242.
19. Oonk, H. A. J.; Tjoa, K. H.; Brants, F. E.; Kroon, J. *Thermochim. Acta* **1977**, *19*, 161–171.
20. Flack, H. D. *Helv. Chim. Acta* **2003**, *86*, 905–921.

21. Gordon, S. G.; Miller, M. W.; Saunders, A. B. *J. Am. Anim. Hosp. Assoc.* **2006**, *42*, 90–93.
22. Chu, K. M.; Shieh, S. M.; Hu, O. Y. Clin. *Pharmacol. Ther.* **1995**, *57*, 610–621.
23. Bell, E. T.; Devi, J. L.; Chiu, S.; Zahra, P.; Whittem, T. J. *Vet. Pharmacol. Ther.* **2015**, *38*, 1–8.
24. Boeren, M. M. M.; Paridaans, R. J.; Petkune, S.; Lusis, V.; Muceniece, D. *Crystalline pimobendan, process for the preparation thereof, pharmaceutical composition and use* European Patent, **2014**.
25. Zvirgzdins, A.; Delina, M.; Mishnev, A.; Actins, A. *Acta Crystallogr. Sect. E Struct. Reports Online* **2013**, *69*, 1677–1677.
26. Malykh, A. G.; Sadaie, M. R. *Drugs* **2010**, *70*, 287–312.
27. Zvejniece, L. Svalbe, B.; Veinberg, G.; Grinberga, S.; Vorona, M.; Kalvinsh, I.; Dambrova, M. *Basic Clin. Pharmacol. Toxicol.* **2011**, *109*, 407–412.
28. Veinberg, G.; Vavers, E.; Orlova, N.; Kuznecovs, J.; Domracheva, I.; Vorona, M.; Zvejniece, L.; Dambrova, M. *Chem. Heterocycl. Compd.* **2015**, *51*, 601–606.
29. Merz Pharma GmbH & Co. KGaA. *Use of (R)-phenylpiracetam for the treatment of sleep disorders* European Patent, **2015**.
30. Zvejniece, L.; Svalbe, B.; Vavers, E; Makrecka-Kuka, M.; Makarova, E.; Liepins, V.; Kalvinsh, I.; Liepinsh, E.; Dambrova M. *Pharmacol. Biochem. Behav.* **2017**, *160*, 21–29.
31. Ksenafontov, D. N.; Moiseeva, N. F.; Rykov, A. N.; Shishkov, I. F.; Oberhammer, H. *Struct. Chem.* **2013**, *24*, 171–179.
32. d'Agostino, S.; Braga, D.; Grepioni, F.; Taddei, P. *Cryst. Growth Des.* **2014**, *14*, 821–829.
33. Hilfiker, R. *Polymorphism: In the Pharmaceutical Industry* **2006**, Wiley.
34. Ivantchev, S.; Kroumova, E.; Madariaga, G.; Pérez-Mato, J. M.; Aroyo, M. I. *J. Appl. Crystallogr.* **2000**, *33*, 1190–1191.
35. Teteruk, J. L.; Glinnemann J.; Heyse W.; Johansson K. E.; van de Streek J.; Schmidt M. U. *Acta Crystallogr. Sect. B Struct. Sci. Cryst. Eng. Mater.* **2016**, *72*, 416–433.

PIELIKUMI / APPENDICES

I

Rekis, T.; Bērziņš, A.; Sarceviča, I.; Kons, A.;
Balodis, M.; Orola, L.; Lorenz, H.; Actiņš, A.

A maze of solid solutions of pimobendan enantiomers: an extraordinary case of polymorph and solvate diversity

Cryst. Growth Des. **2018**, 18(1), 264–273

CRYSTAL GROWTH & DESIGN

Article

Cite This: *Cryst. Growth Des.* 2018, 18, 264−273

pubs.acs.org/crystal

A Maze of Solid Solutions of Pimobendan Enantiomers: An Extraordinary Case of Polymorph and Solvate Diversity

Toms Rekis,[*,†,‡] Agris Bērziņš,[†] Inese Sarceviča,[†] Artis Kons,[†] Mārtiņš Balodis,[†,§] Līāna Orola,[†] Heike Lorenz,[‡] and Andris Actiņš[†]

[†]Department of Physical Chemistry, University of Latvia, Riga, Latvia

[‡]Max Planck Institute for Dynamics of Complex Technical Systems, Magdeburg, Germany

[§]Ecole polytechnique fédérale de Lausanne, Lausanne, Switzerland

Supporting Information

ABSTRACT: Over 10 polymorphs and solvatomorphs of the chiral pharmaceutically active ingredient pimobendan were found to lack enantioselectivity in the solid state, accordingly, forming solid solutions of enantiomers, which is reported to be a rare phenomenon. Solid form screening was performed on different enantiomeric composition samples to analyze obtained phases with powder X-ray diffraction and thermogravimetric differential scanning calorimetry. For nonsolvated forms, a melt phase diagram has been constructed convincingly showing the existence of stable and metastable solid solutions near the pure enantiomer and around the racemic composition regions. A crystal structure study combined with solid-state NMR experiments was performed to analyze and explain structural aspects of pimobendan solid solutions. Furthermore, the driving force for the existence of such a surprisingly large amount of different solid state phases lacking enantioselectivity for a single compound is elucidated tracking down the origin of their formation to the molecular level.

INTRODUCTION

Chirality plays a significant role in many divisions of science. It is particularly important in pharmacy, agrochemistry, and food industry where occasionally a single molecule with a specific configuration is desired over a mixture of enantiomers or diastereomers.[1] Therefore, an increasing number of studies have been conducted to investigate the routes for obtaining a single enantiomer.[2] Besides enantioselective synthesis, a set of physicochemical methods are extensively used for the separation of enantiomers which involve solid crystalline phases of the compound of interest.[2,3] Understanding the enantioselectivity in the solid state is therefore crucial.

Usually chiral substances show very high enantioselectivity at the crystallization stage. More than 99% of racemic enantiomeric mixtures are reported to crystallize either forming racemic compounds or conglomerates,[3] where the former is a racemic crystalline phase with a strict order of both components, and the latter contains two crystalline (mirror) phases where each component has formed its own phase. Extremely rarely, however, single phases form where there is only partial or no recognition of the enantiomers in the solid state.[3−7] Consequently, scalemic compositions are able to form isostructural phases. Such solid solutions are an interesting phenomenon since it hides the answers of how the enantioselectivity is governed in the solid state.

From a structural point of view, two cases can be distinguished regarding enantioselectivity in the solid state: (1) complete lack of enantioselectivity (Type I); (2) partial enantioselectivity is present (Type II). Type I has been defined as follows: within a crystal containing x R molecules and $(1-x)$ S molecules the probability of finding an R molecule on a given site is proportional to x, and the probability of finding an S molecule is proportional to $(1-x)$.[8] Two compounds have been reported to belong to this case by the authors of the classification.[8,9] Furthermore, two mandelic acid derivatives[10,11] can be classified as Type I solid solutions as there is only one symmetrically independent site in the unit cells of the respective enantiopure structures. Consequently, no partial enantioselectivity is possible for that as at least two symmetrically independent sites are required in the enantiopure structures.[8] Type II in the present study is left for structures showing a certain degree of enantioselectivity which arises from reasonable structural aspects. The definition of Type II has been therefore slightly revised compared to that introduced decades ago in the pioneering study of structural aspects of solid solutions of enantiomers.[8] As it can be observed in several structures determined recently[6,12] for which partial enantioselectivity is evidently present, the structural aspects do not fully correspond to the given definition, which rather describes an idealized case of partially enantioselective solid solutions. For Type II solid solutions ($Z' \geq 2$), the asymmetric molecules in the enantiopure structures are typically *quasi*-centrosymmetri-

Received: August 28, 2017
Revised: November 6, 2017
Published: December 4, 2017

DOI: 10.1021/acs.cgd.7b01203
Cryst. Growth Des. 2018, 18, 264−273

cally related, which is achieved by different conformations of the molecules of the same handedness. In such cases a single enantiomer is forming a *quasi*-centrosymmetric structure. When the opposite enantiomer is introduced, genuine centrosymmetry can be achieved locally. At the racemic composition a true racemic compound (an ordered centrosymmetric structure) is possible; however, usually some degree of disorder is observed. Nevertheless, the racemic structure can be solved in a centrosymmetric supergroup of the Sohncke space group of the enantiopure structure. Consequently, the value of Z' is halved. These structural aspects are well illustrated with a phenylpiracetam solid solution example[6] where two pairs of *quasi*-centrosymmetric molecules are present in the enantiopure structure (see Figure 1). There is a pseudoinversion center

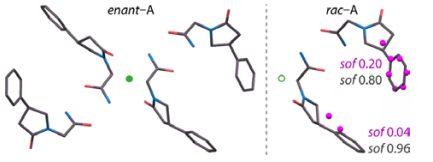

Figure 1. Asymmetric units of phenylpiracetam solid solution α limiting cases *enant*-A ($P1$, $Z' = 4$) and *rac*-A ($P\bar{1}$, $Z' = 2$)[6] showing disorder with corresponding site occupancy factor (sof) values given.

(depicted with a closed circle) in the enantiopure structure and a statistical inversion center in the racemic structure. For both asymmetric sites in the racemic structure, there is a probability of finding an R or S enantiomer of phenylpiracetam. This probability, however, is not 50%. One of the sites is nearly ordered showing disorder as low as 4%, and the other one is largely ordered. From the structure of racemic phenylpiracetam alone, it is evident that at a certain degree the enantiomers are recognized in the solid state. Several other compounds possessing exactly the same structural features and consequently having partial enantioselectivity are reported (tazofelone,[13] citalopram oxalate,[14] atenolol,[15] carvedilol phosphate,[16] timolol maleate,[17] and two naphthalimide derivatives[12]). Such structures correspond to Type II solid solutions.

In this study a chiral pharmaceutically active ingredient pimobendan (4,5-dihydro-6-[2-(*p*-metoxyphenyl)-5-benzimidazolyl]-5-methyl-3(2*H*)-pyridazinone) has been investigated. Pimobendan is used to treat heart failure either in veterinary or human medicine.[18,19] The chemical scheme of pimobendan is shown in Figure 2. In this study pimobendan is found to form a variety of polymorphs and solvates in its racemic and enantiopure form. Furthermore, it is an extraordinary case as more than 10 of the nonsolvated and solvated forms are proven to be solid solutions, while also the others are in fact not strictly classified as enantioselective.

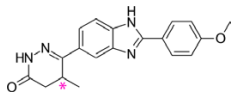

Figure 2. Chemical scheme of pimobendan (4,5-dihydro-6-[2-(*p*-metoxyphenyl)-5-benzimidazolyl]-5-methyl-3(2*H*)-pyridazinone).

The aim of this study was to present the known solid form diversity of racemic and enantiopure pimobendan, characterize the solid solutions of the compound, and finally track down the structural aspects responsible for the formation of such a large number of nonenantioselective crystalline phases.

EXPERIMENTAL METHODS

Materials. Racemic pimobendan (>99.8%) was supplied by JSC Grindeks (Riga, Latvia). Pure enantiomer of pimobendan was resolved from the racemic mixture by classical resolution using (−)−*O*,*O*′−dibenzoyl-L-tartric acid according to methods available in the patent literature.[20] The method was not further optimized; as a result the yield for the enantioseparation was as low as around 4%, similarly as given in the source. Purity (99.7% *ee*) was confirmed by chiral chromatography. (−)−*O*,*O*′-Dibenzoyl-L-tartric acid, phosphorus pentoxide, and aqueous ammonia were purchased from commercial sources. Solvents used in the study were HPLC grade or intended for organic synthesis with purity >99%. Water (<0.01 μS cm^{-1}) was deionized at the laboratory using ion-exchange resins.

Polymorph and Solvate Screening. Solid form screening was performed on racemic pimobendan by crystallizing from different solvents, desolvating solvates, exposing solid forms to solvent vapors, and annealing the amorphous form at elevated temperatures. Stoichiometry of solvates was elucidated based on repeated thermogravimetric (TG) studies. Detailed procedures for obtaining presented pimobendan crystal forms are given in the Supporting Information.

Extensive solid form screening of enantiopure pimobendan, however, was not performed, since it is not available on the market, and classical resolution of pimobendan enantiomers gave extremely low yields. However, a few forms have been obtained via crystallization from different solvents.

Single Crystals. Single crystals of pimobendan form *rac*-A were grown by slow evaporation of a dry acetonitrile and ethyl acetate solution (1:1 v/v) at room temperature in a P_2O_5 desiccator (to prevent the formation of the monohydrate due to air moisture) over the course of several months.

SCXRD. The data were collected at 293 K temperature on a Bruker Nonius Kappa CCD diffractometer using Mo−Kα radiation (graphite monochromator, wavelength of 0.710 73 Å) (Bruker, Germany). The structure was solved by direct methods and refined by full-matrix least-squares on F^2 for all data, using SHELX-2014 software suite.[21] The non-hydrogen atoms were refined anisotropically. As disorder was found, the site occupancy factors (sof) of atoms were refined using SHELX command PART and an additional free variable.

PXRD. PXRD patterns were determined on a Bruker D8 Advance diffractometer (Bruker, Germany) using copper radiation (Cu−Kα) at a wavelength of 1.541 80 Å equipped with a LynxEye position sensitive detector (Bruker, Germany). The tube voltage and current were set to 40 kV and 40 mA. The divergence slit was set at 0.6 mm, and the antiscattering slit was set at 8.0 mm. The diffraction pattern was recorded using a scanning speed of 0.2 s/0.02° from 3° to 35° on 2θ scale.

For indexation or structure determination PXRD patterns were recorded on a Bruker D8 Discover diffractometer (Bruker, Germany) using copper radiation (Cu−Kα) at a wavelength of 1.54180 Å equipped with a LynxEye (1D) detector in transmission mode. The tube voltage and current were set to 40 kV and 40 mA. The samples were loaded into special glass Nr. 10 capillaries (0.5 mm in diameter). Capillary spinner (60 rpm) was used to minimize instrumental and sample packing aberrations. An upper knife edge was used to reduce the background produced by air scattering and lower knife edge was used to block the primary beam. The diffractometer incident beam path was equipped with a Gbel mirror, Soller slit, and a 0.6 mm divergence slit, while the diffracted beam path was equipped only with Soller slit. The diffraction patterns were recorded on 2θ scale from 3° to 70° with 0.01° increments, using a scan speed of 36 s per step.

Structure Determination from PXRD Data. Indexing, space group determination, structure solution, and Rietveld refinement were

DOI: 10.1021/acs.cgd.7b01203
Cryst. Growth Des. 2018, 18, 264−273

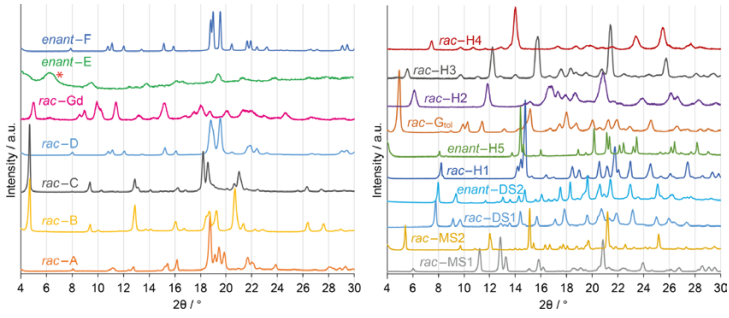

Figure 3. PXRD patterns of nonsolvated (left) and solvated (right) pimobendan crystal forms (* – the broad peak observed at 6.3 2θ for *enant*-E arises from the film of the variable temperature chamber).

performed using EXPO2014.[22] The unit cell dimensions were determined by applying the N-TREOR09[23] and Dicvol06[24] indexing procedures, with a set of 20–25 reflections found in the 3–30° 2θ range. Space group determination was carried out using a statistical assessment of systematic absences, and Z' was determined based on solid-state NMR (SSNMR) results. The cell and diffraction pattern profile parameters were refined according to the LeBail algorithm.[25] The background was modeled by a 20th order polynomial function of the Chebyshev type, and peak profiles were described by the Pearson VII function.

The initial geometry of molecules was taken from the crystal structure of *rac*-A. The Monte Carlo/simulating annealing technique was used to constantly adjust the conformation, position, and orientation of the trial model in the unit cell in order to maximize the agreement between calculated and measured diffraction data. The Rietveld refinement was carried out using soft constraints on bond distances and angles. In the Rietveld refinement, profile and cell parameters, isotropic thermal vibration, and preferred orientation parameters (using March-Dollase model[26,27]) were optimized to get the optimal crystal structure. The planar conjugated rings were separately treated as rigid bodies, whereas soft constraints on bond distances and angles were used. The final Rietveld refinement showed a good agreement between the observed and the calculated profiles.

After the Rietveld refinement, the atomic positions of the final structure were relaxed in Quantum ESPRESSO[28] using the PBE functional with ultrasoft pseudopotentials from the original pseudopotential library and a 44 Ry planewave cutoff energy with vdW interactions treated according to the D2 method of Grimme.[29] The parameters of convergence, pseudopotentials, and the *k*-point grid were used as suggested for structure optimizations of organic molecules.[30] The relaxed structure was compared to the refined one to check for the reliability of the structure solution. Atomic positions did not differ significantly. The experimental and calculated PXRD patterns including difference function and Bragg positions are given in Figure S14. Furthermore, an SSNMR spectrum of the refined structure was simulated (see below) and compared to that of the experimental one, obtaining a good correlation between the experimental and calculated chemical shifts.

Thermal Methods of Analysis. The TG/DSC curves were obtained using a TG/DSC STAR^e system (Mettler Toledo, Switzerland). A 5–10 mg sample was weighed on an open aluminum pan and heated at the rate of 5 to 10 K min^{-1} from 25 to 250 °C under a continuous nitrogen flow (100 mL min^{-1}).

The DSC curves were recorded on a SETARAM DSC 131 instrument (SETARAM Instrumentation, France) at the heating rate of 0.5 to 5 K min^{-1}. Temperature and enthalpy calibration was done using indium, tin, and lead reference materials. A 4–10 mg sample was weighed in an aluminum crucible and the crucible was crimped.

Melt Phase Diagram. The mixtures of different compositions were prepared by weighing racemic and enantiopure samples on an analytical balance (d = 0.1 mg). Different enantiomeric composition samples were then fully dissolved in acetonitrile/ethyl acetate (1:1 v/v) and crystallized in dry conditions. After complete evaporation of the solvent, the samples were homogenized in a mortar prior the DSC measurements. For the metastable solid solutions δ and γ the respective forms were obtained by desolvating the hydrate H1 and methanol solvate MS2, respectively. The samples then were homogenized in a mortar prior the DSC measurements. PXRD analysis were performed to analyze obtained products. The DSC analyses were performed as described above. For construction of the solidus lines, the onset temperatures of the respective DSC peaks were taken. The DSC peak maxima were used for determination of the corresponding liquidus lines.

^{13}C SSNMR Spectroscopy. Spectra of pimobendan *rac*-D and *enant*-F were recorded at a nominal temperature of 300 K with a Bruker Avance-III 11.7 T spectrometer equipped with a 3.2 mm low-temperature CPMAS probe operating at Larmor frequencies of 500 and 125 MHz for ^{1}H and ^{13}C, respectively. ^{13}C CP-MAS NMR spectra were recorded at 12.0 kHz. ^{13}C Chemical shifts were referenced to the CH_2 resonance observed for adamantane at 38.48 ppm with respect to the signal for neat TMS.[31]

Simulation of Solid-State NMR Spectra. Chemical shift calculations for *enant*-F and *rac*-D were carried out using the GIPAW method implemented in CASTEP 6.0 software,[32−35] after geometry optimization by relaxing all atomic positions. The calculations were performed with the PBE[36] functional using on-the-fly generated ultrasoft pseudopotentials and a cutoff energy of 600 eV. The Tkatchenko-Scheffler dispersion correction scheme[37] was used. The computed ^{13}C chemical shifts were referenced by linear regression of the computed shielding values to the experimentally observed chemical shifts.[35,38]

RESULTS AND DISCUSSION

Polymorphs and Solvates of Pimobendan. Several crystal forms of racemic pimobendan are already reported in the literature, including pimobendan monohydrate[39,40] (referred to as *rac*-H1 in the present study), pimobendan 1,4-dioxane monosolvate[39] (*rac*-DS1), pimobendan methanol monosolvate[39] (*rac*-MS1), as well as polymorphs *rac*-A,[39,41] *rac*-B,[39,42] and *rac*-D.[40] A recent own study showed the existence of an enantiopure monohydrate *enant*-H5 and its dehydration product—a poorly crystalline form *enant*-E.[40] In the present study, however, several novel crystal forms from racemic pimobendan were obtained, namely, a monohydrate (*rac*-H2), a hemihydrate (*rac*-H3), a trihydrate (*rac*-H4), a

DOI: 10.1021/acs.cgd.7b01203
Cryst. Growth Des. 2018, 18, 264–273

methanol hemisolvate (*rac*-MS2), an isostructural nonstoichiometric solvate family (*rac*-G; toluene, cyclohexane, 1,4–dioxane, ethyl acetate, acetone, cyclohexanol, xylene, buthyl acetate, ethyl formate, methyl acetate, propyl acetate, and propyl formate solvates), two polymorphs—*rac*-C, and *rac*-G_d (the isostructural desolvate of solvates *rac*-G). For enantiopure pimobendan along with the already reported hydrate *enant*-H5[40] and its dehydration product (*enant*-E), a 1,4-dioxane monosolvate (*enant*-DS2) and a polymorph (*enant*-F) was obtained. PXRD patterns of all known pimobendan crystal forms are given in Figure 3. The transition scheme between the crystalline forms of racemic pimobendan is shown in Figure 4

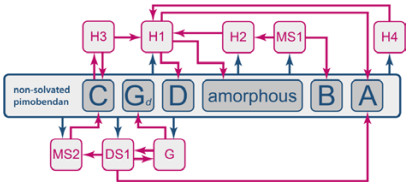

Figure 4. Principal transitions between the crystalline forms of racemic pimobendan (with H, MS, DS, and G solvates with water, methanol, 1,4-dioxane, toluene (or others), respectively).

(see also Figure S1 in Supporting Information for transition conditions). In Table 1 thermochemical data of racemic and

Table 1. Melting Onsets and Enthalpies of Melting of Pimobendan Crystal Forms[a]

form	melting point/°C	ΔH^f/kJ mol^{-1}
rac-A	240	40.1
rac-D	224	31.0
rac-B	189*	≈25**
rac-C	176*	≈25**
rac-G_d	163*	≈3
enant-F	231	33.2

[a]* — peak maximum; ** — due to immediate recrystallization event no precise enthalpy of melting can be assessed.

enantiopure pimobendan polymorphs are given. From heat of fusion rule[43] it follows that polymorphic form systems *rac*-A and *rac*-D, *rac*-A and *rac*-B, *rac*-D and *rac*-B, and *rac*-D and *rac*-C are monotropic, so *rac*-A is the most stable polymorph in all temperatures, while *rac*-D is the second most stable. No relationship between *rac*-B and *rac*-C can be assessed as the enthalpy of melting cannot be determined clearly for the respective forms. No slurry experiments are suitable in this case as both *rac*-B and *rac*-C are not stable in solvents and can be in fact obtained only by desolvating respective solvates of pimobendan and never crystallizing from solvents.

Extensive System of Solid Solutions of Pimobendan Enantiomers. Thermodynamic evidence of solid solution existence of a given two-component system can be summarized in a form of a melt phase diagram. Furthermore, it gives a complete picture of the system of interest showing thermodynamic stability and miscibility limits of the existing solid solutions.[6,10,44] The melt phase diagram of pimobendan enantiomers (Figure 5) shows the existence of four different solid solutions, namely, α, γ, δ, and ζ ($\alpha_{X=50}$ corresponds to previously mentioned form *rac*-A, $\gamma_{X=50}$—to form *rac*-C,

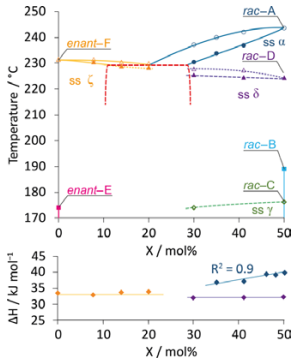

Figure 5. Melt phase diagram of pimobendan enantiomers and Melting enthalpy–temperature plot (in the phase diagram: closed markers—solidus, open markers—liquidus; lines are guides for the eyes).

$\delta_{X=50}$—to *rac*-D, and $\zeta_{X=0}$—to *enant*-F). The DSC and PXRD data used to establish the phase diagram are given in Figures S2–S7. Concerning the thermodynamically stable phases the diagram indicates that there is a eutectic system of two solid solutions (α and ζ), and consequently, miscibility is present around the racemic composition and near the pure enantiomer region, similarly like that observed, e.g., in the cases of phenylpiracetam[6] and malic acid.[5] Because of experimental limitations no equilibrated samples could be obtained representing the miscibility gap of solid solutions α and ζ, and therefore no eutectics could be experimentally accessed. However, the liquidus lines indicate that the eutectic composition is around 20%. Therefore, the eutectic temperature is estimated to be of around 229 °C, and the miscibility gap exists between roughly 10 and 30% composition. There is a good correlation between the enthalpy value and the composition (Figure 5) for α(R^2 = 0.9); however, in the case of ζ the low coefficient value rather indicates no significant composition dependent variation of the enthalpy of melting for solid solutions ζ. As shown in the phase diagram, the ζ + *liquid* region is relatively flat. It indicates that pimobendan enantiomers tend to form what is called an ideal solid solution. Close-to-ideal behavior is rare, it is reported for two glycerol ethers[45,46] and a slightly concaved dome is given for tazofelone.[13] There is also another nearly ideal but metastable solid solution δ present (metastable solid solutions have already been previously reported[47,48]). Similarly, there is no composition-dependent variation of the enthalpy of melting. The liquidus and solidus ofδ form a convex dome, which indicates a slightly lower stability of the racemic composition phase. The observed convex behavior is not typical for solid solutions showing miscibility around the racemic composition as mostly concave behavior is reported.[13,14,16,17,45,46,49–51]

The very similar PXRD patterns observed for *enant*-F and *rac*-D (Figure 3) as well as melting data represented in the phase diagram might suggest that it is a single continuous solid solution in part of the composition range being metastable. However, results of the structural and SSNMR study of *enant*-F and *rac*-D presented later indicate that these phases are not

DOI: 10.1021/acs.cgd.7b01203
Cryst. Growth Des. 2018, 18, 264–273

completely isostructural thus confirming the existence of two distinct solid solutions.

Finally, the solid solution γ is also metastable and like solid solution δ supposedly due to metastability can be accessed to only in a limited composition range. Forms *rac*-B and *enant*-E are depicted as metastable polymorphs; however, due to experimental limitations obtaining the forms, no strong statements could be made whether forms are strictly enantioselective, or if any miscibility of the enantiomers is possible.

The large amount of solid solutions found for pimobendan enantiomers is surprising, and to the best knowledge of the authors no other compound is reported to show such a diversity of structures able to form single scalemic phases. Moreover, the list of solid solutions formed by pimobendan enantiomers does not end with nonsolvated phases. *rac*-C ($\gamma_{X=50}$) could only be obtained by desolvating the methanol hemisolvate *rac*-MS2 upon heating (see Figure 4), and because the transition from *rac*-MS2 to *rac*-C is direct (see the DSC curves in Figure 6 and data on transformation kinetics given in

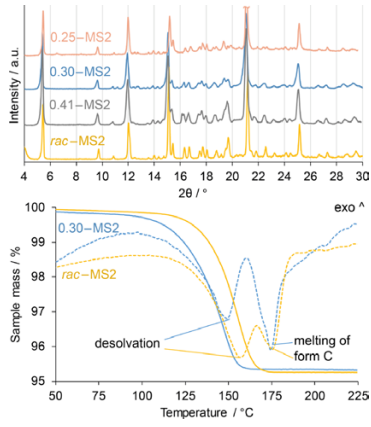

Figure 6. PXRD patterns, TG (solid lines), and DSC (dashed lines) curves of racemic and scalemic composition samples of pimobendan methanol hemisolvate MS2.

the Supporting Information), it follows that form MS2 itself must be a solid solution as well. Although an isopleth section of the ternary melt phase diagram could also be constructed, it meets additional experimental difficulties (DSC analysis must be carried out in hermetically sealed pans to avoid desolvation prior the melting. Furthermore, the interpretation of the data could be complicated if the solvate melts incongruently.). The existence of solid solutions of pimobendan methanol hemisolvate MS2 is thus proven by PXRD, TG, and DSC analysis. Figure 6 clearly shows that PXRD patterns of different enantiomeric composition samples are very similar as expected for solid solutions.[6,10,14,16] Furthermore, TG curves show that for example racemic and 30% composition samples both lose approximately 4.6% of the initial mass corresponding to 0.5 methanol molecules per one pimobendan molecule, therefore excluding the existence of an additional minor phase of the excess enantiomer in the 30% sample, that may be missed or overlooked in the PXRD analysis. In addition, the DSC curves show similar thermal behavior.

Further exploration of the pimobendan solid forms revealed that majority of the solvates are actually solid solutions. Previously reported structural and stability study[40] of pimobendan monohydrates showed that structurally distinct racemic and enantiopure monohydrates (namely, *rac*-H1 and *enant*-H5) exist. It would be expected that scalemic mixtures would show enantioselectivity of pimobendan enantiomers—equimolar amounts of opposite enantiomers forming *rac*-H1 and the remaining excess enantiomer forming *enant*-H5. However, crystallizing scalemic pimobendan mixtures from solvents containing water, solid solutions formed instead. In Figure 7 PXRD patterns of H1 and H5 are depicted. Although

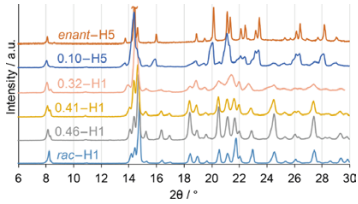

Figure 7. PXRD patterns of racemic, enantiopure, and scalemic composition samples of pimobendan monohydrates H1 and H5.

PXRD patterns of the enantiopure and racemic monohydrates are very similar (due to the already described similarities of the structures[40]), PXRD patterns of scalemic mixtures are not superposition of *rac*-H1 and *enant*-H5 patterns. In fact, PXRD patterns of 46, 41, and 32% mixtures are more similar to that of *rac*-H1, whereas that of the 10% sample is more similar to *enant*-H5, with the corresponding peak positions and intensities slightly varying. Another proof that the scalemic composition samples are single phases (and not mixtures of *rac*-H1 and *enant*-H5) can be found in the recorded TG/DSC traces. Both monohydrates are reported to dehydrate at different temperatures, and furthermore the dehydration products differ.[40] If there were different amounts of *rac*-H1 and *enant*-H5 present, the TG curve would contain two steps corresponding to the dehydration of each of the hydrates; however, TG curves of 46, 41, and 32% composition samples are very smooth showing that the removal of water occurs in a single step (see Figure S8). Furthermore, DSC curves are similar to that of *rac*-H1 showing that similar dehydration product (amorphous phase) forms (see Figure S8). DSC curve of 10% sample is similar to that reported for *enant*-H5[40] showing an additional endothermic event corresponding to the melting of the poorly crystalline dehydration product E (see Figure S9). It can be concluded that *rac*-H1 and *enant*-H5 are in fact limiting cases of two solid solutions apparently showing limited miscibility around the racemic and near the pure enantiomer composition regions, respectively.

Similarly, two pimobendan 1,4-dioxane monosolvates can be obtained—the already known *rac*-DS1 and *enant*-DS2 discovered in this study. Both solvates have similar PXRD patterns; however, careful examination of the patterns (Figure 9) of scalemic samples showed that those are not two extremes of one solid solution, but (similarly like in the case of *rac*-H1 and *enant*-H5) there are two solid solutions—one around the racemic and the other near the pure enantiomer composition

DOI: 10.1021/acs.cgd.7b01203
Cryst. Growth Des. 2018, 18, 264–273

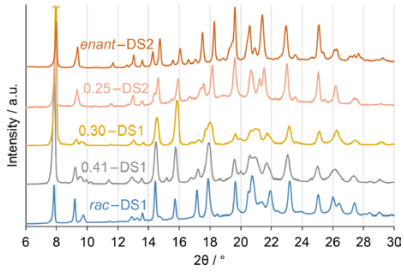

Figure 8. PXRD patterns of racemic, enantiopure, and scalemic composition samples of pimobendan 1,4-dioxane monosolvates DS1 and DS2.

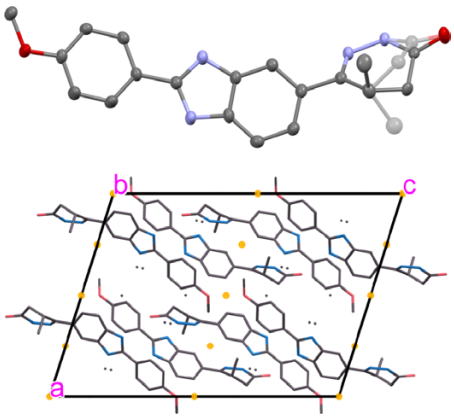

Figure 9. Asymmetric unit (showing the superimposition of both enantiomers with occupancy factors 0.74 and 0.26) and packing representation (centers of inversion depicted in yellow) of pimobendan *rac*-A. Hydrogen atoms omitted for the sake of clarity.

region. PXRD patterns show that *rac*-DS1, 0.41-DS1, and 0.30-DS1 are similar, and furthermore peak broadening resulting from the increase of the disorder is observed. On the contrary, the 25% sample resembles more that of *enant*-DS2. No smooth and continuous transition of the peak properties is present across the concentration range, but rather discontinuity can be observed between 25 and 30% enantiomeric composition samples. Also the TG/DSC analysis show considerably different behavior of 25 and 30% phases (see Figure S10).

Considering the diversity of pimobendan crystal forms existing as solid solutions already discussed, it is not surprising that a few more of the remaining racemic solvates were found to be solid solutions showing at least some miscibility of the enantiomers around the racemic composition. For example, a single phase—solvate $G_{toluene}$ was obtained also for the 30% composition sample as concluded from the PXRD data (see Figure S11) and TG analysis results (showing around 19% weight loss similarly as for the *rac*-$G_{toluene}$). It is therefore likely that also other isostructural solvates G (containing another solvent) having scalemic compositions exist. Pimobendan hemihydrate H3 was found to exist as a solid solution showing very similar PXRD patterns (see Figure S12) and around 2.5% weight loss on heating corresponding to the hemihydrate. Furthermore, also pimobendan methanol monosolvate MS1 most likely represents another solid solution (Figure S13).

The large amount of solid solutions identified for both nonsolvated and solvated pimobendan phases raises a question about what are the underlying reasons responsible for the formation of those commonly extremely rare type of phases[3] in such a large diversity for a single compound. Structural study was performed to better explore the observed phenomenon.

Structural Study of Pimobendan Solid Forms. Previous studies have shown that there must be very specific structural features present for solid solutions to exist,[6,7] which is the reason they occur so extremely rarely.[3] Surprisingly, in the case of pimobendan almost all of the crystal forms found are convincingly proven to exist in a form of solid solutions (with the remaining crystalline phases being rather questionable not strongly proven to be completely enantioselective). Furthermore, solid solutions form regardless of whether nonsolvated or solvated phases are considered. It follows that the driving force of solid solution formation in this case could be tracked down to the molecular level.

Structural study of pimobendan crystal forms was performed to explore the structural aspects governing the solid solution formation. For racemic pimobendan single crystals, however, were obtained only in the case of *rac*-A ($\alpha_{X=50}$) since it is the only racemic nonsolvated form obtainable from a solution. Unfortunately, no single crystals were obtained for any of the solvates except for the racemic monohydrate *rac*-H1 already reported.[40] SCXRD structure of a monohydrate of enantiopure pimobendan (*enant*-H5) is also reported,[40] but no single crystals of any other enantiopure forms were obtained. Crystal structure determination from powder X-ray diffraction data of several phases was considered (the structure of *rac*-B from the PXRD data has already been reported[42]). The structure solution was successful and reliable only in the case of the enantiopure polymorph *enant*-F ($\zeta_{X=0}$). Furthermore, SSNMR spectroscopy served as a crucial technique to facilitate the structure determination. Selected crystallographic data of *rac*-A and *enant*-F are presented in Table 2.

Structure of rac-A. The asymmetric unit of *rac*-A (or $\alpha_{X=50}$) is a superimposition of both enantiomers R and S. Their occupancies are 0.74 and 0.26, respectively (see Figure 9). Each of the enantiomers occupies a different conformation, e.g., RI and SII. Furthermore, concerning the apparent centrosymmetry of the structure there are also SI and RII conformers present (with the opposite occupancies giving overall racemic composition of the crystal). Thus, in the crystal structure of *rac*-A for every each pair of crystallographic molecular positions that are related by symmetry elements changing the handedness (centers of inversion and glide planes in this case) there is in fact a probability (approximately 3:1) whether a pair of pimobendan molecules is genuinely symmetric (RI–SI or RII–SII) or is it *quasi*-symmetric (RI–RII or SI–SII). Note that according to the determined structure there are never RI–SII or RII–SI pairs present if the locus of symmetry for the pair of two crystallographic positions is an inversion center or a glide plane. Therefore, as the occupancy of both enantiomers is not 1:1, there is inevitably some degree of enantioselectivity present. The structure tend to be an ordinary racemic compound. Furthermore, it can be noted that the same chirality conformers I and II found in the crystal structure are

DOI: 10.1021/acs.cgd.7b01203
Cryst. Growth Des. 2018, 18, 264–273

Table 2. Selected Crystallographic Data of Pimobendan Crystal Structures *rac*-A and *enant*-F

	rac-A ss $\alpha_{X=50}$	*enant*-F ss $\zeta_{X=0}$
empirical formula	$C_{19}H_{18}N_4O_2$	$C_{19}H_{18}N_4O_2$
formula weight/g mol^{-1}	334.37	334.37
T/K	293	293
sample type	single crystal	powder
crystal system	monoclinic	trigonal
space group	$C2/c$	$P3_121$ ($P3_221$)
a/Å	16.9418(5)	9.3798(6)
b/Å	9.1256(3)	9.3798(6)
c/Å	22.9751(8)	33.194(3)
α/°	90	90
β/°	107.3133(16)	90
γ/°	90	120
V/Å^3	3391.11(19)	2529.2(5)
ρ_{calc}/g cm^{-3}	1.310	1.317
Z, Z'	8, 1	6,1
reflns. collected	3276	
reflns. with $I > 2\sigma(I)$	2132	
R_1 ($I > 2\sigma(I)$)	0.0643	
S	1.045	
R_{wp} (R_p)		0.0740(0.0494)

approximate mirror images of each other ensuring *quasi*-centrosymmetric (or *quasi*-glide-symmetric) relationship. Structural origin of solid solution existence for *rac*-A (as proved by the melt phase diagram represented in the Figure 5) is therefore evident. It is comprehensible that in scalemic crystals more *quasi*-symmetric pairs of the enantiomer in majority may form in that way preserving the apparent centrosymmetry and general packing of the structure. Because of the observed structural aspects present and, thus, partial enantioselectivity in the solid state, the solid solution α is Type II solid solution.

Structure of enant-F. (*R*)-Pimobendan was found to crystallize in $P3_121$ space group. As it is one of the 11 enantiomorphic pairs of chiral space groups, the structure of the opposite enantiomer belongs to the $P3_221$ space group. The ^{13}C SSNMR spectrum was simulated to compare that with the experimentally obtained one by thus assessing if the structure solved from the PXRD data is reasonable (see Figure 10). A good fit between the experimental and theoretical values is obtained. The largest differences from the fitted straight line are

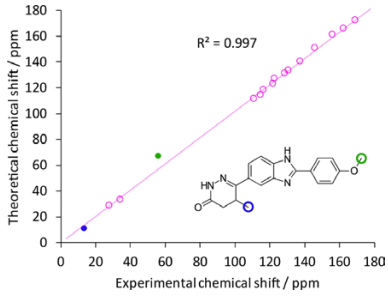

Figure 10. Correlation between the theoretical and experimentally determined chemical shifts in ^{13}C SSNMR spectra of *enant*-F.

observed for both methyl groups which could be explained by relative freedom of those substituents in the crystal structure. Furthermore, the SSNMR spectrum was also exploited to define the structural aspects of pimobendan solid solution ζ. The spectrum (Figure 11) of *enant*-F ($\zeta_{X=0}$) convincingly shows

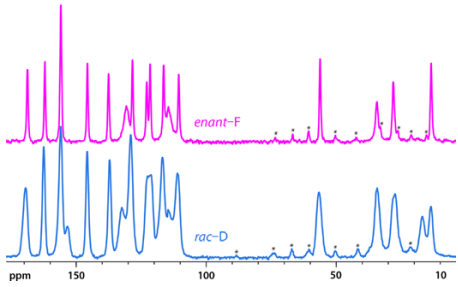

Figure 11. ^{13}C SSNMR spectra of *enant*-F and *rac*-D (spinning sidebands depicted with an asterisk).

that there is only one pimobendan molecule in the asymmetric unit ($Z' = 1$). As $Z' = 1$ it follows that no partial enantioselectivity is possible, and it indicates that solid solution ζ is of a Type I. Moving toward racemic composition statistically there will be a probability of finding R or S enantiomer in any molecular site equal to the mole fraction of R or S enantiomer in the crystal, respectively. Inevitably it leads that probability of finding an R or S molecule in any molecular site for such structure is exactly 50% for racemic composition. SSNMR spectra of *enant*-F and *rac*-D were compared to elucidate whether those phases could be isostructural corresponding to limiting cases of only one solid solution, or are they rather limiting cases of two distinct solid solutions. Peak count of *rac*-D spectrum indicates that also there is only one pimobendan molecule in the asymmetric unit ($Z' = 1$). The peaks are broader indicating that *rac*-D is considerably disordered. Although the PXRD patterns of both forms are very similar (Figure 3) and the melting data of corresponding scalemic phases could be interpreted as belonging to a single continuous solid solution (Figure 5), further analysis of the SSNMR data confirms the presence of two distinct solid solutions. The two additional peaks (at around 17 and 153 ppm) in the spectrum of *rac*-D indicate the static disorder. However, the split (same atom) peak area ratio is not 1:1, indicating that one of the conformer is more abundant in the crystal structure of *rac*-D. If *rac*-D was the limiting case of the solid solution ζ, then at racemic composition as mentioned before probability of finding one enantiomer in a crystallographic molecular site would be exactly 50%, consequently giving equal areas for the split atom peaks. As it is not so, by definition solid solution δ cannot be Type I solid solution, but on the contrary there is some enantioselectivity present leading to Type II for δ.

Similarities and Differences of rac-A and enant-F Structures. The stability of a crystal structure is ensured by favorable intermolecular interactions. Pimobendan molecule has several electron-donor/acceptor sites as well as aromatic rings that can be exploited to form such favorable interactions in a form of hydrogen bonds or $\pi\cdots\pi$ sackings. In the structure of *rac*-A and *enant*-F hydrogen bonds are present (Figure 12).

DOI: 10.1021/acs.cgd.7b01203
Cryst. Growth Des. 2018, 18, 264−273

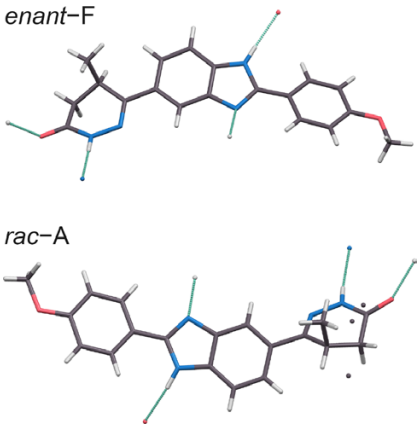

Figure 12. Asymmetric units of pimobendan *rac*-A and *enant*-F showing hydrogen bonds.

In both cases none of the chiral carbon substituents are directly involved in hydrogen bond network which is undoubtedly the main stabilizing force determining the stability of the crystal structures. Existence of solid solutions α and ζ can be therefore explained by the fact that apparently due to conformational flexibility the hydrogen bond network can be preserved regardless of which enantiomer is exploited similarly like in the case of, e.g., two solid solutions reported for phenylpiracetam,[6] a chiral pyrrolidine derivative,[52] and drugs tazofelone[13] and atenolol.[15]

Hydrogen networks in both structures in fact are identical (see the representation in Figure 13). There are $R_2^2(16)$ rings

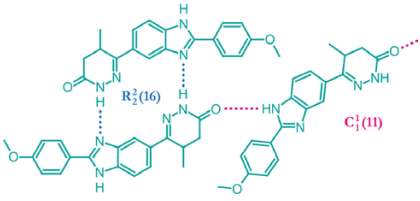

Figure 13. Representation of hydrogen bond network in the structures of *rac*-A and *enant*-F.

and $C_1^1(11)$ chains present. The differences between the structures are found in molecule conformations and packing of the molecules. In the structure of *rac*-A the molecules forming $R_2^2(16)$ rings are (*quasi*−)centrosymmetric, while in that of *enant*-F they are not even close to centrosymmetry. In the structure of *rac*-A the infinite $C_1^1(11)$ chains stacked parallel are forming layers which are interconnected via before mentioned $R_2^2(16)$ hydrogen bonds. In *enant*-F the $C_1^1(11)$ chains form rods which have 3-fold screw axis symmetry. The rods are interconnected via $R_2^2(16)$ hydrogen bonds (see Figure 14).

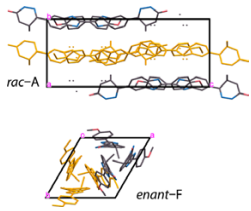

Figure 14. Packing representation of *rac*-A and *enant*-F along the crystallographic *a* and *c*-axis, respectively. Layers and rods formed via $C_1^1(11)$ hydrogen bonds shown in orange.

CONCLUSIONS

In this and previous studies of the authors the pharmaceutically active ingredient pimobendan was found to form five racemic and two enantiopure polymorphs as well as eight racemic and two enantiopure solvates. Surprisingly, four of six polymorphic forms were proven to exist as solid solutions, consequently showing limited or no enantioselectivity in the solid state. Furthermore, also at least 7 out of 10 solvates were found to be solid solutions. None of the 11 solid solutions exist in the full composition range. Therefore, for a distinct set of racemic and a distinct set of enantiopure structures there is an ability to host amounts of (excess or the opposite) enantiomers preserving the crystal structure. The considerable number of different structures (nonsolvated and solvated) that may be obtained as single phases of scalemic compositions means that the driving force of solid solution formation could be tracked down to the molecular structure level.

As the chiral center is fixed in a pyridazinone cycle with the remaining two substituents being a hydrogen atom and a methyl group, it is assumed that the lack of the enantioselectivity is as follows: the changes introduced by placing one or another enantiomer in a crystallographic molecular position are not crucial, because in terms of intermolecular interactions: (1) no steric effect hindrance is expected because of comparable sizes of the nonring chiral center substituents; (2) only dispersion energy term is affected by the change, which obviously has a minor importance determining the lattice energy as efficient hydrogen bond network can be expected. The mentioned reasons are in agreement with the two determined crystal structures. Furthermore, the most crucial aspect of solid solution formation is molecular flexibility, which allows the hydrogen bond network to be maintained regardless of the configuration of the chiral center of pimobendan molecule. The study also showed that solid solutions α and δ are Type II solid solutions, which means there is some enantioselectivity in the solid state while solid solution ζ is Type I solid solution—without any enantioselectivity.

Finally, it is intriguing that none of the solid solutions exist in the whole enantiomeric composition range. Although crystallographic molecular positions in the pimobendan polymorph and solvate crystal structures seem to be fairly indifferent regarding both enantiomers, different structures form at two extreme cases—racemic and enantiopure compositions. It shows that apparently it is energetically more favorable to pack racemic (or close-to-racemic) composition systems differently than those of enantiopure (or close-to-enantiopure) composition.

DOI: 10.1021/acs.cgd.7b01203
Cryst. Growth Des. 2018, 18, 264−273

■ ASSOCIATED CONTENT

Supporting Information

The Supporting Information is available free of charge on the ACS Publications website at DOI: 10.1021/acs.cgd.7b01203.

Transition scheme between pimobendan forms, preparation of pimobendan forms, thermal analysis of pimobendan forms, DSC and PXRD data used to establish the phase diagram of pimobendan enantiomers, evidence of solvated pimobendan solid solutions, experimental and calculated PXRD patterns of pimobendan polymorph *enant*-F (PDF)

Accession Codes

CCDC 1050684 and 1571124 contain the supplementary crystallographic data for this paper. These data can be obtained free of charge via www.ccdc.cam.ac.uk/data_request/cif, or by emailing data_request@ccdc.cam.ac.uk, or by contacting The Cambridge Crystallographic Data Centre, 12 Union Road, Cambridge CB2 1EZ, UK; fax: +44 1223 336033.

■ AUTHOR INFORMATION

Corresponding Author

*E-mail: toms.rekis@lu.lv.

ORCID

Toms Rekis: 0000-0001-5128-4611

Agris Bērziņš: 0000-0002-4149-8971

Artis Kons: 0000-0002-4055-8442

Heike Lorenz: 0000-0001-7608-0092

Notes

The authors declare no competing financial interest.

■ REFERENCES

(1) Rouhi, A. M. Chiral Business. *Chem. Eng. News* **2003**, *81*, 45−61.

(2) Lorenz, H.; Seidel-Morgenstern, A. Processes To Separate Enantiomers. *Angew. Chem., Int. Ed.* **2014**, *53*, 1218−1250.

(3) Jacques, J.; Collet, A.; Wilen, S. *Enantiomers, Racemates, and Resolutions*; Wiley, 1981.

(4) Kaemmerer, H.; Lorenz, H.; Black, S. N.; Seidel-Morgenstern, A. Study of System Thermodynamics and the Feasibility of Chiral Resolution of the Polymorphic System of Malic Acid Enantiomers and Its Partial Solid Solutions. *Cryst. Growth Des.* **2009**, *9*, 1851−1862.

(5) Kotelnikova, E. N.; Isakov, A. I.; Lorenz, H. Non-equimolar discrete compounds in binary chiral systems of organic substances. *CrystEngComm* **2017**, *19*, 1851−1869.

(6) Rekis, T.; Bērziņš, A.; Orola, L.; Holczbauer, T.; Actiņš, A.; Seidel-Morgenstern, A.; Lorenz, H. Single enantiomer's urge to crystallize in centrosymmetric space groups: solid solutions of phenylpiracetam. *Cryst. Growth Des.* **2017**, *17*, 1411−1418.

(7) Brandel, C.; Petit, S.; Cartigny, Y.; Coquerel, G. Structural Aspects of Solid Solutions of Enantiomers. *Curr. Pharm. Des.* **2016**, *22*, 4929−4941.

(8) Chion, B.; Lajzerowicz, J.; Bordeaux, D.; Collet, A.; Jacques, J. Structural aspects of solid solutions of enantiomers: the 3-hydroxymethyl- and 3-carboxy-2,2,5,5-tetramethylpyrrolidinyl 1-oxyl systems as examples. *J. Phys. Chem.* **1978**, *82*, 2682−2688.

(9) Bordeaux, D.; Lajzérowicz, J. Structure cristalline du tétraméthyl-2,2,6,6 (hydroxyimino)-4 pipéridine oxyl-1. *Acta Crystallogr., Sect. B: Struct. Crystallogr. Cryst. Chem.* **1977**, *33*, 1837−1840.

(10) Taratin, N. V.; Lorenz, H.; Kotelnikova, E. N.; Glikin, A. E.; Galland, A.; Dupray, V.; Coquerel, G.; Seidel-Morgenstern, A. Mixed Crystals in Chiral Organic Systems: A Case Study on (R)- and (S)-Ethanolammonium 3-Chloromandelate. *Cryst. Growth Des.* **2012**, *12*, 5882−5888.

(11) Wermester, N.; Aubin, E.; Pauchet, M.; Coste, S.; Coquerel, G. Preferential crystallization in an unusual case of conglomerate with partial solid solutions. *Tetrahedron: Asymmetry* **2007**, *18*, 821−831.

(12) Rekis, T.; D'Agostino, S.; Braga, D.; Grepioni, F. Designing solid solutions of enantiomers: lack of enantioselectivity of chiral naphthalimide derivatives in the solid state. *Cryst. Growth Des.* **2017**, *17*, 6477.

(13) Huang, J.; Chen, S.; Guzei, I. A.; Yu, L. Discovery of a Solid Solution of Enantiomers in a Racemate-Forming System by Seeding. *J. Am. Chem. Soc.* **2006**, *128*, 11985−11992.

(14) de Diego, H. L.; Bond, A. D.; Dancer, R. J. Formation of solid solutions between racemic and enantiomeric citalopram oxalate. *Chirality* **2011**, *23*, 408−416.

(15) de Castro, R. A. E.; Canotilho, J.; Barbosa, R. M.; Silva, M. R.; Beja, A. M.; Paixão, J. A.; Redinha, J. S. Conformational Isomorphism of Organic Crystals: Racemic and Homochiral Atenolol. *Cryst. Growth Des.* **2007**, *7*, 496−500.

(16) Vogt, F. G.; Copley, R. C. B.; Mueller, R. L.; Spoors, G. P.; Cacchio, T. N.; Carlton, R. A.; Katrincic, L. M.; Kennady, J. M.; Parsons, S.; Chetina, O. V. Isomorphism, Disorder, and Hydration in the Crystal Structures of Racemic and Single-Enantiomer Carvedilol Phosphate. *Cryst. Growth Des.* **2010**, *10*, 2713−2733.

(17) Bredikhin, A. A.; Bredikhina, Z. A.; Zakharychev, D. V.; Gubaidullin, A. T.; Fayzullin, R. R. Chiral drug timolol maleate as a continuous solid solution: Thermochemical and single crystal X-ray evidence. *CrystEngComm* **2012**, *14*, 648−655.

(18) Gordon, S. G.; Miller, M. W.; Saunders, A. B. Pimobendan in Heart Failure Therapy - A Silver Bullet? *J. Am. Anim. Hosp. Assoc.* **2006**, *42*, 90−93.

(19) Chu, K. M.; Shieh, S. M.; Hu, O. Y. Pharmacokinetics and pharmacodynamics of enantiomers of pimobendan in patients with dilated cardiomyopathy and congestive heart failure after single and repeated oral dosing. *Clin. Pharmacol. Ther.* **1995**, *57*, 610−621.

(20) Austel, V.; Noll, K.; Eberlein, W.; Heider, J.; Van Dr Meel, J.; Diederen, W.; Haarmann, W. Neue (−)-benzimidazole, deren herstellung und diese verbindungen enthaltende arzneimittel. DE Patent App. DE19,873,728,244, 1989; https://encrypted.google.com/patents/DE3728244A1?cl/it.

(21) Sheldrick, G. M. A short history of SHELX. *Acta Crystallogr., Sect. A: Found. Crystallogr.* **2008**, *64*, 112−122.

(22) Altomare, A.; Cuocci, C.; Giacovazzo, C.; Moliterni, A.; Rizzi, R.; Corriero, N.; Falcicchio, A. EXPO2013: a kit of tools for phasing crystal structures from powder data. *J. Appl. Crystallogr.* **2013**, *46*, 1231−1235.

(23) Altomare, A.; Campi, G.; Cuocci, C.; Eriksson, L.; Giacovazzo, C.; Moliterni, A.; Rizzi, R.; Werner, P. E. Advances in powder diffraction pattern indexing: N-TREOR09. *J. Appl. Crystallogr.* **2009**, *42*, 768−775.

(24) Boultif, A.; Louer, D. Powder pattern indexing with the dichotomy method. *J. Appl. Crystallogr.* **2004**, *37*, 724−731.

(25) Le Bail, A.; Duroy, H.; Fourquet, J. L. Ab-initio structure determination of LiSbWO6 by X-ray powder diffraction. *Mater. Res. Bull.* **1988**, *23*, 447−452.

(26) Dollase, W. A. Correction of intensities for preferred orientation in powder diffractometry: application of the March model. *J. Appl. Crystallogr.* **1986**, *19*, 267−272.

(27) March, A. Z. Mathematische Theorie der Regelung nach der Korngestalt bei affiner Deformation. *Z. Kristallogr. - Cryst. Mater.* **1932**, *81*, 285−297.

(28) Giannozzi, P.; et al. QUANTUM ESPRESSO: a modular and open-source software project for quantum simulations of materials. *J. Phys.: Condens. Matter* **2009**, *21*, 395502.

(29) Grimme, S. Semiempirical GGA-type density functional constructed with a long-range dispersion correction. *J. Comput. Chem.* **2006**, *27*, 1787−1799.

(30) Lund, A. M.; Orendt, A. M.; Pagola, G. I.; Ferraro, M. B.; Facelli, J. C. Optimization of Crystal Structures of Archetypical Pharmaceutical Compounds: A Plane-Wave DFT-D Study Using Quantum Espresso. *Cryst. Growth Des.* **2013**, *13*, 2181−2189.

DOI: 10.1021/acs.cgd.7b01203
Cryst. Growth Des. 2018, 18, 264−273

(31) Morcombe, C. R.; Zilm, K. W. Chemical shift referencing in {MAS} solid state {NMR}. *J. Magn. Reson.* **2003**, *162*, 479−486.
(32) Pickard, C. J.; Mauri, F. All-electron magnetic response with pseudopotentials: NMR chemical shifts. *Phys. Rev. B: Condens. Matter Mater. Phys.* **2001**, *63*, 245101.
(33) Clark, S.; Segall, M.; Pickard, C.; Hasnip, P.; Probert, M.; Refson, K.; Payne, M. First principles methods using CASTEP. *Z. Kristallogr. - Cryst. Mater.* **2005**, *220*, 567−570.
(34) Yates, J.; Pickard, C.; Mauri, F. Calculation of NMR chemical shifts for extended systems using ultrasoft pseudopotentials. *Phys. Rev. B: Condens. Matter Mater. Phys.* **2007**, *76*.10.1103/PhysRevB.76.024401
(35) Harris, R. K.; Hodgkinson, P.; Pickard, C. J.; Yates, J. R.; Zorin, V. Chemical shift computations on a crystallographic basis: some reflections and comments. *Magn. Reson. Chem.* **2007**, *45*, S174−S186.
(36) Perdew, J. P.; Burke, K.; Ernzerhof, M. Generalized Gradient Approximation Made Simple. *Phys. Rev. Lett.* **1996**, *77*, 3865−3868.
(37) Tkatchenko, A.; Scheffler, M. Accurate Molecular Van Der Waals Interactions from Ground-State Electron Density and Free-Atom Reference Data. *Phys. Rev. Lett.* **2009**, *102*, 073005.
(38) Bērziņš, A.; Hodgkinson, P. Solid-state {NMR} and computational investigation of solvent molecule arrangement and dynamics in isostructural solvates of droperidol. *Solid State Nucl. Magn. Reson.* **2015**, *65*, 12−20.
(39) Boeren, M. M. M.; Paridaans, R. J.; Petkune, S.; Lusis, V.; Muceniece, D. Crystalline pimobendan, process for the preparation thereof, pharmaceutical composition and use. 2014.
(40) Rekis, T.; Bērziņš, A.; Džabijeva, D.; Nakurte, I.; Orola, L.; Actiņš, A. Structure and stability of racemic and enantiopure pimobendan monohydrates: on the phenomenon of unusually high stability. *Cryst. Growth Des.* **2017**, *17*, 1814−1823.
(41) Rekis, T.; Oša, G.; Bērziņš, A.; Actiņš, A. Process for preparation of crystalline form A of pimobendan. 2013.
(42) Zvirgzdins, A.; Delina, M.; Mishnev, A.; Actins, A. Pimobendan B from powder diffraction data. *Acta Crystallogr., Sect. E: Struct. Rep. Online* **2013**, *69*, o1677.
(43) Hilfiker, R. *Polymorphism: In the Pharmaceutical Industry* **2006**, 1−414.
(44) Coquerel, G. Review on the heterogeneous equilibria between condensed phases in binary systems of enantiomers. *Enantiomer* **2000**, *5*, 481−498.
(45) Bredikhin, A. A.; Bredikhina, Z. A.; Zakharychev, D. V. Crystallization of chiral compounds: thermodynamical, structural and practical aspects. *Mendeleev Commun.* **2012**, *22*, 171−180.
(46) Fayzullin, R. R.; Zakharychev, D. V.; Gubaidullin, A. T.; Antonovich, O. A.; Krivolapov, D. B.; Bredikhina, Z. A.; Bredikhin, A. A. Intricate Phase Behavior and Crystal Structure Features of Chiral para-Methoxyphenyl Glycerol Ether Forming Continuous and Partial Solid Solutions. *Cryst. Growth Des.* **2017**, *17*, 271−283.
(47) Brandel, C.; Amharar, Y.; Rollinger, J. M.; Griesser, U. J.; Cartigny, Y.; Petit, S.; Coquerel, G. Impact of Molecular Flexibility on Double Polymorphism, Solid Solutions and Chiral Discrimination during Crystallization of Diprophylline Enantiomers. *Mol. Pharmaceutics* **2013**, *10*, 3850−3861.
(48) Bredikhin, A. A.; Bredikhina, Z. A.; Antonovich, O. A.; Zakharychev, D. V.; Krivolapov, D. B. Crystallization features and spontaneous resolution of 3-(2,6-dimethoxyphenoxy)propane-1,2-diol: The case of stable conglomerate and metastable solid solution. *J. Mol. Struct.* **2017**, *1144*, 443−450.
(49) Li, Y.; Zhao, Y.; Zhang, Y. Solid Tryptophan as a Pseudoracemate: Physicochemical and Crystallographic Characterization. *Chirality* **2015**, *27*, 88−94.
(50) Gallis, H.; Bougrioua, F.; Oonk, H.; van Ekeren, P.; van Miltenburg, J. Mixtures of d- and l-carvone: I. Differential scanning calorimetry and solid-liquid phase diagram. *Thermochim. Acta* **1996**, *274*, 231−242.
(51) Oonk, H.; Tjoa, K.; Brants, F.; Kroon, J. The carvoxime system. *Thermochim. Acta* **1977**, *19*, 161−171.
(52) Lajzerowicz, J.; Chion, B.; Lajzerowicz, J. Two dimensional order in a solid solution of molecules of opposite chirality. *J. Chem. Phys.* **1981**, *74*, 3500−3509. cited By 5

DOI: 10.1021/acs.cgd.7b01203
Cryst. Growth Des. 2018, 18, 264−273

II

Rekis, T.; d'Agostino, S.; Braga, D.; Grepioni, F.

Designing solid solutions of enantiomers: lack of enantioselectivity of chiral naphthalimide derivatives in the solid state

Cryst. Growth Des. **2017**, 17(12), 6477–6485

CRYSTAL GROWTH & DESIGN

Article

pubs.acs.org/crystal

Designing Solid Solutions of Enantiomers: Lack of Enantioselectivity of Chiral Naphthalimide Derivatives in the Solid State

Toms Rekis,*[,†,‡] Simone d'Agostino,[†] Dario Braga,[†] and Fabrizia Grepioni[†]

[†]Department of Chemistry, University of Bologna, Bologna, Italy

[‡]Department of Physical Chemistry, University of Latvia, Riga, Latvia

Supporting Information

ABSTRACT: The enantiomers of a previously reported naphthalimide derivative are shown in this study to form a solid solution; furthermore, on the basis of the knowledge of solid solution structural aspects other naphthalimide derivatives have been synthesized and shown to lack the enantioselectivity in the solid state. The structural origin of solid solution formation is the same as observed in most of the cases in the literature—*quasi*-centrosymmetric structures form at nonracemic compositions where the most abundant enantiomer adjusts its conformation to mimic the absent one. Such solid solutions belong to the type showing some enantioselectivity. An extended single crystal X-ray diffraction study of the crystals of different enantiomeric compositions reveals the nature of the disorder in studied solid solutions. Intermolecular interactions are analyzed in terms of Hirshfeld surfaces and by means of density functional theory calculations to explore the differences of isostructural *quasi*-centrosymmetric (enantiopure) and genuine centrosymmetric (racemic) packings to shed light on the energetic aspects of solid solution formation as well as to explain the origin of partial enantioselectivity. Furthermore, lattice energy calculations explain why two structurally distinct solid solutions (around the racemic and near the pure enantiomer regions) form as found for one of the studied compounds.

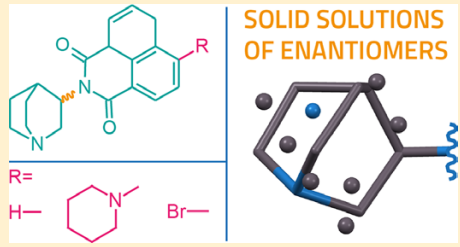

INTRODUCTION

Chirality has always been an intriguing issue in chemistry and other branches of science. It is especially crucial in the pharmaceutical industry and other fields where biological systems interact with chiral molecules.[1] The two enantiomers of a chiral compound are indistinguishable with respect to an achiral media; however, there are crucial differences of the mutual interactions if other species possessing handedness are introduced in the system. It also applies when a single enantiomer or a racemic mixture is considered. In the solid state for an enantiopure system comprising, e.g., *S* molecules, there are certain spatial arrangements possible. Furthermore, because of the symmetry a system comprising only *R* molecules of the same compound possesses the same possible (but mirror) spatial arrangements. For racemic mixtures, however, there is a possibility of additional symmetry elements between the molecules, namely, inversion centers, improper rotation axes, and mirror and glide planes. It is well-known that achiral organic molecules as well as racemic mixtures of chiral molecules tend to crystallize in centrosymmetric space groups.[2] It is therefore not surprising that according to the literature[3] in around 90% of cases so-called racemic compounds form from racemic mixtures. In 10% of cases conglomerates form, which stands for both enantiomers of the racemic mixture crystallizing in distinct (mirror) crystal structures. Thus, it can be concluded that molecular crystals in general show very high enantioselectivity as there is a strong preference of a specific enantiomer in every crystallographic molecular position. However, formation of solid solutions can also be observed. From a crystallographic point of view two types are distinguished: (1) showing complete lack of enantioselectivity; (2) showing partial enantioselectivity.[4−6] A recent study has shown[7] that most often the latter type solid solutions form. The underlying structural origin for such solid solution formation is as follows—nonracemic mixtures form *quasi*-centrosymmetric structures where the amount of the absent enantiomer is compensated by the abundant one adopting a conformation that resembles the enantiomer which is in minority.[6,7] The phenomenon could be referred to as shape mimicry.[8] The enantiopure and racemic structures are therefore isostructural, and continuous change of enantiomeric composition in between is possible forming the same isostructural packing.

The structural aspects of solid solutions of enantiomers have been studied recently[6,7] as well as in the past[9,10] and are quite well understood. Furthermore, growth of mixed crystals in terms of stereospecific interactions has been studied.[11,12] Defining a

Received: August 15, 2017
Revised: October 24, 2017
Published: October 26, 2017

DOI: 10.1021/acs.cgd.7b01146
Cryst. Growth Des. 2017, 17, 6477−6485

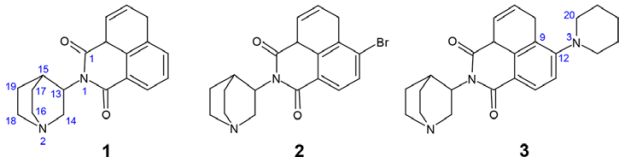

Figure 1. Chemical scheme of 2-(quinuclidin-3-yl)-(1,8-naphthalimide) (**1**), 4-bromo-*N*-(quinuclidin-3-yl)-1,8-naphthalimide (**2**), and 4-(piperidin-1-yl)-*N*-(quinuclidin-3-yl)-1,8-naphthalimide (**3**). Both racemic and enantiopure forms were synthesized.

profound structural origin of solid solution formation actually gives a tool for spotting them based on the structural data as previously the solid solutions of enantiomers were largely rather identified in terms of melt phase diagrams.[3] Their seldom formation up to now cannot be predicted based on the molecular structure. Solid solutions, however, could be an interesting subject in terms of crystal engineering since solids with finely tunable properties depending on the enantiomeric composition could be designed. To the best knowledge of the authors, no attempts have been made thus far to intentionally design structures that would lack such an enantioselectivity in the solid state.

The aim of this study was, first, to prove that the enantiomers of previously reported compound[13] 2-(quinuclidin-3-yl)-(1,8-naphthalimide) (**1**) could indeed form solid solutions in the whole composition range as suggested on the basis of the knowledge of the structural aspects of solid solution formation and of the enantiopure and racemic crystal structures of **1**. Second, the aim was to design other chiral naphthalimide derivatives whose enantiomers would show miscibility in the solid state. To achieve the aim along with **1** two novel compounds were synthesized (namely, 4-bromo-*N*-(quinuclidin-3-yl)-1,8-naphthalimide (**2**) and 4-(piperidin-1-yl)-*N*-(quinuclidin-3-yl)-1,8-naphthalimide (**3**) (see Figure 1)), and extensive crystal structure studies on different enantiomeric composition phases of those compounds were performed.

EXPERIMENTAL METHODS

Synthesis of Enantiopure and Racemic 1, 2, and 3. All the starting compounds and solvents used were purchased from commercial sources and used without further purification. The water was doubly distilled at the laboratory. **1** was synthesized by weighing 0.33 g (2 mmol) of 3-aminoquinuclidine hydrochloride (racemic or enantiopure), a 0.28 g (2 mmol) of potassium carbonate, and a 0.40 g (2 mmol) of 1,8-naphthalic anhydride into a 50 mL round-bottom flask. Around 30 mL of ethanol and 1.5−2 mL of water was added. The suspension was then refluxed overnight. After cooling, 0.28 g (2 mmol) of potassium carbonate was added together with 10−15 mL of water. The pale-yellow precipitate that formed was filtered, rinsed with cold water, and dried at 75 °C. Synthesis of **2** and **3** were done similarly, except 4-bromo-1,8-naphthalic anhydride and 4-(piperidin-1-yl)-1,8-naphthalic anhydride was used, respectively.

Single Crystals. Single crystals of different enantiomeric composition samples of **1** (initial mole fractions of the S enantiomer in the solutions: 1, 0.80, 0.75, 0.60, and 0.5) were grown by slow evaporation of acetonitrile and *N*,*N*-dimethylformamide solutions at room temperature. Those of **3** (initial mole fractions of the S enantiomer in the solutions: 1, 0.90, 0.70, 0.60, and 0.5) were grown by slow evaporation of ethyl acetate solutions at 75 °C.

Single Crystal X-ray Diffraction. The data were collected at room temperature on an Oxford X'Calibur S CCD diffractometer using Mo−Kα radiation (graphite monochromator, wavelength of 0.710 73 Å) (Oxford Instruments, UK). The structures were solved by direct methods and refined by full-matrix least-squares on F^2 for all data, using SHELX-2014 software suite.[14] The non-hydrogen atoms were refined anisotropically. When disorder was present, the site occupancy factors (sof) of atoms were refined using SHELX command PART and an additional free variable was added. The absolute structures were not determined by means of Flack parameter as compound with a known configuration was used for the synthesis of the derivatives. Mercury[15] was used for the analysis and visualization of the structures and figure preparation.

Powder X-ray Diffraction. PXRD patterns were determined on a Panalytical X'Pert PRO diffractometer (Panalytical, Japan) using copper radiation (Cu−Kα) at a wavelength of 1.541 80 Å equipped with a X'Celerator detector (Panalytical, Japan). The tube voltage and current were set to 40 kV and 40 mA. The diffraction pattern was recorded using a scanning speed of 0.5 s/0.02° from 5° to 35° on 2θ scale.

Quantum Chemical Calculations. Density functional theory (DFT) calculations were performed in Gaussian 09.[16] For potential energy surface (PES) scans atomic positions of the analyzed molecules were extracted from experimentally determined structures and total energy calculations were performed at the B3LYP/6-311g(d,p) level of theory using 'opt = ModRedundant' key-word and 15° increments of the chosen torsion angle. Total energy calculations of the conformers found in the experimentally determined structures were performed in Gaussian 09 at the same level of theory. Interaction energy between a pair of molecules in the experimental structures was calculated in Gaussian 09 at the M06-2X/6-311g(d,p) level of theory which includes dispersion correction. The basis set superposition error was corrected using the counterpoise method in this case.

Hypothetical packings of compound **3** were generated by a self-written code in PHP programming language using Cartesian coordinates of the atomic positions of corresponding asymmetric units and corresponding space group symmetry operators, as well as experimentally determined unit cell parameters as input data. The generated structures and the experimentally determined ones were then relaxed (both atomic positions and unit cell parameters) in program Quantum ESPRESSO[17] with ultrasoft pseudopotentials from the original pseudopotential library and a 44 Ry planewave cutoff energy using PBE functional with vdW interactions treated according to the D2 method of Grimme.[18] The parameters of convergence, pseudopotentials, and the *k*-point grid were used as suggested for structure optimizations of organic molecules.[19] The calculations of lattice energies afterward were performed according to the semiempirical PIXEL methodology (code provided in the CLP software suite).[20] Empirical parameters were used as provided in the literature.[20] The atom positions were obtained by standard procedure using RETCIF and RETCOR modules. The hydrogen atom positions were renormalized. Molecular electron density calculations were performed in Gaussian 09 at the MP2/6-31g(d,p) level using standard grid parameters. The condensation level 4 and a cutoff distance of 44 to 48 Å were used (in the case of the enantiopure hypothetical structure $P2_12_12$ with no shift between the layers the relaxation of the atomic positions lead to a *P*1 structure with Z' = 8 (resembling $P2_12_12$ packing but not possessing complete symmetry). PIXEL methodology, however, does not allow one to calculate the lattice energy for structures with $Z' > 2$).

RESULTS AND DISCUSSION

Solid Solutions of 1 and 2. As a recent study has shown[7] in most of the cases when miscibility in the solid state is present

DOI: 10.1021/acs.cgd.7b01146
Cryst. Growth Des. 2017, 17, 6477−6485

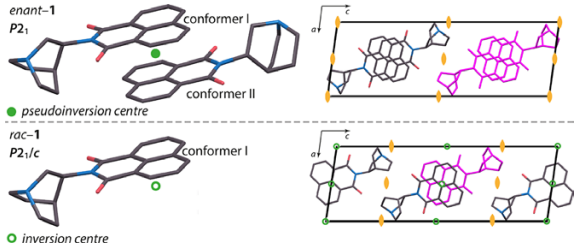

Figure 2. Asymmetric units (left) and packing representation (right, asymmetric units colored in magenta) of *enant*-**1** and *rac*-**1** (hydrogen atoms omitted and disorder of the racemic structure not shown at this point for the sake of clarity).

there is a common structural origin responsible for that. For enantiopure samples two molecules with the same configuration can adjust the conformations to form an apparent centrosymmetric pair, as a result *quasi*-centrosymmetric structures form able to host also the opposite enantiomer when scalemic composition phases are considered. Requirement for such structures therefore is that two (or other even number) of single enantiomer molecules in the asymmetric unit are approximate mirror images to each other. The study of **1**[13] has shown that all the structural prerequisites for solid solution existence are present; furthermore, the racemic structure is isostructural with the enantiopure one (see Figure 2).

Previously reported cases[5,7,21−23] of solid solutions show that molecules possessing relatively large conformational freedom around the chiral center are able to form *quasi*-centrosymmetric pairs. Studied quinuclidine derivatives on the contrary are rather rigid molecules and for **1** only rotation around the N1—C13 bond is possible (see Figure 1 for atom numbering); however, because of steric hindrance (due to the oxygen atoms of the naphthalimide moiety) rotation may not be so feasible. PES scan of **1** in the gas phase was calculated (Figure 3) showing that there

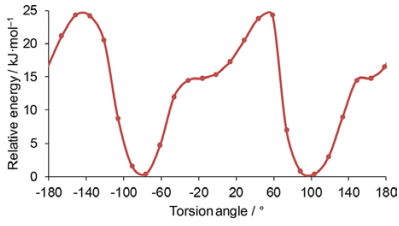

Figure 3. Relative energy of **1** in the gas phase as a function of the torsion angle C1—N1—C13—C15.

are two deep minima (corresponding to two symmetrically identical states). The torsion angle C1—N1—C13—C15 does not differ significantly from the minimum energy value also in the crystal structures. However, the conformations of both symmetrically independent molecules in the crystal structure of *enant*-**1** in fact are not identical (see Figure 4). Nevertheless, they are very similar, and the torsion angles C1—N1—C13—C15 are 86° (conformer I) and 104° (conformer II).

Concerning the enantiopure *quasi*-centrosymmetric structure (see Figure 2), it is clear that genuine centrosymmetry at the racemic composition can be achieved either by a pair S_I—R_I or a

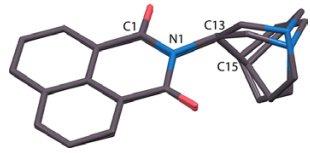

Figure 4. Overlay of conformer S_I and conformer S_{II} (hydrogen atoms omitted for the sake of clarity).

pair S_{II}—R_{II}. Experimental data show that the pair S_I—R_I is preferred in this case as the racemic crystal contains molecules mostly occupying conformation I. DFT calculations showed that the energy of conformer I is by 0.8 kJ mol^{-1} lower than that of conformer II. This small difference, however, does not fully justify the conformational preference in the racemic crystal structure as it is known that not always the energetically most favorable conformer is found in the crystal structure.[24,25] In the case of conformationally flexible molecules, the stability of a crystal structure is often determined by a subtle compromise between molecular energy and packing efficiency represented by lattice energy. The hypothetical conformational polymorph possessing the same packing as in *rac*-**1** but with molecules occupying conformation II was modeled. Relaxation of the atomic positions and unit cell parameters was performed before calculating the lattice energy. However, upon relaxation the hypothetical structure *rac*$_{II}$-**1** converged to experimentally determined *rac*$_I$-**1** indicating that the former is not energetically favorable. The main reason for that may be that in the packing comprising conformers II there are too short H···H contacts present (see Figure S1) which are not energetically favorable. The question might arise about why conformer II is preferred at all in the enantiopure structure if it differs only slightly from the conformer I. In other words, why would, e.g., a pair S_I—S_{II} be preferable over a pair S_I—S_I in the enantiopure structure. Figure 5a shows an overlay of the target conformer R_I (required for genuine centrosymmetric pair with S_I) and S_I, and Figure 5 depicts R_I and S_{II} showing that the overlapping ball-shaped volume of the quinuclidine substituent and therefore resemblance of the absent R_I enantiomer is better in the latter. Therefore, inclusion of a slightly energetically less favorable conformer II in the crystal structure of enantiopure **1** results in a packing more sterically resembling more that of a centrosymmetric one.

The intermolecular interactions were analyzed in the crystal structures of *rac*-**1** and *enant*-**1** to further explore similarities and differences of those structures. Hirshfeld surfaces of the

DOI: 10.1021/acs.cgd.7b01146
Cryst. Growth Des. 2017, 17, 6477−6485

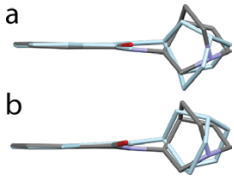

Figure 5. Overlay of (a) target conformer R_I (colored by element) and S_I (light blue); (b) target conformer R_I (colored by element) and S_{II} (light blue) (hydrogen atoms omitted for clarity).

symmetrically independent species proved to serve as an excellent tool for contact analysis in crystal structures.[26,27] Fingerprint plots of the Hirshfeld surfaces are given in Figure 6. General shape of all three fingerprint plots is very similar since the packings are isostructural and the conformations do not differ much. Furthermore, no significant differences are observed in the plots of conformers I; however, they are not completely identical as the Hirshfeld surface is solely a property in the context of a crystal structure thus being dependent on the environment around the molecule of interest. Most characteristic contacts of all three molecules are C···C contacts (corresponding to $\pi\cdots\pi$ stacking of the naphthalene moieties) denoted with a yellow circle. The regions are very similar indicating that conformational (hence enantiomeric composition) differences do not affect these contacts. No significant differences of the minor O···H contacts are observed (see pairs of the light blue stripes between the depicted ellipses characteristic for the respective contacts). The plot actually indicates that there are no hydrogen bonds present in the studied structures. Additional contact density appears in the fingerprint plot of conformer II (compare the ellipses in magenta). Those contacts correspond to N···H and H···H interactions arising from a different position of the quinuclidine moiety (see Figure 5b). The region denoted with a white ellipse (H···H contacts) differs for conformer II in a way that it is approximately equally dense in the whole area, on contrary in the plots of conformer I the contact density is more concentrated in the upper part of the given range in the ellipse. Thus, in the case of *enant*-**1** there is a larger number of short H···H contacts present (compared to those in *rac*-**1**) originating from the molecules of conformer II. Finally, the region depicted in the rounded rectangle in green shows that in the case of conformer II there are some contacts present in the structure of *enant*-**1** being relatively long. That indicates for existence of space in the unit cell not as efficiently packed as in the structure of *rac*-**1**. Indeed, a tiny void could be found in the structure of *enant*-**1** (using the algorithm implemented in Mercury) that occupies 0.1% of the unit cell volume if the default probe radius for finding voids is lowered to 0.82 Å. On the contrary, no voids can be found with the same settings in the structure of *rac*-**1**.

To explore the energetic aspects of crystal packings, lattice energies were calculated for *rac*-**1** and *enant*-**1**. The lattice energy values and their breakdown are summarized in Table 1. The lattice energy is slightly lower for the crystal structure of *rac*-**1**. The main stabilizing forces in both crystal structures are dispersion interactions arising from efficient $\pi\cdots\pi$ stacking of naphthalene moieties. As there are no hydrogen bonds present and no ions are involved, the Coulombic interactions are of a minor importance in determining the stability of the lattices. The energy stabilizing terms are roughly the same in both cases; however, the repulsion energy terms are considerably different (8 kJ mol^{-1} difference). When identical packings and the same molecules comprising the crystal structures are considered, the higher repulsion energy term can be associated with atoms of the neighboring molecules being too close to each other. It is compatible with the analysis of the Hirshfeld surfaces showing that conformer II has higher contact density at lower d_e and d_i values (see the ellipses in white and magenta in Figure 6) corresponding to N···H and H···H contacts.

Table 1. Lattice Energy Values and Their Components of the Crystal Structures of *rac*-1 and *enant*-1

	E_{Coul}/ kJ mol^{-1}	E_{Pol}/ kJ mol^{-1}	E_{Disp}/ kJ mol^{-1}	E_{Rep}/ kJ mol^{-1}	E_{Tot}/ kJ mol^{-1}
rac-**1**	−35.1	−18.5	−174.3	98.9	−129.0
enant-**1**	−36.6	−19.9	−177.4	106.9	−127.2

Although it is symmetrically forbidden, enantiopure **1** tries to crystallize in a centrosymmetric structure. The analysis of intermolecular contacts and interactions stabilizing the crystal show that apparent centrosymmetry is facilitated by dominating dispersion interactions arising mostly from $\pi\cdots\pi$ stacking, which are not stereospecific and are primarily responsible for the stability of the crystal lattice. Moreover, there are no specific intermolecular interactions (e.g., hydrogen bonds) of the atoms

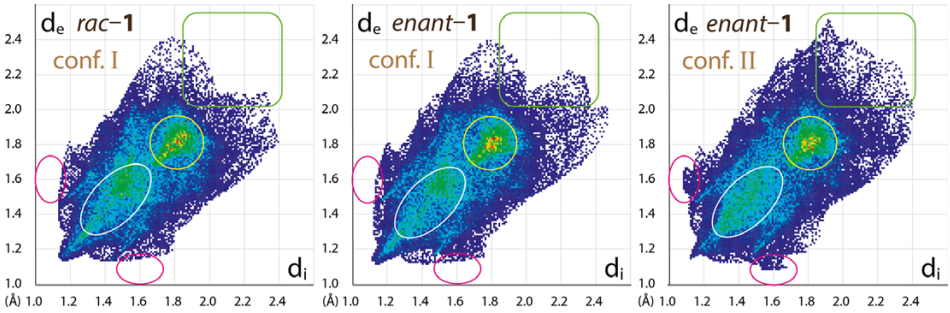

Figure 6. Fingerprint plots of the Hirshfeld surfaces of symmetrically independent molecules in the crystal structures of *rac*-**1** and *enant*-**1** (see Table S1 for the breakdown of the fingerprint plots).

DOI: 10.1021/acs.cgd.7b01146
Cryst. Growth Des. 2017, 17, 6477−6485

Table 2. Selected Crystallographic Data of 1 Structures

	enant-**1**	0.82-**1**	0.76-**1**	0.63-**1**	*rac*-**1**
temperature/K	298	298	298	298	298
crystal system	monoclinic	monoclinic	monoclinic	monoclinic	monoclinic
space group	$P2_1$	$P2_1$	$P2_1$	$P2_1$	$P2_1/c$
a/Å	8.4199(10)	8.4594(9)	8.4637(7)	8.4726(4)	8.4871(11)
b/Å	6.9924(11)	6.9775(9)	6.9747(4)	6.9547(6)	6.9736(6)
c/Å	25.013(4)	25.010(4)	24.9956(17)	24.9403(18)	24.943(3)
β/°	97.653(12)	98.071(12)	98.189(7)	98.329(6)	98.280(11)
V/Å^3	1459.5(4)	1461.6(3)	1460.49(18)	1454.09(18)	1460.9(3)
ρ_{calc}/g cm^{-3}	1.394	1.392	1.393	1.399	1.393
Z, Z'	4, 2	4, 2	4, 2	4, 2	4, 1
$R_{1[I>2\sigma(I)]}$	0.0594	0.0672	0.0900	0.0607	0.0770
S	1.008	1.032	1.093	1.026	1.017

of the quinuclidine moiety. As a result enantiopure **1** can crystallize in a *quasi*-centrosymmetric structure, and the absence of the opposite enantiomer is accommodated by altering the conformations of half of the molecules in the crystal structure to the conformation II. Computations show that the interaction energy of an S_I—R_I pair is −67.3 kJ mol^{-1}, while that of an S_I—S_{II} (R_I—R_{II}) pair is −65.0 kJ mol^{-1}, thus showing that a genuine centrosymmetric pair is energetically more favorable. Analysis of the Hirshfeld surfaces and energy calculations therefore strongly suggests that conformer II is not favored in the overall crystal structure, yet it is still preferred in the case the opposite enantiomer is missing.

To prove that there is a lack of enantioselectivity in the solid state, the structures were determined also for scalemic crystals. The structural study clearly shows the disordered nature of the studied scalemic crystals; moreover, single phases could have been obtained comprising the initial scalemic compositions, therefore fully verifying the existence of solid solutions of **1**. Selected crystallographic data for *enant*-**1**, *rac*-**1**, and the studied scalemic composition crystals are presented in Table 2. There is a systematic variation of the unit cell parameters a, c, and β across the composition range (see Figure 7). Parameter a and β

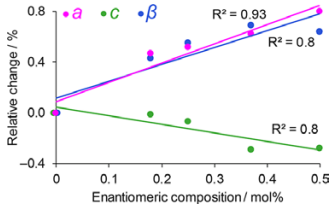

Figure 7. Dependence of the unit cell parameter relative change of **1** as a function of enantiomeric composition.

increases by 0.8% and parameter c decreases by 0.3% as the composition reaches racemic one. Parameter b, however, does not show any significant variation on the composition since the correlation coefficient is small ($R^2 = 0.5$). Furthermore, there is no significant enantiomeric composition dependent variation of the unit cell volume ($R^2 = 0.04$) and hence also the crystallographic density. It can be concluded that either racemic samples or enantiopure samples of **1** can form crystal structures equally well packed (packing index for *rac*-**1** and *enant*-**1** calculated to be 74.2 and 74.3%, respectively).

For scalemic crystals disorder of only one of the molecular sites in the asymmetric units is present; furthermore, the disordered site corresponds to conformer II. Intermolecular interaction analysis already showed that the conformer II is not favored in the overall crystal structure. It is therefore comprehensible that those sites would be occupied by conformer I, if possible. The crystallographic data indeed show that when the opposite enantiomer is introduced into the enantiopure structure it adopts conformation I and therefore substitutes conformer II molecules. As a result as many as possible genuine centrosymmetric pairs S_I—R_I are formed in the structures. It would be expected that racemic crystals only contain molecules occupying conformation I giving a genuine racemic compound. However, the asymmetric unit of *rac*-**1** contains one molecule, which is in fact disordered occupying conformation I and II. As found in three different single crystals the conformer ratio (I:II) varies—85:15, 87:13, and 90:10. Asymmetric units and conformer abundance as a function of enantiomeric composition is depicted in Figure 8. It must be noted that after careful examination of the data the disorder was found also in the original crystal structure reported years ago.[13] However, due to its minor extent, it was only possible intentionally searching for additional electron density in the positions corresponding to conformer II and in general reasonable structure solutions could be obtained ignoring any disorder.

Although a racemic composition phase in the case of solid solutions having the same structural origin could exist as a true racemic compound (thus being completely ordered), several of the cases reported[7,21−23] also show that a certain degree of disorder is present. It is questionable whether the analyzed crystals represent thermodynamically equilibrated phases, in other words, whether the disorder is a thermodynamically inherited phenomenon or it has a kinetic origin. Slow growth of a single crystal may be imagined as a process carried out at near-equilibrium conditions, therefore suggesting that the disorder observed in *rac*-**1** crystals has a thermodynamic origin. Slight variation of the conformer ratio observed in a few analyzed crystals of *rac*-**1** (from different batches) can also stand for a single value within the refinement error. Nevertheless, the disorder systematically observed and reported also for many other cases of racemic crystals being limiting cases of solid solutions leads us to believe that it is rather governed by thermodynamics. In the literature it has been shown that the disorder found in molecular crystals can be treated according to Boltzmann distribution.[28−30] If the lattice energy difference of, e.g., two locally ordered extreme structures is small enough, then depending on this difference and the equilibration temperature

DOI: 10.1021/acs.cgd.7b01146
Cryst. Growth Des. 2017, 17, 6477−6485

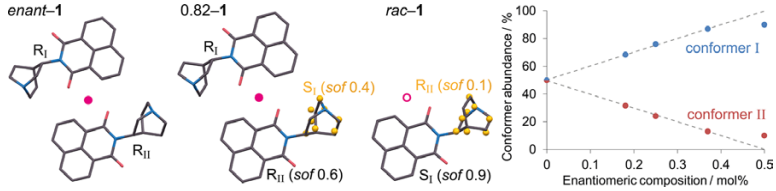

Figure 8. Asymmetric units of studied solid solutions of **1** (hydrogen atoms omitted for the sake of clarity) and conformer abundance in the crystal structure as a function of enantiomeric composition.

both can be found in the general structure with a certain probability. This approach could probably explain why there is a deviation from the straight line in the plot depicted in Figure 8 as the enantiomeric composition approaches racemic one. However, a detailed study on the lattice energies of different ordered extreme cases should be performed to justify the statement.

In the case of the bromine substituted compound (**2**), neither single crystals were obtained for the structure analysis, nor reliable structure refinement from powder X-ray diffraction data was possible. The PXRD patterns of different enantiomeric composition samples are nearly identical with only minor differences of some peak positions and intensities (see Figure 9),

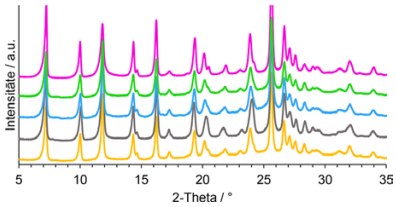

Figure 9. PXRD patterns of different enantiomeric composition samples of **2** (from bottom to top: enantiopure, 0.80, 0.75, 0.60, racemic).

which is typical in the case of solid solutions as there is a composition dependent systematic change of the unit cell parameters.[7,31] Unfortunately, due to compound degradation prior to melting it was not possible to construct a melt phase diagram for the system of interest, which would prove solid solution existence from a thermodynamic point of view. However, the PXRD data convincingly suggest that the compound **2** forms solid solutions in the whole composition range, and therefore also in this case there is no complete enantioselectivity in the solid state.

Solid Solutions of 3. On the basis of the knowledge about the solid solution formation of compound **1** and **2** it was inferred that also compound **3** would show miscibility of the enantiomers in the solid state since non-stereospecific $\pi\cdots\pi$ stacking of the naphthalene moieties, and no specific interactions of the quinuclidine moiety are expected in the crystal structure. The structural study confirmed that solid solution formation for **3** is also possible. Selected crystallographic data of different enantiomeric composition crystals are presented in the Table 3. *enant*-**3** crystallizes in $P2_12_12_1$ space group with two molecules in the asymmetric unit. Figure 10 shows an overlay of the two

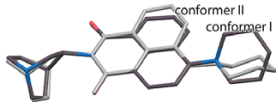

Figure 10. Overlay of conformer R_I (colored by element) and conformer R_{II} (gray) (hydrogen atoms omitted for the sake of clarity).

conformers. In the case of *enant*-**3** the naphthalimide core moiety is no longer planar but skewed. PES scan of **3** in the gas phase was calculated for two torsion angles C1—N1—C13—C15 and C9—C12—N3—C20 representing the rotation of the quinuclidine and piperidine substituents, respectively (Figure 11). As observed previously for **1** there are two minima in the scan of C1—N1—C13—C15. Furthermore, the graph is again sinusoidal indicating that the rotation of the quinuclidine substituent in terms of energy is independent of the presence of an additional

Table 3. Selected Crystallographic Data of 3 Structures

	enant-**3**	0.86-**3**	0.70-**3**[a]	0.58-**3**	*rac*-**3**
temperature/K	298	298	298	298	298
crystal system	orthorhombic	orthorhombic	orthorhombic	orthorhombic	orthorhombic
space group	$P2_12_12_1$	$P2_12_12_1$	$P2_12_12_1$	$P2_12_12$	*Pccn*
a/Å	7.4629(5)	7.4674(7)	7.4648(9)	30.622(8)	30.669(4)
b/Å	17.4188(8)	17.4222(11)	17.5053(18)	17.290(3)	17.302(2)
c/Å	30.117(3)	30.317(3)	30.871(4)	7.3918(11)	7.3829(9)
V/Å^3	3915.0(5)	3944.3(6)	4034.0(8)	3913.7(13)	3917.7(9)
ρ_{calc}/g cm^{-3}	1.322	1.312	1.283	1.322	1.321
Z, *Z*′	8, 2	8, 2	8, 2	8, 2	8, 1
$R_{1[I>2\sigma(I)]}$	0.0598	0.0823	N/A	0.0811	0.0964
S	1.049	0.948	N/A	0.965	0.959

[a]For 0.70-**3** only indexation was possible and no complete structure solution was obtained.

DOI: 10.1021/acs.cgd.7b01146
Cryst. Growth Des. 2017, 17, 6477−6485

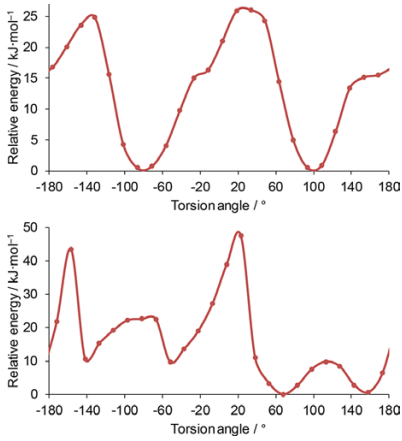

Figure 11. Relative energy of **3** in the gas phase as a function of the torsion angles C1—N1—C13—C15 (top) and C9—C12—N3—C20 (bottom).

piperidine substituent in the compound **3**. Two minima are observed for the angle C9—C12—N3—C20 occurring at 68 and 158°. The crystal structure study shows that the two reasonable torsion angles analyzed fall into the calculated energy minimum. The torsion angle C1—N1—C13—C15 is around 90° for both conformers, and the angle C9—C12—N3—C20 is around 161 and 68° for conformer I and II, respectively. However, the conformer I and II energy difference is considerably large being 6.6 kJ mol^{-1} (lower for conformer I). The rather unfavorable conformer II is included in the crystal structure ensuring relative centrosymmetry. It has been argued in several studies that centrosymmetric structures offer better opportunities for close-packing of molecules[32,33] and it has been shown that one of the strongest interactions between the molecules in the crystals can be achieved when they are related by centers of inversion.[2,34] It could explain the single enantiomer's tendency to form such a *quasi*-centrosymmetric structure rather than crystallizing in an ordinary Sohncke space group structure.

Surprisingly, Hirshfeld surface fingerprint plots are very similar for both conformers in the structure of *enant*-**3** (see Figure S2), and unlike in case of *enant*-**1** no straightforward evidence is present that one of the conformers would seem less favorable in the particular crystal structure. However, in the structure of 0.80-**3** the disorder is only found in the conformer II site; consequently as many as possible molecules of **3** occupy conformation I. The scenario does not seem to differ from that discussed in the case of **1**. Furthermore conformer I is present in the crystal structure of *rac*-**3**. However, note that the space groups of *enant*-**3** and *rac*-**3** are not compatible. $P2_12_12_1$ is not a subgroup of *Pccn*, and therefore the limiting structures cannot be and are not isostructural (see Figure 12). However, there are considerable structural similarities present. Both structures comprise nearly identical $\pi\cdots\pi$ stacked blocks. In fact, the only difference between those blocks in *enant*-**3** and *rac*-**3** is that (due to crystal enantiomeric composition) they are enantiopure *quasi*-centrosymmetric in the former and genuinely centrosymmetric in the latter. Both structures in general differ by the shift between

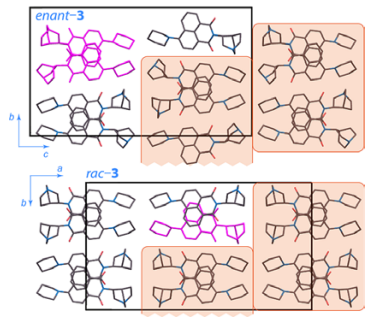

Figure 12. Structures of *enant*-**3** and *rac*-**3** (asymmetric units colored in magenta).

the adjacent blocks—1/4 shift of the cell edge in the enantiopure structure and 1/2 in the racemic one (see the rounded rectangles in Figure 12). Therefore, unlike in the case of **1**, no continuous stable solid solution exists in the complete composition range, but two distinct solid solutions (around the racemic and near the pure enantiomer composition regions) are present. It apparently indicates that a crystal structure is more stable if enantiopure blocks are packed with 1/4 shift and racemic ones—with 1/2 shift. The single crystal data (Table 3) indicate that 0.86-**3** and 0.70-**3** samples crystallize in $P2_12_12_1$ space group. The structures are isostructural to that of *enant*-**3**. Consequently, it can be concluded that also 86 and 70% enantiomeric composition samples like the enantiopure one tends to form structures with 1/4 shift of the adjacent blocks. On the contrary, the structure of 0.58-**3** is isostructural to that of *rac*-**3** (*Pccn* is a supergroup of $P2_12_12$) showing that 1/2 shift of the adjacent blocks is preferred in such composition samples. Unlike in the case of *rac*-**1**, no disorder of the asymmetric unit of *rac*-**3** could be successfully refined. Although there was some electron density in the positions corresponding to the atoms belonging to conformer II, the final structure model was better without any disorder. It is comprehensible that to refine a disorder for example of a carbon atom, the electron density to detect is comparable and lower than that of a hydrogen atom when the occupancy factor of the carbon atom is below 10%. Therefore, no strong statement can be made that the racemic crystal is indeed completely ordered, and there is no conformer II present in the crystal structure. Conformer II, however, is present in the 0.58-**3** and also in this case serves as a structural unit to form some *quasi*-centrosymmetric pairs due to lack of the opposite enantiomer.

Lattice energy calculations were performed to shed a light on the energetic aspects governing the reasons of differently shifted blocks in the experimental crystal structures. As lattice energy calculations cannot be directly carried out on disordered structures, only ordered phases were considered —enantiopure and racemic structures. It was also intriguing to explore the energetic aspects of other hypothetical but similar structures than those obtained experimentally (with different shifts of the blocks and blocks being either enantiopure of racemic). In Figure 13 all the variations of the structures are shown. Furthermore, the racemic structures were generated either with conformer I or conformer II in the asymmetric unit. The lattice energy values (and their breakdown) of the relaxed structures are shown in Table 4. The lattice energy calculations show that the most

DOI: 10.1021/acs.cgd.7b01146
Cryst. Growth Des. 2017, 17, 6477−6485

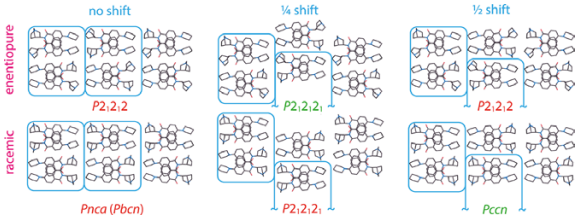

Figure 13. Experimental (space groups in green) and hypothetical (space groups in red) structures of compound **3**.

Table 4. Lattice Energy Values and Their Components of the Experimental and Hypothetical Crystal Structures of *rac*-3 and *enant*-3

	shift	structure	E_{Coul}/kJ mol^{-1}	E_{Pol}/kJ mol^{-1}	E_{Disp}/kJ mol^{-1}	E_{Rep}/kJ mol^{-1}	$E_{Lattice}$/kJ mol^{-1}
racemic	1/2	*Pccn* I[a]	−96.1	−51.8	−286.8	286.2	−148.5
	1/4	$P2_12_12_1$[b]	−100.2	−56.4	−295.2	311.6	−140.1
	1/2	*Pccn* II	−92.1	−54.0	−278.7	286.4	−138.4
	0	*Pnca* I	−90.6	−48.7	−269.9	271.2	−138.0
	0	*Pnca* II	−98.9	−56.4	−293.8	312.1	−137.1
enantiopure	1/4	$P2_12_12_1$[a]	−97.3	−50.6	−288.6	291.0	−145.6
	1/2	$P2_12_12$	−94.5	−50.7	−281.6	286.0	−140.8
	0	$P2_12_12$			[c]		

[a]Experimental structures. [b]Distinction between the conformers I and II lost upon the relaxation of the structure. [c]See the Experimental Methods.

favorable packings are formed when racemic blocks are packed with 1/2 shift and enantiopure ones with 1/4 shift, which corresponds to experimentally obtained structures. It can also be seen that unlike in racemic case the enantiopure structure with 1/2 shift is less stable than 1/4 shift phase, which is mostly due to less efficient dispersion and Coulombic interactions. For the racemic composition, however, the 1/4 shift phase looses to the 1/2 shift phase due to far more inefficient repulsion energy term, although the lattice energy stabilizing terms are in fact lower than those of the 1/2 shift phase. The lattice energy calculations are consistent with the experimentally determined structures. Furthermore, the calculations explain why two structurally distinct solid solutions form—one around the racemic composition and the other one near the enantiopure composition region.

CONCLUSIONS

On the basis of the knowledge of structural aspects of solid solutions of enantiomers a previously reported naphthalimide derivative **1** was found to show miscibility of the enantiomers in the solid state. Furthermore, two other compounds (**2** and **3**) were designed, synthesized, and shown to exist as solid solutions. Structural analysis showed that like in several other cases reported in the literature the driving force for solid solution formation is the possibility of forming *quasi*-centrosymmetric molecular arrangements in nonracemic crystals. It is ensured by existence of two conformers which are approximate mirror images within the one enantiomer. Such solid solutions belong to the type of solid solutions (classified based on crystallographic assumptions), which show some enantioselectivity in the solid state.[4−6] In the case of compounds for which the crystal structures were obtained (**1** and **3**) it was shown that both conformers are close to the minima in PES scans. The stability of the crystal structures is largely ensured by nondirectional interactions which are rather independent of the configuration of the molecule. Therefore, it can be concluded that formation of this type of solid solutions can be expected when (1) there are two reasonably favorable conformers possible of the enantiomer that are nearly mirror images to each other; and (2) the substituents of the chiral carbon are not directly involved in any specific interactions determining the stability of the packing. On the basis of these findings, it is thus possible to intentionally design solid solutions of enantiomers that rarely mix in the solid state.

The analysis of the intermolecular interactions either by Hirshfeld surfaces or DFT calculations revealed that one of the conformers is rather not favored in the crystal structures and was avoided when it was possible. Those findings actually explain reasons for partial enantioselectivity in this type of solid solutions. However, although racemic composition crystalline phases would be expected to show complete enantioselectivity, several racemic crystals of **1** were found to be disordered with approximately constant disorder degree. There was also a weak evidence of slightly disordered racemic structures of **3**. It is believed that the disorder has a thermodynamic origin and it is governed by the energetic aspects of the structures. For enantiopure and scalemic structures it seems that the less favorable conformer is tolerated to achieve apparent centrosymmetry, which yet again shows its importance in the crystal structures as the question might arise why do enantiopure samples not crystallize in ordinary Sohncke space group structures.

ASSOCIATED CONTENT

Supporting Information

The Supporting Information is available free of charge on the ACS Publications website at DOI: 10.1021/acs.cgd.7b01146.

Additional Hirsfeld surface fingerprint plots (PDF)

Accession Codes

CCDC 1569157−1569165 contain the supplementary crystallographic data for this paper. These data can be obtained free of

DOI: 10.1021/acs.cgd.7b01146
Cryst. Growth Des. 2017, 17, 6477−6485

charge via www.ccdc.cam.ac.uk/data_request/cif, or by emailing data_request@ccdc.cam.ac.uk, or by contacting The Cambridge Crystallographic Data Centre, 12 Union Road, Cambridge CB2 1EZ, UK; fax: +44 1223 336033.

AUTHOR INFORMATION

Corresponding Author

*E-mail: toms.rekis@lu.lv.

ORCID

Toms Rekis: 0000-0001-5128-4611
Simone d'Agostino: 0000-0003-3065-5860
Fabrizia Grepioni: 0000-0003-3895-0979

Notes

The authors declare no competing financial interest.

REFERENCES

(1) Murakami, H. In *Novel Optical Resolution Technologies*; Sakai, K., Hirayama, N., Tamura, R., Eds.; Springer: Berlin, Heidelberg, 2007; pp 273−299.
(2) Pidcock, E. Achiral molecules in non-centrosymmetric space groups. *Chem. Commun.* **2005**, *27*, 3457−3459.
(3) Jacques, J.; Collet, A.; Wilen, S. *Enantiomers, Racemates, and Resolutions*; Wiley, 1981.
(4) Chion, B.; Lajzerowicz, J.; Bordeaux, D.; Collet, A.; Jacques, J. Structural aspects of solid solutions of enantiomers: the 3-hydroxymethyl- and 3-carboxy-2,2,5,5-tetramethylpyrrolidinyl 1-oxyl systems as examples. *J. Phys. Chem.* **1978**, *82*, 2682−2688.
(5) Bredikhin, A. A.; Bredikhina, Z. A.; Zakharychev, D. V.; Gubaidullin, A. T.; Fayzullin, R. R. Chiral drug timolol maleate as a continuous solid solution: Thermochemical and single crystal X-ray evidence. *CrystEngComm* **2012**, *14*, 648−655.
(6) Brandel, C.; Petit, S.; Cartigny, Y.; Coquerel, G. Structural Aspects of Solid Solutions of Enantiomers. *Curr. Pharm. Des.* **2016**, *22*, 4929−4941.
(7) Rekis, T.; Bērziņš, A.; Orola, L.; Holczbauer, T.; Actiņš, A.; Seidel-Morgenstern, A.; Lorenz, H. Single enantiomer's urge to crystallize in centrosymmetric space groups: solid solutions of phenylpiracetam. *Cryst. Growth Des.* **2017**, *17*, 1411−1418.
(8) Whitesell, J. K.; Davis, R. E.; Wong, M. S.; Chang, N. L. Molecular crystal engineering by shape mimicry. *J. Am. Chem. Soc.* **1994**, *116*, 523−527.
(9) Kitaigorodsky, A. *Mixed Crystals*; Springer, 1984; pp 1−390.
(10) Chion, B.; Lajzerowicz, J.; Bordeaux, D.; Collet, A.; Jacques, J. Structural aspects of solid solutions of enantiomers: the 3-hydroxymethyl- and 3-carboxy-2,2,5,5-tetramethylpyrrolidinyl 1-oxyl systems as examples. *J. Phys. Chem.* **1978**, *82*, 2682−2688.
(11) Vaida, M.; Weissbuch, I.; Lahav, M.; Leiserowttz, L. Mixed Crystals as Host-Guest Systems for Probing Molecular Interactions. *Isr. J. Chem.* **1992**, *32*, 15−21.
(12) Shimon, J.; Vaida, M.; Addadi, L.; Lahav, M.; Leiserowitz, L. Molecular Recognition at the Solid-Solution Interface: A "Relay" Mechanism for the Effect of Solvent on Crystal Growth and Dissolution. *J. Am. Chem. Soc.* **1990**, *112*, 6215−6220.
(13) d'Agostino, S.; Braga, D.; Grepioni, F.; Taddei, P. Intriguing Case of Pseudo-Isomorphism between Chiral and Racemic Crystals of rac- and (S)/(R)2-(1,8-Naphthalimido)-2-quinuclidin-3-yl, and Their Reactivity Toward I2 and IBr. *Cryst. Growth Des.* **2014**, *14*, 821−829.
(14) Sheldrick, G. M. A short history of SHELX. *Acta Crystallogr., Sect. A: Found. Crystallogr.* **2008**, *64*, 112−122.
(15) Macrae, C. F.; Bruno, I. J.; Chisholm, J. A.; Edgington, P. R.; McCabe, P.; Pidcock, E.; Rodriguez-Monge, L.; Taylor, R.; van de Streek, J.; Wood, P. A. *Mercury CSD 2.0* − new features for the visualization and investigation of crystal structures. *J. Appl. Crystallogr.* **2008**, *41*, 466−470.
(16) Frisch, M. J. et al. *Gaussian Inc 09*, Revision D.01; Gaussian Inc.: Wallingford, CT, 2009.
(17) Giannozzi, P.; et al. QUANTUM ESPRESSO: a modular and open-source software project for quantum simulations of materials. *J. Phys.: Condens. Matter* **2009**, *21*, 395502.
(18) Grimme, S. Semiempirical GGA-type density functional constructed with a long-range dispersion correction. *J. Comput. Chem.* **2006**, *27*, 1787−1799.
(19) Lund, A. M.; Orendt, A. M.; Pagola, G. I.; Ferraro, M. B.; Facelli, J. C. Optimization of Crystal Structures of Archetypical Pharmaceutical Compounds: A Plane-Wave DFT-D Study Using Quantum Espresso. *Cryst. Growth Des.* **2013**, *13*, 2181−2189.
(20) Gavezzotti, A. Efficient computer modeling of organic materials. The atom-atom, Coulomb-London-Pauli (AA-CLP) model for intermolecular electrostatic-polarization, dispersion and repulsion energies. *New J. Chem.* **2011**, *35*, 1360−1368.
(21) Huang, J.; Chen, S.; Guzei, I. A.; Yu, L. Discovery of a Solid Solution of Enantiomers in a Racemate-Forming System by Seeding. *J. Am. Chem. Soc.* **2006**, *128*, 11985−11992.
(22) de Castro, R. A. E.; Canotilho, J.; Barbosa, R. M.; Silva, M. R.; Beja, A. M.; Paixão, J. A.; Redinha, J. S. Conformational Isomorphism of Organic Crystals: Racemic and Homochiral Atenolol. *Cryst. Growth Des.* **2007**, *7*, 496−500.
(23) Vogt, F. G.; Copley, R. C. B.; Mueller, R. L.; Spoors, G. P.; Cacchio, T. N.; Carlton, R. A.; Katrincic, L. M.; Kennady, J. M.; Parsons, S.; Chetina, O. V. Isomorphism, Disorder, and Hydration in the Crystal Structures of Racemic and Single-Enantiomer Carvedilol Phosphate. *Cryst. Growth Des.* **2010**, *10*, 2713−2733.
(24) Buttar, D.; Charlton, M. H.; Docherty, R.; Starbuck, J. Theoretical investigations of conformational aspects of polymorphism. Part 1: o-acetamidobenzamide. *J. Chem. Soc., Perkin Trans. 2* **1998**, *2*, 763−772.
(25) Starbuck, J.; Docherty, R.; Charlton, M.; Buttar, D. A theoretical investigation of conformational aspects of polymorphism. Part 2. Diarylamines. *J. Chem. Soc., Perkin Trans. 2* **1999**, *2*, 677−692.
(26) McKinnon, J. J.; Jayatilaka, D.; Spackman, M. A. Towards quantitative analysis of intermolecular interactions with Hirshfeld surfaces. *Chem. Commun.* **2007**, 3814−3816.
(27) Spackman, M. A.; Jayatilaka, D. Hirshfeld surface analysis. *CrystEngComm* **2009**, *11*, 19−32.
(28) Schmidt, M. U.; Glinnemann, J. Explanation for the stacking disorder in tris(bicyclo[2.1.1]hexeno)benzene using lattice-energy minimisations. *Z. Kristallogr. - Cryst. Mater.* **2012**, *227*, 805−817.
(29) Teteruk, J. L.; Glinnemann, J.; Gorelik, T. E.; Linden, A.; Schmidt, M. U. Explanation of the stacking disorder in the beta-phase of Pigment Red 170. *Acta Crystallogr., Sect. B: Struct. Sci., Cryst. Eng. Mater.* **2014**, *70*, 296−305.
(30) Teteruk, J. L.; Glinnemann, J.; Heyse, W.; Johansson, K. E.; van de Streek, J.; Schmidt, M. U. Local structure in the disordered solid solution of cis- and trans-perinones. *Acta Crystallogr., Sect. B: Struct. Sci., Cryst. Eng. Mater.* **2016**, *72*, 416−433.
(31) Taratin, N. V.; Lorenz, H.; Kotelnikova, E. N.; Glikin, A. E.; Galland, A.; Dupray, V.; Coquerel, G.; Seidel-Morgenstern, A. Mixed Crystals in Chiral Organic Systems: A Case Study on (R)- and (S)-Ethanolammonium 3-Chloromandelate. *Cryst. Growth Des.* **2012**, *12*, 5882−5888.
(32) Kitaigorodsky, A. *Organic Chemical Crystallography*; Consultants Bureau, 1961.
(33) Brock, C.; Dunitz, J. Towards a grammar of crystal packing. *Chem. Mater.* **1994**, *6*, 1118−1127.
(34) Filippini, G.; Gavezzotti, A. A quantitative analysis of the relative importance of symmetry operators in organic molecular crystals. *Acta Crystallogr., Sect. B: Struct. Sci.* **1992**, *48*, 230−234.

DOI: 10.1021/acs.cgd.7b01146
Cryst. Growth Des. 2017, 17, 6477−6485

III

Rekis, T.; Bērziņš, A.; Džabijeva, D.; Nakurte, I.;
Orola, L.; Actiņš, A.

Structure and Stability of Racemic and Enantiopure Pimobendan Monohydrates: On the Phenomenon of Unusually High Stability

Cryst. Growth Des. **2017**, 17(4), 1814–1823

CRYSTAL GROWTH & DESIGN

Article

pubs.acs.org/crystal

Structure and Stability of Racemic and Enantiopure Pimobendan Monohydrates: On the Phenomenon of Unusually High Stability

Toms Rekis,* Agris Bērziņš, Diāna Džabijeva, Ilva Nakurte, Liāna Orola, and Andris Actiņš

Department of Physical Chemistry, University of Latvia, Riga, Latvia

Supporting Information

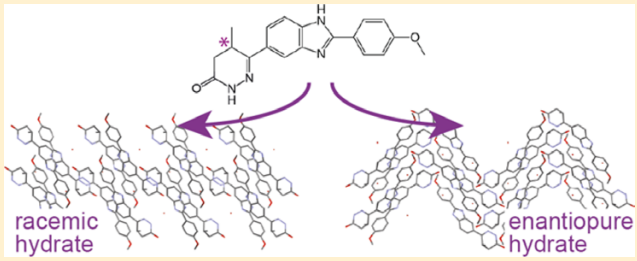

ABSTRACT: Study of structures and physicochemical properties of racemic (*rac*-H) and enantiopure (*enant*-H) hydrates of the active pharmaceutical ingredient pimobendan revealed that both hydrates have highly similar crystal structures and exhibit unusually high stability. Both structures contain identical two-dimensional layers and very similar conformations. The most significant difference is the stacking of these layers. The high stability of both hydrates appeared as extremely low solubility over a wide temperature range as well as an exceptionally high dehydration temperature and melting point. Study of the dehydration process showed that both hydrates have different activation energies of dehydration and kinetic model. Intermolecular interaction energy calculations showed that the dispersion interactions provide a highly significant stabilizing force in both pimobendan hydrates, while their exceptionally high stability can be associated with an efficient interplay between the hydrogen bonding and the dispersion interactions.

INTRODUCTION

Hydrates are of particular interest in the pharmaceutical industry. The occurrence of hydrates among organic compounds also applies to a significant fraction of pharmaceuticals (29% of active pharmaceutical ingredients (APIs) listed in the Pharmacopoeia European[1] or even 38% of APIs studied in SSCI polymorph screenings[2]). When selecting the most appropriate crystal form for manufacturing, its solubility, thermal stability over a range of water vapor pressure, mechanical properties, and other aspects are taken into account.[1] The possible formation of hydrates of a compound and the relevant stability studies are therefore important.

The stability of hydrates in general is determined by the crystal structure[3−5] (if other factors including the sample itself and its preparation can be assumed to be of a minor importance[6]) and depends on temperature and water activity it is exposed to.[7−9] However, dehydration as a process is affected by particle size and the crystallinity of the sample, as well as dehydration conditions, such as the heating rate, humidity, and inert gas flow rate.[10−15] Nevertheless, dehydration temperature, if determined for a well described system under well-defined conditions, is a meaningful parameter that can be used to compare the stability of hydrates (solvates).[16,17] Usually, by performing the dehydration of organic molecule hydrates upon heating, the onset temperature is below the boiling point of water.[10,16,18−21] Because of strong ion−dipole interactions, higher dehydration temperatures are observed for ionic organic compounds,[22] especially when a metal ion is present.[23,24]

Another way to assess the hydrate stability is to determine the temperature above which the hydrate is no longer thermodynamically stable. When a two-component phase diagram between the host compound and water is considered and the temperature of a hydrate is increased along an isopleth, congruent melting or incongruent melting (peritectic invariant) can be observed. Experimentally, fast heating rates can be applied or closed crucibles can be used to determine the melting point of a hydrate (solvate) by means of differential scanning calorimetry (DSC) or differential thermal analysis (DTA).[17,20,25,26] Furthermore, hydrate solubility studies in water are in fact sufficient to determine the peritectic points.[27,28]

Received: December 7, 2016
Revised: March 3, 2017
Published: March 10, 2017

DOI: 10.1021/acs.cgd.6b01780
Cryst. Growth Des. 2017, 17, 1814−1823

Among the usual techniques most conveniently used to explore hydrate stability and dehydration behavior, computational methods can be used to try to explain the stability of hydrates (solvates) and dehydration behavior,[17] as well as to explain or predict their formation.[29−31]

Pimobendan is an API used as a positive ionotrop and vasodilator mainly to treat heart failure either in veterinary or human medicine.[32,33] The chemical structure of pimobendan is shown in Figure 1. The molecule is chiral and it is marketed as

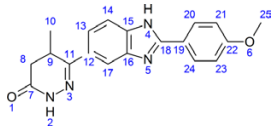

Figure 1. Chemical structure of pimobendan with the numbering scheme of non-hydrogen atoms used in this study.

a racemate. However, there are increasing demands for selecting only one enantiomer of an API for pharmaceutical use. As observed for enantiomers of many other chiral compounds, the pharmacokinetics and pharmacodynamics of pimobendan enantiomers differ.[33,34] So far only solid forms of racemic pimobendan have been reported—a number of polymorphs, solvates (1,4-dioxane, methanol), and a monohydrate have been described.[35,36] The solid form diversity of enantiopure pimobendan has not yet been discussed either in the scientific or patent literature. In the literature it is described that the dehydration of racemic pimobendan monohydrate occurs at 140 to 160 °C,[35] suggesting it has unusually high thermal stability. Besides, after resolving a racemic mixture of pimobendan, it was found that also enantiopure pimobendan very easily forms a monohydrate. Therefore, the aim of this study was to analyze the stability of racemic and enantiopure hydrates of pimobendan (*rac*-H and *enant*-H, respectively) by studying their solubility, dehydration behavior and kinetics, as well as crystal structures. As unusually high stability of both monohydrates was in fact observed, quantum chemistry calculations were performed to try to understand and explain this phenomenon based on the crystal structure information.

EXPERIMENTAL SECTION

Materials. Racemic pimobendan (>99.8%) was supplied by JSC Grindeks (Riga, Latvia). Pure enantiomer of pimobendan was resolved from the racemic mixture by classical resolution using (−)-*O*,*O*′-dibenzoyl-L-tartric acid. Purity (99.7% *ee*) was confirmed by chiral chromatography as described below. (−)-*O*,*O*′-dibenzoyl-L-tartric acid, phosphorus pentoxide, sodium dihydrogen phosphate, aqueous ammonia, and solvents (*N*,*N*-dimethylformamide, acetonitrile, ethanol, acetone, diethyl ether, methanol) were purchased from commercial sources. Water (<0.01 μS cm^{-1}) was deionized at the laboratory using ion-exchange resins, while that for chromatography (18.2 MΩcm) was prepared by a Milli-Q water purification system from Millipore (Billerica, Massachusetts, USA).

UPLC−TOF−MS. Chromatographic analyses were performed on a modular Agilent 1290 Infinity series UPLC system (Agilent Technologies, Germany). The experimental data were handled using MassHunter version B05.00 software (Agilent Technologies). LC separations were achieved by using an Extend-C18 RRHD 1.8 μm, 2.1 × 50 μm column (Agilent Technologies, USA). The elution solvents consisted of 0.1% formic acid in water and 0.1% formic acid in acetonitrile mixed in a linear gradient mode. The high resolution mass spectra were recorded on an Agilent 6230 TOF LC/MS instrument (Agilent Technologies, Germany) with electrospray ionization. The flow rate was maintained at 0.3 mL min^{-1}. The injection volume was 1.0 μL. More details are given in the Supporting Information.

Enantioseparations were achieved by using an ULTRON ES-OVM 5 μm, 4.6 × 150 μm column (Shinwa Chemical Industries Ltd., Japan) with a mobile phase composed of 90% 20 mol^{-1} sodium dihydrogen phosphate buffer solution with pH 6.0 (channel A) and 10% ethanol (channel B) in the isocratic mode at a flow rate of 1.0 mL min^{-1}. The injection volume was 2.0 μL and the column temperature was 25 °C, respectively. The UV detection of enantiomers was performed using a diode array detector at 328 nm. More details are given in the Supporting Information.

Single Crystal X-ray Diffraction. Single crystals of racemic and enantiopure pimobendan monohydrates (*rac*-H and *enant*-H) were grown by slow evaporation of an acetonitrile solution at ambient conditions. The data were collected at 173 K temperature on a Bruker Nonius Kappa CCD diffractometer using Mo−Kα radiation (graphite monochromator, wavelength of 0.71073 Å) (Bruker, Germany) and Oxford Cryostream (Oxford Cryosystems, UK) open-flow nitrogen cryostat for sample temperature control. The structures were solved by direct method and refined by full-matrix least-squares on F^2 for all data, using SHELX-2014 software suite.[37] The non-hydrogen atoms were refined anisotropically. For both crystal structures, the positions of all the hydrogen atoms were refined, and none were added geometrically.

Powder X-ray Diffraction (PXRD). PXRD patterns were determined on a Bruker D8 Advance diffractometer (Bruker, Germany) using copper radiation (Cu−Kα) at a wavelength of 1.5418 Å equipped with a LynxEye position sensitive detector (Bruker, Germany). The tube voltage and current were set to 40 kV and 40 mA. The divergence slit was set at 0.6 mm, and the antiscattering slit was set at 0.8 mm. The diffraction pattern was recorded in reflection mode using a scanning speed of 0.5 s/0.02° from 3° to 35° on 2θ scale. Variable temperature powder X-ray diffraction (VT-PXRD) patterns were measured on a Bruker D8 Discover diffractometer (Bruker, Germany) equipped with an MRI nonambient stage (Bruker, Germany). All of the settings and other equipment were identical to those used for the measurements on the D8 Advance diffractometer.

Solubility Determination. For solubility determination, samples of pimobendan hydrates and water were kept in closed vials for 2 weeks at 30, 40, 60, 70, 80, 90 °C. During that time, the vials were shaken to facilitate the approach to the solubility equilibrium. Aliquots of saturated solutions (200 μL) were taken using a micropipette and diluted with acetonitrile (200 μL) to avoid precipitation during cooling to ambient temperature. Three parallel samples were prepared in the same manner for each case. The concentrations of the samples were determined using high resolution mass spectra as described above and in the Supporting Information. The solubility at each temperature was calculated as an average value from three measurements of different samples. Confidence interval was calculated based on a Student's *t*-distribution with a 5% significance level.

Thermal Methods of Analysis. The DSC curves were recorded on a SETARAM DSC 111 instrument (SETARAM Instrumentation, France) at the heating rate of 1 K min^{-1}. A 40−50 mg sample was weighed in a 150 μL steel crucible, and the crucible was crimped. The air-tightness was verified by weighing the crucible before and after the experiment.

The DTA/TG curves were obtained using an SII Exstar6000 TG/DTA6300 instrument (EXSTAR, Japan). A 5−10 mg sample was weighed on an aluminum pan and heated at the rate of 0.5−20 K min^{-1} from 30 to 250 °C under a continuous nitrogen flow (200 mL min^{-1}).

For hot-stage microscopy, an Axio Lab.A1 (Zeiss, Germany) polarized light microscope equipped with a Standard LTS420 heating stage and a T95-Linksys heating controller (Linkam Scientific Instruments, UK) was used. The heating rate was 1 K min^{-1}. The crystals were heated without embedding into an oil, and no purge gas was used. Images were collected from an Axiocam ICc1 (Zeiss, Germany) digital microscope camera.

DOI: 10.1021/acs.cgd.6b01780
Cryst. Growth Des. 2017, 17, 1814−1823

Calculation of the Intermolecular Interaction Energy. Calculation of the intermolecular interaction energy was performed for the crystal structures of pimobendan monohydrates determined in this work, as well as for the crystal structures of selected monohydrates of other nonionic organic compounds obtained from the Cambridge Structural Database (fluconazole monohydrate (refcode IVUQJZ), nitrofurantoin monohydrate (HAXBUD), citric acid monohydrate (CITARC), lactose monohydrate (LACTOS), neotame monohydrate (HOFNAR), paracetamol monohydrate (HUMJEE), phenobarbital monohydrate (PHBARM), and polymorphs of gallic acid monohydrate IV, I°, and II (KONTIQ, KONTIQ01, and KONTIQ05, respectively)).

Intermolecular interaction energy was calculated according to the semiempirical PIXEL methodology (code provided in the CLP software suite).[38] Empirical parameters were used as provided in the literature.[38] The atom positions were obtained by standard procedure using RETCIF and RETCOR modules. The hydrogen atom positions were renormalized. Molecular electron density calculations were performed in Gaussian 09[39] at the MP2/6-31G(d,p) level using standard grid parameters. The condensation level 4 and a cutoff distance of 31−40 Å were used (depending on the size of the molecules).

RESULTS AND DISCUSSION

Crystal Structures of *rac*-H and *enant*-H Pimobendan. Racemic pimobendan hydrate (*rac*-H) crystallizes in the monoclinic crystal system, $P21/c$ space group. Enantiopure pimobendan hydrate (*enant*-H; the absolute configuration was not determined), however, crystallizes in the orthorhombic crystal system, $P2_12_12_1$ space group (see Table 1 for selected crystallographic data).

Table 1. Selected Crystallographic Data of *rac*-H and *enant*-H Pimobendan

	rac-H	*enant*-H
empirical formula	$C_{19}H_{18}N_4O_2{\cdot}H_2O$	$C_{19}H_{18}N_4O_2{\cdot}H_2O$
formula weight/g mol^{-1}	352.39	352.39
T/K	173	173
Mo Kα wavelength, λ/Å	0.71073	0.71073
crystal system	monoclinic	orthorhombic
space group	$P2_1/c$	$P2_12_12_1$
a/Å	6.5589(3)	6.41280(10)
b/Å	12.3073(4)	12.7755(3)
c/Å	21.1865(7)	20.4984(7)
α/°	90	90
β/°	98.298(2)	90
γ/°	90	90
V/Å^3	1692.32	1679.37
calculated density/g cm^{-3}	1.383	1.394
Z, Z'	4, 1	4, 1
reflections collected	4519	3831
reflections with $I > 2\sigma(I)$	2364	3089
final R ($I > 2\sigma(I)$)	0.0619	0.0487
goodness of fit F^2	0.993	1.047

Both hydrates contain one pimobendan and one water molecule in the asymmetric unit; furthermore, water molecules interact only with pimobendan molecules, and therefore both hydrates are isolated site hydrates with 1:1 pimobendan/water stoichiometry. The unit cell parameters of the studied monohydrates are very similar, and the geometries of the pimobendan molecules in the asymmetric units of *rac*-H and *enant*-H are nearly identical. The phenyl ring and the benzimidazole moiety of the pimobendan molecule are coplanar in both cases. The dihydropyridazone ring assumes a distorted twist-conformation. Rather identical geometries of pimobendan molecules in *rac*-H and *enant*-H crystals were confirmed by comparison of dihedral angles. The corresponding dihedral angle values were almost identical, the largest differences being only around 10° (see Table S1).

In both crystal structures pimobendan molecules form hydrogen bond NH4−H4···O1 and three hydrogen bonds with the water molecule (Figure 2). The corresponding

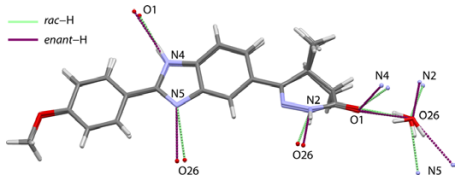

Figure 2. Representation of the asymmetric units of *rac*-H and *enant*-H pimobendan showing hydrogen bonds.

geometrical parameters of these hydrogen bonds as well as interaction energy associated with the molecules forming this bond (presented below) in both cases do not differ significantly (Table 2). On the basis of the geometrical parameters and interaction energy calculations all hydrogen bonds can be classified as medium strong.[40]

In spite of the almost identical asymmetric units and hydrogen bond networks, the structures of *rac*-H and *enant*-H crystals are not isostructural. However, both space groups apart from the identity operator also have a common symmetry operator $-x, 1/2 + y, 1/2 - z$. Furthermore, due to the similar unit cell parameters, two asymmetric units (x, y, z and $-x, 1/2 + y, 1/2 - z$) form periodic isostructural patterns (see Figure 3). This was also confirmed by comparing the molecular packing with the XPac program,[41,42] where identical 2D supramolecular constructs—layers parallel to (004)—were identified. The structural moieties shown in red in Figure 3 are isostructural. Besides, in Figure 2 the most different hydrogen bond O26−H26A···N5 is situated on the edge of these differently stacked layers. It was also observed that the different stacking of identical layers results in differences in hydrogen bond motifs: hydrogen bonds O26−H26B···O1 and N2−H2···O26 linking molecules within the same layer in both structures forms identical $C_2^2(6)$ graph set, while graph sets containing hydrogen bond O26−H26A···N5 linking molecules in adjacent layer differ ($R_4^4(20)$ graph set is formed by O26−H26A···N5 and N2−H2···O26 in *rac*-H, whereas $C_2^2(10)$ (formed by O26−H26A···N5 and N2−H2···O26) and $C_2^2(12)$ (formed by O26−H26A···N5 and O26−H26B···O1) is present in *enant*-H). Despite linking molecules in adjacent layers, in both structures N4−H4···O1 hydrogen bonds form $C_1^1(11)$ graph set, although the relative orientation of the linked molecules is different. Interestingly, the black colored moieties of both structures are mirror images to each other. This, however, leads to an optical phenomenon that when both structures are viewed along the crystallographic *a*-axis, they appear to be isostructural (Figure 3).

A calculation of the intermolecular interaction energy values in racemic and enantiopure pimobendan monohydrates was performed to try to further explore the structural similarities and differences. The corresponding energies associated with the

DOI: 10.1021/acs.cgd.6b01780
Cryst. Growth Des. 2017, 17, 1814−1823

Table 2. Geometrical Parameters for Hydrogen Bonds in *rac*-H and *enant*-H Pimobendan

	D−H···A	symmetry	d(D−H)/ Å	d(H···A)/ Å	d(D···A)/ Å	∠(D−H···A)/ °
rac-H	O26−H26A···N5	$2 - x, -y, 1 - z$	0.88(3)	1.93(3)	2.804(2)	171(3)
enant-H	O26−H26A···N5	$-3/2 + x, -1/2 - y, -z$	0.86(4)	2.03(4)	2.870(3)	166(4)
rac-H	O26−H26B···O1	x, y, z	0.91(3)	1.97(3)	2.876(2)	169(3)
enant-H	O26−H26B···O1	x, y, z	0.89(4)	2.07(4)	2.922(3)	160(4)
rac-H	N2−H2···O26	$-1 + x, y, z$[a]	0.96(2)	1.87(2)	2.809(3)	165.1(18)
enant-H	N2−H2···O26	$-1 + x, y, z$[a]	0.92(3)	1.89(3)	2.779(3)	162(3)
rac-H	N4−H4···O1	$1 + x, 1/2 - y, 1/2 + z$	0.91(2)	2.07(2)	2.977(2)	174.6(19)
enant-H	N4−H4···O1	$-1/2 - x, -y, 1/2 + z$	0.93(4)	2.04(4)	2.970(3)	174(3)

[a]Symmetry operation with respect to water O26 atom.

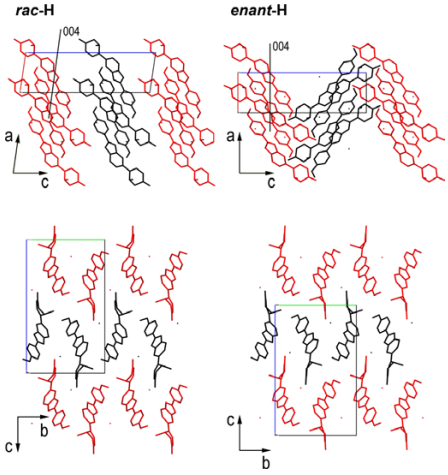

Figure 3. Molecular packing representation of *rac*-H and *enant*-H pimobendan viewed along the crystallographic *a*- and *b*-axis (red colored moieties are isostructural, the black ones are mirror images).

hydrogen bonds formed by water, as well as the most favorable interaction energies between pimobendan molecules are given in the Table 3 (breakdown of the total interaction energy into components is given in Table S2 and Table S3 in Supporting Information). It can be seen that the hydrogen bonding of water molecules is slightly more efficient in the crystal structure of *rac*-H, which correlates with the geometrical parameters of hydrogen bonds (see Table 2). However, *enant*-H has a lower lattice energy (by 5.8 kJ mol^{-1}, see Table S4), which is associated with denser packing (see Table 1) and mostly is due to the lower dispersion energy component in this crystal structure (see Table S3). The highest difference in interaction energy between hydrogen bonded molecules was observed for pimobendan molecules interacting via N4−H4···O1 (3.3 kJ mol^{-1}, due to different relative arrangement of the molecules) as well as, interestingly, between pimobendan and water molecules interacting via O26−H26B···O1 (2.8 kJ mol^{-1}) which in both structures appear to be arranged very similarly. Pimobendan molecules having the most efficient interactions (E_{Tot} being lower than −15 kJ mol^{-1}) are located in the identical layers of molecules (except for already mentioned hydrogen-bonded pimobendan molecules), with the highest difference for identically interacting molecules among both hydrates being only 3.5 kJ mol^{-1}.

Thermodynamic and Thermal Stability of *rac*-H and *enant*-H Pimobendan. Given the role of the crystal structure in determining the hydrate stability described in the Introduction, the observed high similarity in crystal structures of both studied hydrates suggests that both hydrates should have similar physicochemical properties. Initially evaluation of hydrate stability using water sorption−desorption analysis was considered. However, storing *rac*-H at 5% RH at temperatures up to 90 °C over 1 week did not introduce any observable dehydration. As the observed stability could be a result of kinetic factors, stability evaluation by slurrying hydrates in

Table 3. Interaction Energies between Selected Molecules in the Crystal Structure of *rac*-H and *enant*-H Pimobendan

rac-H		*enant*-H	
symmetry	E_{Tot}/ kJ mol^{-1}	symmetry	E_{Tot}/ kJ mol^{-1}
Interaction Energies between Pimobendan and Water Molecules			
x, y, z	−26.5	x, y, z	−23.7
$-1 + x, y, z$	−26.0	$-1 + x, y, z$	−26.4
$2 - x, -y, 1 - z$	−33.9	$-3/2 + x, -1/2 - y, -z$	−32.7
Interaction Energies between Pimobendan Molecules			
$1 + x, y, z$	−45.9	$1 + x, y, z$	−49.4
$-1 + x, y, z$	−45.9	$-1 + x, y, z$	−49.4
$-1 + x, 1/2 - y, -1/2 + z$	−42.8	$-1/2 - x, -y, 1/2 + z$	−39.5
$1 + x, 1/2 - y, 1/2 + z$	−42.8	$-1/2 - x, -y, -1/2 + z$	−39.5
$3 - x, -1/2 + y, 3/2 - z$	−22.9	$-x, 1/2 + y, 1/2 - z$	−20.0
$3 - x, 1/2 + y, 3/2 - z$	−22.8	$-x, -1/2 + y, 1/2 - z$	−20.0
$4 - x, 1/2 + y, 3/2 - z$	−16.1	$1 - x, 1/2 + y, 1/2 - z$	−16.2
$4 - x, -1/2 + y, 3/2 - z$	−16.1	$1 - x, -1/2 + y, 1/2 - z$	−16.2

DOI: 10.1021/acs.cgd.6b01780
Cryst. Growth Des. 2017, 17, 1814−1823

organic solvent−water mixtures with different water activity was also considered.[43,44] However, for example, using dry acetonitrile (water content ≤ 0.1%) and anhydrous pimobendan, the trace amount of water was enough to lead to the formation of pimobendan hydrates during the growth of single crystals. Thus, it was concluded that the phase boundary lies in the region with extremely low water activity, therefore complicating the experimental conditions for accurate phase boundary determination. Nevertheless, this observation confirms that both pimobendan hydrates *rac*-H and *enant*-H have very high thermodynamic stability.

Both hydrates show extremely low solubility in water even at elevated temperatures (see Figure 4). The quantification of pimobendan in saturated solutions was achieved using UPLC−TOF−MS as it was not possible to detect such small concentrations by any other method. The low solubility can be regarded as an indication for high thermodynamic stability as the congruent melting point of a hydrate is implicitly connected to solubility in such a way that it is actually a point on a solubility curve at a concentration equal to hydrate composition (see Figure S2).

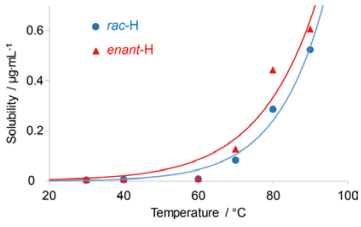

Figure 4. Solubility curves of pimobendan *rac*-H and *enant*-H. Error bars not attained as they were on average smaller than the depicted point size.

The solubility and its temperature dependence of both hydrates were very similar. The solubility curves (Figure 4) were fitted with the widely used Apelblat equation.[45,46] However, for some experimental data points rather strong deviations from the fitted curve was observed, which can be explained by experimental complications in determining such small concentrations. It, however, must be clarified that there are no isobaric invariants (peritectics) present on the solubility curves. The equilibrium solid phases at each temperature were analyzed by PXRD, confirming that the solubility was determined for no other crystal forms but the studied pimobendan monohydrates over the whole temperature range.

Thermal analysis was used to explore the behavior of pimobendan hydrates upon heating. The dehydration onset temperature of powdered pimobendan monohydrate *rac*-H when heated in open pan at 5 K min^{-1}, is 140 °C, whereas for *enant*-H under identical conditions it is 132 °C (see Figure 5). Therefore, the observed dehydration onset temperatures are higher than usually used reference point (boiling point of water) and in fact dehydration temperatures usually reported for hydrates of nonionic organic molecules in general (see Table S5).

The VT-PXRD method was used for a qualitative exploration of the dehydration process. Figure 6 shows the representation of PXRD patterns of *rac*-H and *enant*-H pimobendan as the dehydration occurs. It is seen from Figure 6 that amorphous

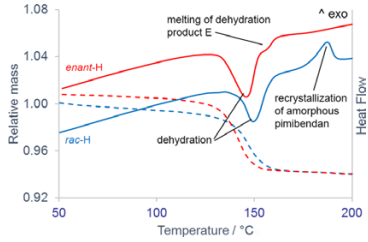

Figure 5. TG/DTA curves of *rac*-H and *enant*-H pimobendan at the heating rate of 5 K min^{-1} in open pans.

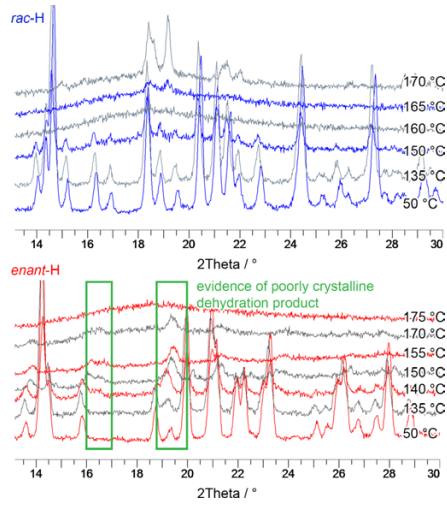

Figure 6. VT-PXRD patterns characterizing the dehydration process of pimobendan *rac*-H and *enant*-H.

pimobendan forms when *rac*-H is heated. At 150 °C, the diffraction peaks of hydrate are still present, whereas at 160 °C only the characteristic diffraction pattern of amorphous phase is observable. Right after that, at around 165 °C, recrystallization occurs and crystalline pimobendan polymorph D forms. In dehydration of *enant*-H, however, a poorly crystalline dehydration product E forms (see also Figure S1). At around 140 °C, a smooth transformation of *enant*-H into the dehydration product E is observed (the shift of hydrate diffraction peaks on the right is due to the sample displacement occurring upon dehydration). At 150 °C, only broad diffraction peaks of the dehydration product E are present, and subsequently it melts at around 165 °C. The phase transitions observed in VT-PXRD experiments are also visible in DTA curves presented above (Figure 5), while dissimilarities in the temperature of thermal events can be explained by the different heating rates applied (5 K min^{-1} for DTA and stepwise heating of around 1 K min^{-1} for VT-PXRD).

It is obvious from both VT-PXRD (Figure 6) and DTA study (Figure 5) that the dehydration product of *enant*-H (form E)

DOI: 10.1021/acs.cgd.6b01780
Cryst. Growth Des. 2017, 17, 1814−1823

had a very low crystallinity. DTA curves showed that the melting event of the *enant*-H dehydration product E was broad and its onset temperature varied depending on the heating rate applied (between 147 and 151 °C with heating rates of 0.5−5 K min^{-1}). As observed in the case of trehalose dihydrate dehydration, the crystallinity of the resulting solid phase significantly decreased as water was removed more rapidly.[47,48] The inability of *enant*-H to dehydrate under mild conditions led to rapid water removal at such high temperatures, resulting in a partially crystalline product E. Moreover, no long-range order was present in the dehydration product of *rac*-H as amorphous dehydration product was obtained.

To further explore the stability of pimobendan hydrates, congruent or incongruent melting points were determined using DCS measurements in closed crucibles. The behavior of pimobendan hydrate solubility curves already point to high thermodynamic stability. The low solubility and absence of a peritectic point up to 90 °C indicate that one has to deal with a two-component system involving non-negligible water vapor pressure to assess hydrate thermodynamic stability (like in the two cases reported for phenobarbital−water[49] and sulfaguanidine−water[21] systems). From DTA curves (Figure 5) it is also comprehensible that the melting points of both *rac*-H and *enant*-H pimobendan lie well above the boiling point of water. It was possible to obtain melting endotherms of pimobendan hydrates only using airtight steel crucibles (see Figure 7). It is

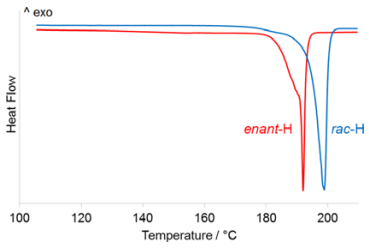

Figure 7. DSC curves of *rac*-H and *enant*-H pimobendan at the heating rate of 1 K min^{-1} in airtight steel crucibles.

seen from Figure 7 that *rac*-H melts at 195 °C, whereas *enant*-H at 191 °C. Broad endotherms prior the melting represent dehydration in the headspace of the crucible. It is, however, not simple in this case and was not in the scope of this study to distinguish whether the studied pimobendan hydrates melt congruently or incongruently. Because of the non-negligible vapor pressure two-component (water/pimobendan; strictly speaking, *rac*-H is a three-component system, however, an isophletal section with respect to pimobendan enantiomer racemic composition can be considered) phase diagrams can be complicated.

The experimental data show that *enant*-H has a lower thermal (kinetic) and thermodynamic stability than *rac*-H as the dehydration occurs at a lower temperature and the melting point is lower.

Dehydration Kinetics of *rac*-H and *enant*-H Pimobendan. To explore the kinetic stability of pimobendan hydrates their dehydration kinetics was studied. Specifically, the isoconversional average linear integral method (ALIM)[50] was used for calculating dehydration activation energy. A graph of the effective activation energy E_a versus the fraction dehydrated for pimobendan hydrates is presented in Figure 8. No systematic change in the effective activation energy is observed

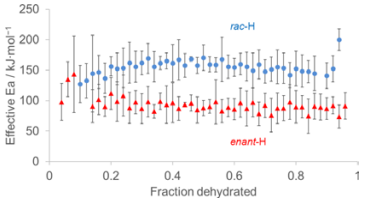

Figure 8. Effective dehydration activation energy versus the dehydrated fraction of *rac*-H and *enant*-H pimobendan.

either for *rac*-H or for *enant*-H. It follows that there is no change of the dehydration mechanism for pimobendan hydrates, considering the experimental conditions applied. The average effective activation energy of dehydration was 155(35) and 93(23) kJ mol^{-1} for *rac*-H and *enant*-H, respectively. Usually it ranges from around 60 to 140 kJ mol^{-1} for the dehydration of hydrates of nonionic organic molecules.[16,51−53] The effective dehydration activation energy of *enant*-H therefore falls into this interval, while that of *rac*-H is rather higher. Surely, the activation energy cannot be related to the thermodynamic stability of hydrates, but rather to how feasible is a structural transformation from one phase to another. As stated previously, the dehydration of *rac*-H leads to the formation of amorphous pimobendan. As the hydrate is of an isolated site type, dehydration requires complete disintegration of the crystal lattice that may be associated with a large energy barrier. On the contrary, dehydration of *enant*-H leads to the formation of a low crystallinity product. In such a case, the effective activation energy might be lower, as it was indeed confirmed experimentally.

The ALIM method also provides information about the kinetic model (assuming that it does not change). Experimental data were used to determine the dehydration kinetic models for pimobendan hydrates.[54] The correlation coefficients (a detailed description is given in an article by Ortega[50]) for the solid state kinetics models with the best fit are listed in Table 4.

For *rac*-H, high correlation coefficients were observed for geometrical contraction models (R3, R2), first-order reaction model (F1), and diffusion models (D1, D2). The statistical data and mechanistic considerations suggest that *rac*-H dehydrates by three-dimensional phase boundary model (R3), which is derived considering that the phase boundary is moving toward the center of a spherical/cubical particle.[54] Hot-stage microscopy results do not contradict this assumption (Figure 9 top). Upon heating of *rac*-H single crystals, their appearance remains unchanged until a liquid layer starts to form around the crystal at 160 °C. However, this must not be mistaken for a melting event, as (1) it is not rapid, but occurs over a wide temperature range, and (2) the determined melting point for this hydrate is significantly higher (see Figure 7). The formation of liquid can be explained by assuming that the amorphous phase formed in the dehydration process is in a liquid state. Such a dehydration could be described by the R3 kinetic model, as the phase boundary is moving inward from all three dimensions. Formation of liquid was also observed during the dehydration of powdered *rac*-H samples.

DOI: 10.1021/acs.cgd.6b01780
Cryst. Growth Des. 2017, 17, 1814−1823

Table 4. Correlation Coefficients Characterizing Linear Fit of *rac*-H and *enant*-H Pimobendan Dehydration to Commonly Used Kinetic Models

rac-H	model	R3	F1	D1	R2	D2	D4	A2	A3	D3	F0/R1
	R^2	0.997	0.997	0.996	0.996	0.995	0.993	0.993	0.988	0.987	0.986
enant-H	model	A3	A4	A2	F0/R1	R2	R3	F1	D1	D2	D4
	R^2	0.998	0.997	0.997	0.997	0.994	0.990	0.98	0.96	0.95	0.94

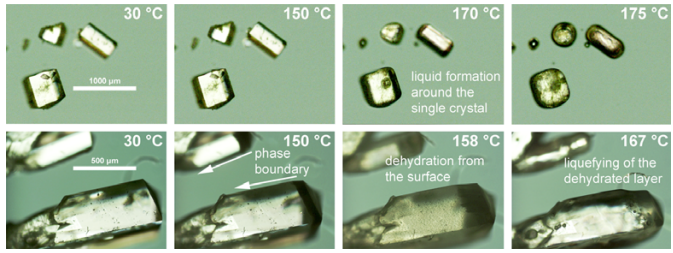

Figure 9. Hot-stage micrographs of *rac*-H (top) and *enant*-H (bottom) pimobendan dehydration.

For the dehydration of *enant*-H the highest correlation coefficients were for Avrami−Erofeev models (A3, A4, A2) and one-dimensional phase boundary model (R1). Avrami−Erofeev nucleation and nuclei growth models are disregarded in this case as it is expected that a high-crystallinity anhydrous phase would form during nuclei growth. However, in dehydration of *enant*-H low crystallinity polymorph E formed instead. It is believed that highly disordered structure results as the water molecules are rapidly removed from the initial solid phase. Therefore, it is reasonable to consider phase boundary model R1 for the dehydration kinetics of *enant*-H. Hot-stage microscopy in fact clearly showed that the phase boundary was moving in one dimension inward to the center of the single crystal (Figure 9 bottom). A noticeable dehydration progress was clearly visible starting from around 140 °C (at the heating rate of 1 K min^{-1}). It correlated with the VT-PXRD results, where diffraction peaks of dehydration product were present at 140 °C (Figure 6). It was noticed that at temperatures above 150 °C, regardless of heating rate, dehydration started in at least one more direction—the transparency of the single crystal was gradually lost (Figure 9). It obviously indicated the change of the dehydration mechanism. However, it should also be clarified that the dehydration of powdered samples and larger crystals may occur differently under the same conditions. In the experiments used for calculation of kinetic parameters, dehydration of *enant*-H had already been finished below 150 °C as the heating rates were small. However, when the kinetic model calculations were performed from experimental data with considerably larger heating rates, the highest correlation coefficient was in fact obtained for the two-phase boundary model (R2) in agreement with the observations in the hot-stage microscopy experiment. It is shown in Figure 9 that at around 167 °C a liquid layer had formed corresponding to the melting of the dehydration product E. After that, dehydration continued until the remaining crystals disappeared in the liquid phase.

Stability of Pimobendan Monohydrates in Context of the General Trends for Stability of Hydrates of Nonionic Organic Compounds. The presented study of pimobendan monohydrates *rac*-H and *enant*-H showed that these hydrates exhibit very high thermodynamic and thermal stability. To put the determined stability of these hydrates in the context, it was compared to the stability of hydrates of other nonionic organic compounds.

First, thermal stability characterized by the onset dehydration temperature of powder samples was determined to be 140 °C for *rac*-H and 132 °C for *enant*-H. For other hydrates of nonionic organic compounds found in the literature onset dehydration temperature are typically below 100 °C (see Table S5). Higher onset dehydration temperatures are reported for nitrofurantoin monohydrate (125 °C),[55] lactose monohydrate (138 °C),[16] as well as for mercaptopurine monohydrate and hemihydrate (125 and 240 °C respectively).[56,57] Therefore, it is clear that the thermal stability of both pimobendan hydrates is exceptionally high.

Second, melting points were determined to be 195 °C for *rac*-H and 191 °C for *enant*-H. On the basis of the values typically reported for hydrates of organic compounds, again it was concluded that so high melting points are not usual. For other hydrates peritectic temperatures are below 100 °C (see Table S5). Higher incongruent melting points up to around 140 °C are reported for phenobarbital monohydrate,[49] nitrofurantoin monohydrate,[55] methylene blue dihydrate,[27] and phloroglucinol dihydrate.[19] Peritectic temperature of mercaptopurine monohydrate is around 160 °C,[56] whereas sulfaguanidine monohydrate is reported to melt congruently at 148 °C.[21]

These observations together with the observed unusually low solubility and phase boundary lying in the region with extremely low water activity therefore put pimobendan monohydrates *rac*-H and *enant*-H among the most stable hydrates of nonionic organic compounds. In order to try to understand the origin of the high stability of pimobendan monohydrates, intermolecular interaction energy values were compared to those in selected few other monohydrates of nonionic organic compounds.

The interaction energies for the interactions formed by the water molecules showed that in pimobendan monohydrates these were among the least efficient if compared to those in other analyzed hydrates and therefore appears not explain the high stability of pimobendan hydrates (see Supporting Information). The contribution of the interaction energies between the host molecules and the water molecules (E_{API}-

DOI: 10.1021/acs.cgd.6b01780
Cryst. Growth Des. 2017, 17, 1814−1823

water) in the sum of all interaction energies for pimobendan monohydrates and other analyzed monohydrates were also compared. This contribution significantly varies (from 20 to 42%) and strongly depends on the size and properties of the APIs, and is 32 and 30% for *rac*-H and *enant*-H, respectively (see Table S6).

The lattice energy values reveal that a very important stabilizing force in the crystal structures of both pimobendan hydrates is the dispersion interactions (42% from the sum of Coulombic, polarization, and dispersion energies, see Table S6, Supporting Information). This is also confirmed by analyzing all pairwise intermolecular interactions (see Tables S2 and S3, Supporting Information), where the highest contribution to the total interaction energy is provided by molecules interacting mainly via dispersion interactions, instead of molecules interacting mainly via hydrogen bonds. In comparison, from the analyzed monohydrates of other APIs similar contribution of the dispersion interactions was present only in phenobarbital monohydrate (43%), whereas for other hydrates it was below 34%. Therefore, the stability of both pimobendan hydrates can be associated with an efficient interplay between the hydrogen bonding network and dispersion interactions in both crystal structures. And even though the interactions between pimobendan and water molecules are not among the most efficient (compared to API−water interactions in other hydrates), intramolecular interactions in pimobendan monohydrates in general apparently are very efficient due to the efficient interactions between pimobendan molecules themselves.

The high stability of phenobarbital monohydrate (melting temperature 123 °C[49]) can also be explained similarly as that of pimobendan monohydrates (with the most apparent difference being higher contribution from the water−API interactions due to smaller size of the API molecules). In comparison, the high thermal stability of lactose monohydrate (dehydration onset temperature 138 °C[16]) can be associated with the extensive hydrogen bond network formed mainly by the lactose molecules rather than the water molecules (the contribution from E_{API}-water in fact is only 20%). Also the most stable of the reported hydrates, mercaptopurine hemihydrate (dehydration onset temperature 240 °C), is stabilized mostly by an efficient hydrogen bond network, with dispersion interactions having a secondary role.[57]

CONCLUSIONS

This study showed that the very high similarity of pimobendan monohydrate *rac*-H and *enant*-H structures are reflected in similar bulk physicochemical properties, such as solubility, thermal stability, and melting point, in accordance with the well-known fact that most of the properties of solids originate from their crystal structure. Furthermore, both pimobendan monohydrates exhibited unusually high stability (confirmed by exceptionally high melting points, thermal stability as well as extremely low solubility) in comparison with that of other nonionic organic molecule hydrates.

Differences, however, were observed for *rac*-H and *enant*-H dehydration kinetics and products, apparently resulting from differences in the solid form landscape of racemic and enantiopure pimobendan. Dehydration of *enant*-H produced low crystallinity polymorph and was best described by the one-dimensional phase boundary model R1. Dehydration of *rac*-H, however, produced an amorphous phase and was best described by the three-dimensional phase boundary model R3. As expected, such a complete disintegration of molecular arrangement was associated with a high energy barrier, reflecting as higher dehydration activation energy, compared to the dehydration of *enant*-H.

Analysis of the intermolecular interaction energies showed that a highly significant stabilizing force in the crystal structures of both *rac*-H and *enant*-H is the dispersion interactions, and the contribution of the dispersion interactions to the total interaction energy is one of the highest among the analyzed API hydrates. Therefore, the exceptionally high stability of both pimobendan hydrates can be associated with an efficient interplay between the hydrogen bonding network and dispersion interactions in both crystal structures.

ASSOCIATED CONTENT

Supporting Information

The Supporting Information is available free of charge on the ACS Publications website at DOI: 10.1021/acs.cgd.6b01780.

Additional experimental details, additional information from crystal structure analysis, lattice energies of pimobendan monohydrates, individual patterns of the VT-PXRD study of *rac*-H and *enant*-H pimobendan dehydration process, dehydration temperatures, activation energies of dehydration, and melting points of selected API hydrates, interaction energy values in pimobendan monohydrates and other analyzed hydrates (PDF)

Accession Codes

CCDC 1453863−1453864 contain the supplementary crystallographic data for this paper. These data can be obtained free of charge via www.ccdc.cam.ac.uk/data_request/cif, or by emailing data_request@ccdc.cam.ac.uk, or by contacting The Cambridge Crystallographic Data Centre, 12 Union Road, Cambridge CB2 1EZ, UK; fax: +44 1223 336033.

AUTHOR INFORMATION

Corresponding Author

*E-mail: toms.rekis@lu.lv.

ORCID

Toms Rekis: 0000-0001-5128-4611

Notes

The authors declare no competing financial interest.

ACKNOWLEDGMENTS

The research work was supported by the University of Latvia Grant No. 6012-A55.2/48. The authors thank professors Heike Lorenz and Andreas Seidel-Morgenstern from the Max Planck Institute for Dynamics of Complex Technical Systems in Magdeburg for the opportunity to perform DSC and hot-stage microscopy measurements.

REFERENCES

(1) *European Pharmacopoeia*, 7th ed.; Council of Europe: Strasbourg, 2001.

(2) Stahly, G. P. Diversity in Single- and Multiple-Component Crystals. The Search for and Prevalence of Polymorphs and Cocrystals. *Cryst. Growth Des.* **2007**, *7*, 1007−1026.

(3) Vogt, F.; Brum, J.; Katrincic, L.; Flach, A.; Socha, J.; Goodman, R.; Haltiwanger, R. Physical, crystallographic, and spectroscopic characterization of a crystalline pharmaceutical hydrate: Understanding the role of water. *Cryst. Growth Des.* **2006**, *6*, 2333−2354.

(4) Byrn, S.; Pfeiffer, R.; Stowell, J. *Solid-State Chemistry of Drugs*; SSCI, Inc., 1999.
(5) Perrier, P.; Byrn, S. R. Influence of crystal packing on the solid-state desolvation of purine and pyrimidine hydrates: loss of water of crystallization from thymine monohydrate, cytosine monohydrate, 5-nitrouracil monohydrate, and 2′-deoxyadenosine monohydrate. *J. Org. Chem.* **1982**, *47*, 4671−4676.
(6) Brown, M.; Brown, R. Kinetic aspects of the thermal stability of ionic solids. *Thermochim. Acta* **2000**, *357*−*358*, 133−140.
(7) Hilfiker, R. *Polymorphism: In the Pharmaceutical Industry*; Wiley: New York, 2006; pp 1−414.
(8) Khankari, R.; Grant, D. Pharmaceutical hydrates. *Thermochim. Acta* **1995**, *248*, 61−79.
(9) Zhu, H.; Yuen, C.; Grant, D. Influence of water activity in organic solvent + water mixtures on the nature of the crystallizing drug phase. 1. *Int. J. Pharm.* **1996**, *135*, 151−160.
(10) Liu, W.; Dang, L.; Wei, H. Thermal, phase transition, and thermal kinetics studies of carbamazepine. *J. Therm. Anal. Calorim.* **2013**, *111*, 1999−2004.
(11) Griesser, U. J.; Burger, A. The effect of water vapor pressure on desolvation kinetics of caffeine 4/5-hydrate. *Int. J. Pharm.* **1995**, *120*, 83−93.
(12) Han, J.; Suryanarayanan, R. Influence of environmental conditions on the kinetics and mechanism of dehydration of carbamazepine dihydrate. *Pharm. Dev. Technol.* **1998**, *3*, 587−596.
(13) Han, J.; Suryanarayanan, R. A method for the rapid evaluation of the physical stability of pharmaceutical hydrates. *Thermochim. Acta* **1999**, *329*, 163−170.
(14) Agbada, C. O.; York, P. Dehydration of theophylline monohydrate powder - Effects of particle size and sample weight. *Int. J. Pharm.* **1994**, *106*, 33−40.
(15) Berzinš, A.; Actinš, A. Effect of experimental and sample factors on dehydration kinetics of mildronate dihydrate: Mechanism of dehydration and determination of kinetic parameters. *J. Pharm. Sci.* **2014**, *103*, 1747−1755.
(16) Shimanovich, R.; Cooke, M.; Peterson, M. L. A rapid approach to the preliminary assessment of the physical stability of pharmaceutical hydrates. *J. Pharm. Sci.* **2012**, *101*, 4013−4017.
(17) Berzinš, A.; Rekis, T.; Actinš, A. Comparison and rationalization of droperidol isostructural solvate stability: An experimental and computational study. *Cryst. Growth Des.* **2014**, *14*, 3639−3648.
(18) Censi, R.; Martena, V.; Hoti, E.; Malaj, L.; Di Martino, P. Sodium ibuprofen dihydrate and anhydrous: Study of the dehydration and hydration mechanisms. *J. Therm. Anal. Calorim.* **2013**, *111*, 2009−2018.
(19) Braun, D. E.; Tocher, D. a.; Price, S. L.; Griesser, U. J. The complexity of hydration of phloroglucinol: A comprehensive structural and thermodynamic characterization. *J. Phys. Chem. B* **2012**, *116*, 3961−3972.
(20) Braun, D. E.; Bhardwaj, R. M.; Arlin, J. B.; Florence, A. J.; Kahlenberg, V.; Griesser, U. J.; Tocher, D. a.; Price, S. L. Absorbing a little water: The structural, thermodynamic, and kinetic relationship between pyrogallol and its tetarto-hydrate. *Cryst. Growth Des.* **2013**, *13*, 4071−4083.
(21) Rouland, J.; Makki, S.; Fournival, J.; Céolin, R. Congruent melting of binary compounds with non-negligible vapour pressure. *J. Therm. Anal.* **1995**, *45*, 1507−1523.
(22) Chakravarty, P.; Berendt, R. T.; Munson, E. J.; Young, V. G.; Govindarajan, R.; Suryanarayanan, R. Insights into the dehydration behavior of thiamine hydrochloride (vitamin B1) hydrates: Part II. *J. Pharm. Sci.* **2010**, *99*, 1882−1895.
(23) Zupančič, V.; Ograjšek, N.; Kotar-Jordan, B.; Vrečer, F. Physical characterization of pantoprazole sodium hydrates. *Int. J. Pharm.* **2005**, *291*, 59−68.
(24) Murakami, F. S.; Lang, K. L.; Mendes, C.; Cruz, A. P.; Filho, M. A. S. C.; Silva, M. A. S. Physico-chemical solid-state characterization of omeprazole sodium: Thermal, spectroscopic and crystallinity studies. *J. Pharm. Biomed. Anal.* **2009**, *49*, 72−80.
(25) B̄erzinš, A.; Actinš, A. Dehydration of mildronate dihydrate: a study of structural transformations and kinetics. *CrystEngComm* **2014**, *16*, 3926−3934.
(26) Zencirci, N.; Gstrein, E.; Langes, C.; Griesser, U. J. Temperature and moisture dependent phase changes in crystal forms of barbituric acid. *Thermochim. Acta* **2009**, *485*, 33−42.
(27) Rager, T.; Geoffroy, A.; Hilfiker, R.; Storey, J. M. D. The crystalline state of methylene blue: a zoo of hydrates. *Phys. Chem. Chem. Phys.* **2012**, *14*, 8074−8082.
(28) Lafontaine, A.; Sanselme, M.; Cartigny, Y.; Cardinael, P.; Coquerel, G. Characterization of the transition between the monohydrate and the anhydrous citric acid. *J. Therm. Anal. Calorim.* **2013**, *112*, 307−315.
(29) Braun, D. E.; Oberacher, H.; Arnhard, K.; Orlova, M.; Griesser, U. J. 4-Aminoquinaldine monohydrate polymorphism: prediction and impurity aided discovery of a difficult to access stable form. *CrystEngComm* **2016**, *18*, 4053−4067.
(30) Braun, D.; Griesser, U. Why Do Hydrates (Solvates) Form in Small Neutral Organic Molecules? Exploring the Crystal Form Landscapes of the Alkaloids Brucine and Strychnine. *Cryst. Growth Des.* **2016**, *16*, 6405−6418.
(31) Loschen, C.; Klamt, A. Computational Screening of Drug Solvates. *Pharm. Res.* **2016**, *33*, 2794−2804.
(32) Gordon, S. G.; Miller, M. W.; Saunders, A. B. Pimobendan in Heart Failure Therapy - A Silver Bullet? *J. Am. Anim. Hosp. Assoc.* **2006**, *42*, 90−93.
(33) Chu, K. M.; Shieh, S. M.; Hu, O. Y. Pharmacokinetics and pharmacodynamics of enantiomers of pimobendan in patients with dilated cardiomyopathy and congestive heart failure after single and repeated oral dosing. *Clin. Pharmacol. Ther.* **1995**, *57*, 610−621.
(34) Bell, E. T.; Devi, J. L.; Chiu, S.; Zahra, P.; Whittem, T. The pharmacokinetics of pimobendan enantiomers after oral and intravenous administration of racemate pimobendan formulations in healthy dogs. *J. Vet. Pharmacol. Ther.* **2016**, *39*, 54−61.
(35) Boeren, M. M. M.; Paridaans, R. J.; Petkune, S.; Lusis, V.; Muceniece, D. Crystalline pimobendan, process for the preparation thereof, pharmaceutical composition and use, Patent EP 2 338 493 A1 The Netherlands, 2014.
(36) Zvirgzdins, A.; Delina, M.; Mishnev, A.; Actins, A. Pimobendan B from powder diffraction data. *Acta Crystallogr., Sect. E: Struct. Rep. Online* **2013**, *69*, o1677.
(37) Sheldrick, G. M. A short history of SHELX. *Acta Crystallogr., Sect. A: Found. Crystallogr.* **2008**, *64*, 112−122.
(38) Gavezzotti, A. Efficient computer modeling of organic materials. The atom-atom, Coulomb-London-Pauli (AA-CLP) model for intermolecular electrostatic-polarization, dispersion and repulsion energies. *New J. Chem.* **2011**, *35*, 1360−1368.
(39) Frisch, M. J. et al. *Gaussian 09*; Gaussian, Inc., Wallingford, CT, 2009.
(40) Steiner, T. The hydrogen bond in the solid state. *Angew. Chem., Int. Ed.* **2002**, *41*, 48−76.
(41) Gelbrich, T.; Hursthouse, M. B. A versatile procedure for the identification, description and quantification of structural similarity in molecular crystals. *CrystEngComm* **2005**, *7*, 324−336.
(42) Gelbrich, T. The XPac Program for Comparing Molecular Packing. *IUCr Newslett.* **2006**, *7*, 39−45.
(43) Touil, A.; Peczalski, R.; Timoumi, S.; Zagrouba, F. Influence of Air Temperature and Humidity on Dehydration Equilibria and Kinetics of Theophylline. *J. Pharm.* **2013**, *2013*, 1−9.
(44) Zhu, H.; Grant, D. Influence of water activity in organic solvent + water mixtures on the nature of the crystallizing drug phase. 2. Ampicillin. *Int. J. Pharm.* **1996**, *139*, 33−43.
(45) Liu, M.-j.; Yin, D.-p.; Fu, H.-l.; Zhang, Y.-l.; Liu, M.-x.; Zhou, J.-y.; Qing, X.-y.; Wu, W.-b. Solid-liquid equilibrium of azithromycin in water+1,2-propanediol solutions from (289.35 to 319.15) K. *J. Mol. Liq.* **2014**, *199*, 51−56.
(46) Dun, W.; Wu, S.; Tang, W.; Wang, X.; Sun, D.; Du, S.; Gong, J. Solubility of Ibuprofen Sodium Dihydrate in Acetone + Water

DOI: 10.1021/acs.cgd.6b01780
Cryst. Growth Des. 2017, 17, 1814−1823

Mixtures: Experimental Measurement and Thermodynamic Modeling. *J. Chem. Eng. Data* **2014**, *59*, 3415−3421.
(47) Rani, M.; Govindarajan, R.; Surana, R.; Suryanarayanan, R. Structure in Dehydrated Trehalose Dihydrate-Evaluation of the Concept of Partial Crystallinity. *Pharm. Res.* **2006**, *23*, 2356−2367.
(48) Willart, J. F.; Danede, F.; De Gusseme, A.; Descamps, M.; Neves, C. Origin of the Dual Structural Transformation of Trehalose Dihydrate upon Dehydration. *J. Phys. Chem. B* **2003**, *107*, 11158−11162.
(49) Fournival, J.; Rouland, J.; Ceolin, R. Le systeme EAU-phenobarbital. *J. Therm. Anal.* **1988**, *34*, 161−175.
(50) Ortega, A. A simple and precise linear integral method for isoconversional data. *Thermochim. Acta* **2008**, *474*, 81−86.
(51) Pinto, M. A. L.; Ambrozini, B.; Ferreira, A. P. G.; Cavalheiro, E. T. G. Thermoanalytical studies of carbamazepine: hydration/dehydration, thermal decomposition, and solid phase transitions. *Braz. J. Pharm. Sci.* **2014**, *50*, 877−884.
(52) Alkhamis, K. A.; Salem, M. S.; Obaidat, R. M. Comparison between dehydration and desolvation kinetics of fluconazole monohydrate and fluconazole ethylacetate solvate using three different methods. *J. Pharm. Sci.* **2006**, *95*, 859−870.
(53) Sheth, A. R.; Zhou, D.; Muller, F. X.; Grant, D. J. W. Dehydration kinetics of piroxicam monohydrate and relationship to lattice energy and structure. *J. Pharm. Sci.* **2004**, *93*, 3013−3026.
(54) Khawam, A.; Flanagan, D. R. Solid-state kinetic models: Basics and mathematical fundamentals. *J. Phys. Chem. B* **2006**, *110*, 17315−17328.
(55) Otsuka, M.; Teraoka, R.; Matsuda, Y. Rotating-Disk Dissolution Kinetics of Nitrofurantoin Anhydrate and Monohydrate at Various Temperatures. *Pharm. Res.* **1992**, *9*, 307−311.
(56) Niazi, S. Thermodynamics of mercaptopurine dehydration. *J. Pharm. Sci.* **1978**, *67*, 488−491.
(57) Kersten, K. M.; Matzger, A. J. Improved pharmacokinetics of mercaptopurine afforded by a thermally robust hemihydrate. *Chem. Commun.* **2016**, *52*, 5281−5284.

DOI: 10.1021/acs.cgd.6b01780
Cryst. Growth Des. 2017, 17, 1814−1823

IV

Rekis, T.; Bērziņš, A.; Orola, L.; Holczbauer, T.;
Actiņš, A.; Seidel-Morgenstern, A.; Lorenz, H.

Single Enantiomer's Urge to Crystallize in Centrosymmetric Space Groups: Solid Solutions of Phenylpiracetam

Cryst. Growth Des. **2017**, 17(3), 1411–1418

CRYSTAL GROWTH & DESIGN

Article

pubs.acs.org/crystal

Single Enantiomer's Urge to Crystallize in Centrosymmetric Space Groups: Solid Solutions of Phenylpiracetam

Toms Rekis,*[,†,‡] Agris Bērziņš,[‡] Līāna Orola,[‡] Tamás Holczbauer,[¶] Andris Actiņš,[‡] Andreas Seidel-Morgenstern,[†] and Heike Lorenz[†]

[†]Max Planck Institute for Dynamics of Complex Technical Systems, 39106 Magdeburg, Germany

[‡]Department of Physical Chemistry, University of Latvia, Riga, LV1004 Latvia

[¶]Institute of Organic Chemistry, Hungarian Academy of Sciences, 1117 Budapest, Hungary

Supporting Information

ABSTRACT: A detailed thermochemical and structural study of the phenylpiracetam enantiomer system was performed by characterizing the solid solutions, rationalizing the structural driving force for their formation, as well as identifying a common structural origin responsible for the formation of solid solutions of enantiomers. Enantiomerically pure phenylpiracetam forms two enantiotropically related polymorphs (*enant*−A and *enant*−B). The transition point (70(7) °C) was determined based on isobaric heat capacity measurements. Structural studies revealed that *enant*−A and *enant*−B crystallize in space groups $P1$ ($Z' = 4$) and $P2_12_12_1$ ($Z' = 2$), respectively. However, pseudoinversion centers were present resulting in apparent centrosymmetric structures. The quasi centrosymmetry was achieved by a large variety of phenylpiracetam conformations in the solid state (six in total). As a result, miscibility of the phenylpiracetam enantiomers in the solid state is present for scalemic and racemic samples, which was confirmed by the melt phase diagram. Racemic phenylpiracetam (*rac*−A) was determined to crystallize in the $P\bar{1}$ space group being isostructural to *enant*−A; furthermore, disorder is present showing that enantiomers are distributed in a random manner. The lack of enantioselectivity in the solid state is explained. Furthermore, structural aspects of phenylpiracetam solid solutions are discussed in the scope of other cases reported in the literature.

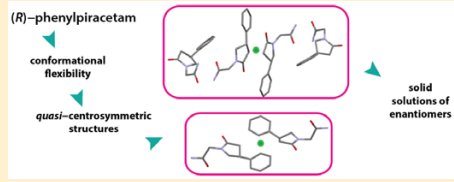

INTRODUCTION

Enantiomers of any chiral compound are indistinguishable with respect to achiral environments, but due to being incongruent objects, represent different building blocks when it comes to the formation of a crystal structure. Occasionally, solid solutions may form, where enantiomers are distributed randomly within the crystal—there is a lack of enantioselectivity in the solid state. However, according to the literature less than 1% of chiral compounds are able to form solid solutions;[1] therefore, they are not extensively studied.

For clear identification and characterization of solid solutions thermal methods of analysis can be employed by studying solid−liquid equilibrium of a given enantiomer system.[2,3] Detailed structural studies, however, help to better understand this rare phenomenon and possibly rationalize conditions governing formation of solid solutions. Nevertheless, comprehensible structural studies are done only for a handful of cases.[4−11]

General structural aspects of solid solutions have already been explained decades ago by Kitaigorodsky.[2] Recently reported cases[4−11] meanwhile serve as working examples for specifying, justifying, and rationalizing structural conditions required to observe the miscibility of enantiomers in the solid state. Formation of solid solutions of enantiomers is such a rare phenomenon because crystal and molecular structure must fulfill certain requirements. The enantiomers must be interchangeable with their opposite counterparts forming energetically efficient lattices. Therefore, to fit the opposite enantiomer in a crystallographic site there must be isosterism (strong analogy of the shapes)[12] present as well as the ability to maintain most stabilizing interactions in the crystal structure. Most of the previously reported cases[4−6,10,11] show a common structural feature—two molecules of the same configuration adjust conformation to form an apparent centrosymmetric relationship. Therefore, to predict if the enantiomers of a chiral compound can form solid solutions one has to answer questions like the following: Can the enantiomer adopt two conformations which are approximate mirror images to each other? Are those conformations energetically favorable? Will the most favorable interactions (e.g., hydrogen bonds or $\pi\cdots\pi$ stacking) stabilizing the crystal structure be preserved?

Here, we present an extended study on two recently reported[13] structurally distinct solid solutions formed by an active pharmaceutical ingredient phenylpiracetam—a mild

Received: December 20, 2016
Revised: January 31, 2017
Published: January 31, 2017

DOI: 10.1021/acs.cgd.6b01867
Cryst. Growth Des. 2017, 17, 1411−1418

nootropic drug (Figure 1). The aim of this study was to explain the lack of enantioselectivity of phenylpiracetam enantiomers in the solid state, as well as to justify the structural aspects of phenylpiracetam solid solutions in the scope of the previously reported cases of solid solutions of enantiomers. To characterize the phenylpiracetam solid solutions and achieve the aim, the melt phase diagram was obtained and crystal structures were studied.

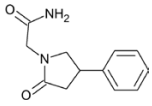

Figure 1. Molecular structure of phenylpiracetam.

EXPERIMENTAL METHODS

Materials. Racemic and (*R*)−phenylpiracetam (>99.8%) was supplied by JSC Olainfarm (Olaine, Latvia). Organic solvents were purchased from commercial sources.

Single Crystals. Single crystals of phenylpiracetam forms were grown by slow evaporation of an ethanol solution at ambient conditions.

Single Crystal X-ray Diffraction. The data were collected at 173 K on a Bruker Nonius Kappa CCD diffractometer using Mo Kα radiation (graphite monochromator, wavelength of 0.71073 Å) (Bruker, Germany) and Oxford Cryostream (Oxford Cryosystems, UK) open-flow nitrogen cryostat for sample temperature control. The structures were solved by direct methods and refined by full-matrix least-squares on F^2 for all data, using the SHELX-2014 software suite.[14] The non-hydrogen atoms were refined anisotropically. For *rac*−A where two independent disordered sites were found, the corresponding site occupancy factors (s.o.f.) of atoms were refined using SHELX command PART and two free variables.

Powder X-ray Diffraction. PXRD patterns were determined on a Bruker D8 Advance diffractometer (Bruker, Germany) using copper radiation (Cu Kα) at a wavelength of 1.5418 Å equipped with a LynxEye position sensitive detector (Bruker, Germany). The tube voltage and current were set to 40 kV and 40 mA. The divergence slit was set at 0.6 mm and the anti-scattering slit was set at 8.0 mm. The diffraction pattern was recorded using a scanning speed of 1 s/0.01° from 5° to 35° on 2θ scale. The lattice parameters were refined using the Rietveld method in the TOPAS5.0 software. The unit cell parameters, cell volume, and sample displacement were refined by minimizing the R_{wp} value.

Thermal Methods of Analysis. The DSC curves were recorded on a SETARAM DSC 131 instrument (SETARAM Instrumentation, France) at the heating rate of 0.5 to 5 K min^{-1}. Temperature and enthalpy calibration was done using indium, tin, and lead reference materials. A 4 to 10 mg sample was weighed in an aluminum crucible and the crucible was crimped. Melting temperatures and enthalpies of melting were calculated from 8 independent runs. Confidence interval was calculated based on a Student's *t*-distribution with a 5% significance level.

The isobaric heat capacity measurements were performed on a SETARAM DSC 111 instrument (SETARAM Instrumentation, France) operating with a Tian-Calvet type sensor. Temperature calibration was done using indium, tin, and lead reference materials. The calorimetric calibration of the sensor was done absolutely by the Joule effect (sapphire and water were used as test substances). An approximately 80 mg sample was weighed in a 150 μL aluminum crucible and the crucible was crimped. For liquid phase heat capacity measurements, the sample was first heated above the melting point and then slowly supercooled. The measurements were performed in a stepwise mode in 8 K steps with a heating rate of 5 K min^{-1}.

Melt Phase Diagram. The mixtures of different compositions were prepared by weighing racemic and enantiomerically pure samples on analytical balance (d = 0.1 mg). The samples were dissolved in ethanol and crystallized at room temperature. To obtain the samples of the biphasic region the melts were seeded with *enant*−B at elevated temperature (100 °C). Afterward the samples were ground in a mortar to ensure homogeneity. The DSC analyses were performed as described above. For solidus line (including the eutectic line) the onset temperatures of the respective DSC peaks were taken to construct the phase diagram. The DSC peak maxima were used for determination of the corresponding liquidus lines.

THEORETICAL BACKGROUND

Thermodynamic Characterization of Solid Solutions of Enantiomers. Solid solutions are isostructural single phases consisting of at least two components with variable compositions. Construction of a melt phase diagram of an enantiomeric system reveals formation of solid solutions (if any) as well as allows characterization of them by, e.g., assessing thermodynamic stability and miscibility limits. Figure 2 shows principal types of phase diagrams involving solid solutions (more sophisticated types of phase diagrams involving polymorphism and other thermodynamic invariants apart from eutectics are discussed in a review by Coquerel[3]). Miscibility around the racemic composition,[15] near the pure enantiomer region,[8,9,12] or covering the whole composition range[5,6,10,11,16−18] has been reported for particular compounds. The phase diagram obtained for a certain compound is governed by the thermodynamics of the respective solid phases. For example, in the case of miscibility around the

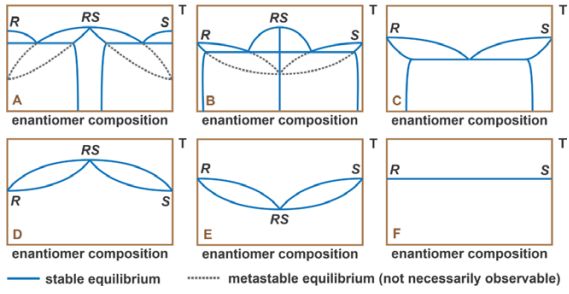

Figure 2. Melt phase diagrams of enantiomer systems involving solid solution formation (A−C partial and D−F full miscibility in solid state).

DOI: 10.1021/acs.cgd.6b01867
Cryst. Growth Des. 2017, 17, 1411−1418

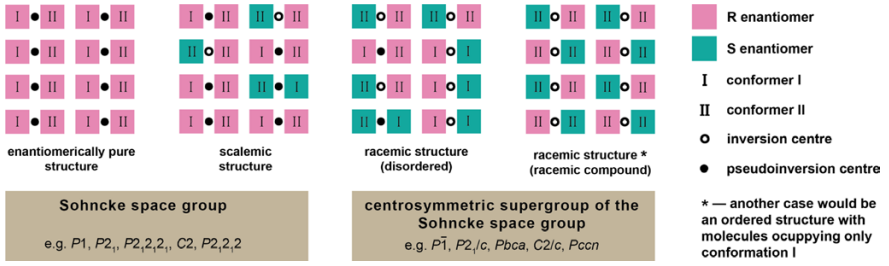

Figure 3. Graphical representation of the solid solution formation from two enantiomers.

racemic composition (Figure 2A) there is a racemic phase *RS* that must have a structural feature which allows exchange of the enantiomers with their opposite counterparts, therefore forming solid solutions with scalemic compositions. However, the miscibility region is not covering the whole composition range due to the existence of a stable structurally different enantiomerically pure solid phase *S* (or *R*). The miscibility region width and other quantitative phase diagram properties like, for example, eutectic composition and temperature are determined by properties of the solid phases *RS* and *S* (or *R*), namely, the enthalpies of melting and melting temperatures. In the case of miscibility close to the pure enantiomer region (Figure 2B and C) there is a solid phase *S* (or *R*) with a structural ability to form solid solutions. For case B a stable racemic compound *RS* emerges. Depicted metastable equilibria are not necessarily observable. For case C, however, limited miscibility arises because the solid solution at a certain composition is no longer thermodynamically stable and a mixture of two phases with the limiting compositions forms instead. Cases D, E, and F represent miscibility in the entire composition range for nonideal solid solutions with maximum and minimum melting temperatures at the racemic composition and ideal solid solutions, respectively. The solid phases *RS* and *S* (or *R*) in those cases are isostructural. Convex, concave, or ideal types of the phase diagram should be related to the relative stability of racemic and enantiomerically pure phases. So far, concave behavior is observed for most of the solid solutions showing miscibility in the complete composition range;[5,6,10,11,16,18,19] however, a convex type phase diagram[17] and nearly ideal behavior are also reported.[16]

Structural Aspects of Solid Solutions of Enantiomers. Due to physical and chemical considerations a single enantiomer can only crystallize in 1 of the 65 Sohncke space groups (without any symmetry element generating the opposite enantiomer, namely, inversion centers, mirror, or glide planes).[20] However, in crystal structures of most of the enantiomer solid solutions reported[4−6,10,11] apparent centrosymmetry is observed: molecules with identical configuration occupy different conformations which are approximate mirror images to each other. This structural feature is the core origin for formation of solid solutions of the first kind (two solid solutions apparently having another structural origin are reported[8,9]). The mentioned structural aspects describing the formation of solid solutions are illustrated in Figure 3. The enantiomerically pure sample crystallizes in a quasi centrosymmetric structure so that the absent enantiomer is mimicked by adjusting the conformation of the present enantiomer. Therefore, such a crystal structure has pseudoinversion centers. Scalemic structures may contain some genuine inversion centers. Two cases are depicted for racemic composition crystals—completely ordered structure (only genuine inversion centers are present; thus, all the molecules occupy only one of the conformations), and disordered structure. Disordered racemic structures form when, for example, an S enantiomer is deposited in a molecular site requiring the R enantiomer. In such cases, the conformation of the S enantiomer is switched to resemble that of the R enantiomer. Therefore, only conformers R_I — S_{II} and R_{II} — S_I are interchangeable in the structure (see Figure 3). Regardless of the disorder, the space group of the racemic composition crystal changes to a centrosymmetric supergroup of the Sohncke space group. In practice the asymmetric unit of the racemic crystal (in the case of disordered structure) appears to be a superimposition of a pair of molecules, e.g., R_I — S_{II}. So, with a certain probability either one or another conformation (and enantiomer) is observed in every molecular site. These probabilities can be determined during the structure solution by refining occupancy factors of the disordered atoms. Enantiomerically pure samples, on the contrary, can never be disordered (as long as any disorder does not arise for other reasons); therefore, their asymmetric unit contains an even number of molecules occupying different conformations—those superimposed in the racemic structure.

For example, (*RS*)-tazofelone[10] and (*RS*)-citalopram oxalate[6] crystallize in the P2$_1$/*c* space group showing disorder around the chiral center, while (*R*)-tazofelone[10] and (*S*)-citalopram oxalate[6] crystallize in the P2$_1$ space group with two molecules in the asymmetric unit occupying both conformations observed in the corresponding racemic crystals. Similarly, (*S*)-atenolol[4] and (*R*)-carvedilol phosphate hydrate[5] crystallize in the *C*2 space group (Z' = 2), while the respective racemic structures crystallize in the *C*2/*c* space group (Z' = 1, superimposition of the two conformers). Racemic timolol maleate is reported to crystallize in P$\bar{1}$ showing additional static disorder not involving the chiral center.[11] Scalemic timolol maleate crystallizes in the *P*1 space group with two quasi centrosymmetrically related timolol molecules in the asymmetric unit. Diprophylline solid solution with racemic composition is reported to crystallize in the P2$_1$/*c* space group with the asymmetric unit being a superimposition of two diprophylline conformers.[7] To draw a conclusion, the cases of solid solutions reported show that regardless of enantiomeric composition apparent centrosymmetric structures are formed.

DOI: 10.1021/acs.cgd.6b01867
Cryst. Growth Des. 2017, 17, 1411−1418

RESULTS AND DISCUSSION

Characterization of Phenylpiracetam Crystal Forms. Investigation of racemic and enantiomerically pure phenylpiracetam reveals that the racemic mixture crystallizes in one form (*rac*−A); however, two different crystal forms *enant*−A and *enant*−B can be obtained for an enantiomerically pure sample. PXRD patterns of all three crystalline phases are given in Figure 4. Nearly identical PXRD patterns of *rac*−A and

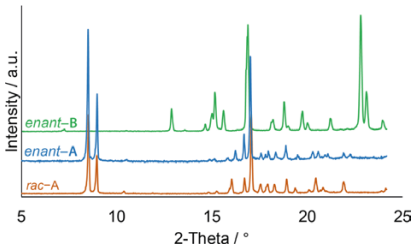

Figure 4. PXRD patterns of racemic and enantiomerically pure phenylpiracetam crystalline phases.

enant−A indicate very high structural similarity of those crystalline phases and yet, because of noticeable differences, conglomerate formation is disregarded in this case. However, it is suggested and further confirmed by the phase diagram that both phases are extreme cases of a solid solution. DSC study (Figure 5) shows that the melting of *enant*−A is accompanied

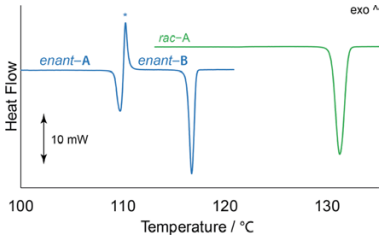

Figure 5. DSC curves of phenylpiracetam crystal forms (crystallization event marked with an asterisk).

by a subsequent crystallization of *enant*−B, which is observed as an exothermic peak. Melting points and enthalpies of melting are listed in Table 1. Melting enthalpy of *enant*−A was calculated taking into account that the overlapping exothermic peak must be of the same area as the peak of *enant*−B melting. As there are two single component phases (*enant*−A and *enant*−B) in the scope of studied system, the question arises whether there is a monotropic or an enantiotropic relationship between them. This was determined using the heat of fusion rule,[21] and according to the values of the enthalpy of melting (Table 1), it is suggested that *enant*−A and *enant*−B are enantiotropically related. The enantiotropic relationship was confirmed by slurrying the higher melting *enant*−B seeded with *enant*−A for a few days at room temperature in different solvents, after which only the characteristic PXRD peaks of *enant*−A were observed. Furthermore, when samples of pure *enant*−A were annealed at 100 °C, the unambiguous presence of *enant*−B was detected within a few days in terms of PXRD analysis. As the enantiotropic relationship holds, transition point (taking into account the experimental results just mentioned, between room temperature and 100 °C) must exist, at which both polymorphs are in thermodynamic equilibrium. Not a minor endothermic event, however, was observed in DSC analysis indicating the transition, when *enant*−A was used as a starting material. Since solid−solid transformations at the transition temperatures are most often kinetically hindered,[21] they are rarely clearly observed. In fact, *enant*−A was kinetically rather stable, as annealing samples of *enant*−A at 100 °C for 24 h lead to formation of *enant*−B only to a minor extent, while complete transformation was observed only after several days (see Figure S1). Although the thermodynamic transition point could not have been observed in DSC analysis, there are several accurate methods for determining the transition temperature of an enantiotropically related phase pair.[22] In the present study the transition point was determined based on a purely thermodynamic approach by calculating the Gibbs free energy difference of *enant*−A and *enant*−B as a function of temperature using isobaric heat capacity measurements (see Figure S2) and the determined melting temperatures and enthalpies of melting (Table 1). Figure 6 shows that the transition point for *enant*−A and

Table 1. Melting Points and Enthalpies of Melting of Phenylpiracetam Crystal forms

form	melting point/°C	ΔH^f/kJ mol^{-1}
rac−A	130.4	30.0(3)
enant−A	109.2	25.1(6)
enant−B	116.3	22.4(3)

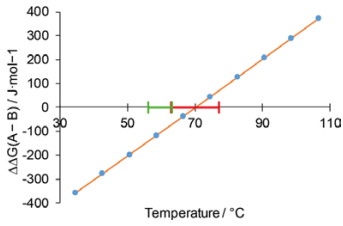

Figure 6. Gibbs free energy difference of *enant*−A and *enant*−B as a function of temperature (the green bar denotes an estimate transition temperature interval as determined from slurry bridging experiments).

enant−B transition is 70(7) °C. The detailed explanation and formulas for the Gibbs free energy difference calculation are given in the Supporting Information. The data points were fitted to the equation

$$\Delta G = A - BT + CT\ln T \quad (1)$$

which was derived based on thermodynamic grounds. Although coefficient standard errors were negligible, the large uncertainty arises from the total contribution of the errors for the enthalpy of melting (Table 1). Therefore, to calculate the transition point more precise, the enthalpy of melting has to be determined with higher accuracy. Furthermore, slurry bridging experiments in butanone and isopropyl acetate suggested that the transition point lies between 55 and 63 °C. Such a

DOI: 10.1021/acs.cgd.6b01867
Cryst. Growth Des. 2017, 17, 1411−1418

disagreement presents the role of precise enthalpy determination which in this case is particularly problematic for phase *enant*–A since the melting is followed by an overlapping crystallization event.

Two Component Phase Diagram of Phenylpiracetam Enantiomers. To clearly identify that *enant*–A and *rac*–A are limiting cases of a solid solution (*ss* $\alpha_{x=0}$ and *ss* $\alpha_{x=0.5}$, respectively), the melting behavior of samples with different composition was studied and the melt phase diagram was constructed (Figure 7). Furthermore, it was found also that

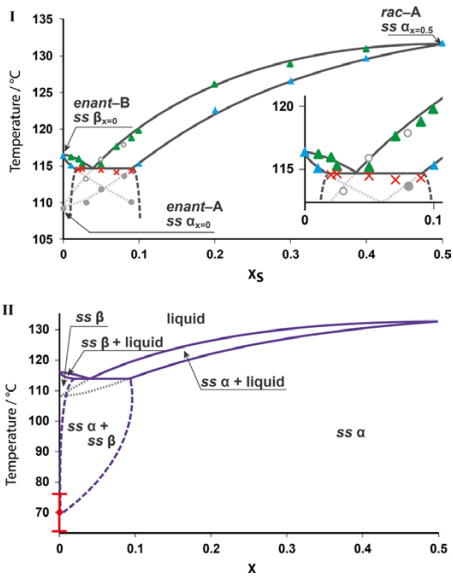

Figure 7. Two component phase diagram of phenylpiracetam enantiomer system. I: Showing experimental data points from DSC measurements (green ▲, liquidus of the stable equilibrium, cyan ▲, solidus of the stable equilibrium, red ×, eutectics, gray ○, liquidus of the metastable equilibrium, gray ●, solidus of the metastable equilibrium; the lines are guides for the eyes). II: Proposed general shape of the phase diagram taking into account the enantiotropic transition (red ●, transition temperature).

enant–B is a limiting case of another solid solution (*ss* $\beta_{x=0}$). There is a relatively narrow miscibility gap of phenylpiracetam enantiomer solid solutions α and β. Close to the eutectic temperature the biphasic region exists in enantiomeric composition range between 2% and 9%. This is because there is a large difference in melting points of the racemic composition phase and the enantiomerically pure phenylpiracetam *enant*–B. Therefore, it follows that the liquidus lines intersect far from the racemic composition. The eutectic invariant is observed at 114.4 °C and around enantiomeric composition 3:97. Due to the narrow miscibility gap and the position of the eutectic point it is not possible to determine the eutectic composition more accurately using the Tamman plot.

The metastable equilibrium of solid solution α can also be observed. As the enantiotropic relationship holds, samples where the mole fraction of the opposite enantiomer is below 0.1 crystallized at room temperature show absence of the eutectic melting. Continuation of the solidus and liquidus of the solid solution α reaching single enantiomer composition is therefore easily experimentally accessible. At temperatures below the enantiotropic phase transition point, phenylpiracetam enantiomers show complete miscibility in the solid state. Existence of the solid solution β may seem arguable as it is shown to exist in such a narrow composition region; however, β with a metastable composition can be accessed experimentally by seeding melts of different enantiomer compositions with *enant*–B. It is either depicted by continuation of the solidus line (Figure 7) or systematic and consistent lattice parameter change observed and discussed below (Figure 10). In general, the solvus can be determined by PXRD study of different composition phases,[8] as it cannot be done by means of DSC alone. In this case, however, a great many attempts to produce thermodynamically completely equilibrated biphasic compositions failed. Annealing samples at elevated temperature over several days usually resulted in partial decomposition of phenylpiracetam. Slurry–bridging experiments were not suitable in this case, as the studied compound showed extremely high solubility in many different solvents at elevated temperature. Finally, vapor-mediated equilibration was not successful and led to decomposition of the starting material. Deliquescence was also observed in some of the cases.

Structural Aspects of Phenylpiracetam Solid Solutions. To explore the structural aspects of solid solutions formed by the phenylpiracetam enantiomers, structures of *enant*–A, *enant*–B, and *rac*–A were determined. Selected crystallographic data of phenylpiracetam crystal structures are presented in Table 2. *enant*–A crystallizes in the triclinic crystal

Table 2. Selected Crystallographic Data of Phenylpiracetam Crystal Structures

	enant–B *ss* $\beta_{x=0}$	*enant*–A *ss* $\alpha_{x=0}$	*rac*–A *ss* $\alpha_{x=0.5}$
Crystal system	Orthorhombic	Triclinic	Triclinic
Space group	$P2_12_12_1$	$P1$	$P\bar{1}$
a/Å	8.1318(2)	6.11810(10)	6.07790(10)
b/Å	11.4712(3)	10.8017(3)	10.7615(3)
c/Å	24.0264(7)	17.2658(5)	17.4660(4)
α/°	90	76.5724(12)	76.6562(15)
β/°	90	84.5852(11)	85.8089(15)
γ/°	90	81.4105(18)	81.7617(9)
V/Å^{-3}	2241.22(10)	1095.27(5)	1099.14(4)
ρ_{calc}/g cm^{-3}	1.294	1.324	1.319
Z, Z'	8, 2	4, 4	4, 2
$R_{1[I>2\sigma(I)]}$	0.0603	0.0408	0.0448
S	1.037	1.080	1.044

system $P1$ space group, while *enant*–B crystallizes in the orthorhombic crystal system $P2_12_12_1$ space group. Both space groups as restricted by chemical composition are Sohncke space groups.[20] However, ignoring the positions of chiral carbons and a few surrounding atoms in the unit cell, both enantiomerically pure structures seem to possess higher symmetry resulting in the description of *enant*–A and *enant*–B structures with centrosymmetric space groups $P\bar{1}$ and $Pbca$, respectively (see Figure S3). The respective apparent space groups are supergroups of the former ones.[23] Quasi centrosymmetry is ensured by asymmetric units (Figure 8 I) containing even

DOI: 10.1021/acs.cgd.6b01867
Cryst. Growth Des. 2017, 17, 1411–1418

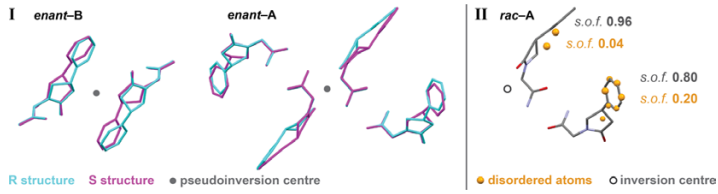

Figure 8. I: Superimposition of the asymmetric units of the enantiomorphic structures of *enant*−B (Z' = 2) and *enant*−A (Z' = 4). II: Asymmetric unit of *rac*−A (Z' = 2) showing disorder.

numbers of molecules related by a pseudoinversion center. Obviously, conformations of the molecules in these pairs differ—one of the conformers is mimicking the opposite enantiomer of the former conformer (pay attention to the overlay of the structures of opposite chirality). Furthermore, structures of *enant*−A and *rac*−A are isostructural and represent limiting cases of solid solution α as $\alpha_{x=0}$ and $\alpha_{x=0.5}$, respectively. The space groups of the corresponding structures are $P1$ and $P\bar{1}$, and the asymmetric unit of *rac*−A is therefore half that of *enant*−A and shows disorder around the chiral carbon (Figure 8 II). All four conformers found in the enantiomerically pure structure (*enant*−A) are present in the racemic one (*rac*−A). The occupancy factors of the conformers were refined for both molecular sites separately. As seen in Figure 8 I the largest differences for atomic positions in an overlaid pair are found for chiral carbons, whereas carbon atoms in the phenyl group show only minor differences. In the structure of *rac*−A, chiral carbons were clearly found to be disordered over two positions for both symmetrically independent molecules. However, the positions of some of the phenyl group carbons are obviously not refinable, as the electron density is describing thermal ellipsoids for atoms of the most probable conformer. In fact, only two of four conformers are most abundant in the racemic structure (*rac*−A). Even more, one of the molecular sites is nearly ordered showing disorder as low as 4%. The observed conformer abundance must be related to energetic causes. To sum up, structural origin of the formation of both solid solutions of phenylpiracetam is the same as that in most cases reported and discussed in the Theoretical Background section.

It is also worth noting the large variety of phenylpiracetam conformers within only two crystal structures: the *enant*−B asymmetric unit contains two symmetrically independent molecules, while there are four different conformers present in the *enant*−A (and *rac*−A) crystal structure. Conformers in pairs are approximate mirror images to each other, and are therefore able to form quasi centrosymmetric structures. It is surprising that a single enantiomer would rather occupy such a large diversity of conformations to try to form centrosymmetric structures rather than crystallizing in ordinary chiral structures. However, centrosymmetry in general is indeed very common among structures of organic molecules since nearly 90% of achiral molecules crystallize in centrosymmetric space groups.[24] As shown in numerous studies, centrosymmetric structures offer better opportunities for close-packing of molecules,[25,26] and inversion centers are favorable and can provide one of the strongest interactions between the molecules in the crystals.[24,27]

The crystal structures of solid solutions α and β are very different. In both cases each phenylpiracetam molecule forms four hydrogen bonds; however, the structures possess very different synthons and, thus, molecular packings. In *enant*−A there are two types of simple NH···O dimer synthons present (see Figure 9). The synthons are quasi centrosymmetric.

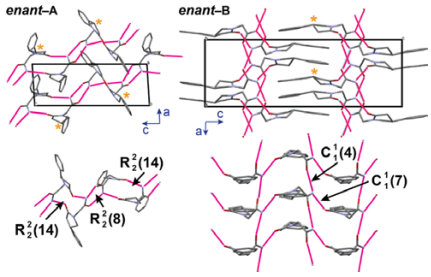

Figure 9. Packing representation and hydrogen bonding motifs of *enant*−A and *enant*−B structures (chiral centers marked with an asterisk).

Consequently, chains linked with hydrogen bonding motifs represented by $R_2^2(14)$ and $R_2^2(8)$ graph sets are observed. Different hydrogen bonding motifs represented by $C_1^1(4)$ and $C_1^1(7)$ graph sets have formed in *enant*−B (Figure 9), resulting in formation of layers. Quasi centrosymmetry is present between the molecules of two adjacent layers instead of hydrogen-bonded molecules like in *enant*−A. Therefore, the overall structures of phenylpiracetam crystal forms can be considered to be built by packing together chains in the case of α and layers in the case of β. The chains and layers are held together via dispersion interactions. It is worth noting that the substituents of the chiral carbons are not directly involved in the hydrogen bond network which therefore can be preserved if the configuration of the molecule is inverted. Furthermore, the inversion would rather affect dispersion interactions, which are significantly less directional and therefore probably would result only minor changes in the lattice energy. It is believed that in the case of phenylpiracetam the ability to preserve an efficient hydrogen bonding network and limited changes introduced to the overall lattice energy are the energetic reasons for the lack of recognition of the enantiomers in the solid state. However, detailed quantum chemical calculations would be required to justify this argument.

Variation of the lattice parameters over composition range were studied (Figure 10). Lattice parameter c in solid solution β and angle α in solid solution α are nearly constant over the studied composition range, which explains the observed low correlation coefficients for the respective relationships.

DOI: 10.1021/acs.cgd.6b01867
Cryst. Growth Des. 2017, 17, 1411−1418

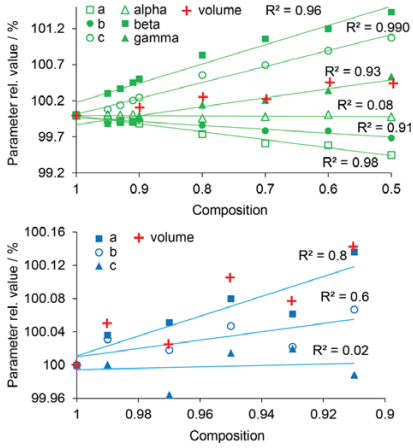

Figure 10. Dependence of the unit cell parameters and volume on the composition of the solid solutions α and β (top and bottom).

Interestingly, although solid solution β is thermodynamically stable only up to around 1% composition, a non-negligible change of parameters a and b can be observed up to around 9% composition (metastable equilibria as observed in the phase diagram (Figure 7)). For both solid solutions, change of the phase composition from enantiopure to racemic increases the unit cell volume. Therefore, the packing efficiency of structures with different enantiomeric compositions cannot be correlated to the stability if the melting point is chosen as a reference. Although both solid solutions α and β show higher packing efficiency for $x = 0$, the phase diagram (Figure 7) shows that the melting of different composition phases is of a concave type for α and convex for β.

CONCLUSIONS

A study of the active pharmaceutical ingredient phenylpiracetam showed that it forms two structurally distinct solid solutions α and β. Furthermore, the compound shows no recognition of the enantiomers in the solid state, as the whole enantiomeric composition range is composed of a solid solution or a mixture of two. The structural origin of phenylpiracetam solid solutions α and β is the same as that found for most of the already reported solid solutions formed by optically active compounds. Besides, α serves as an extraordinary example having up to 8 different species in the crystal structure (2 enantiomers able to occupy 4 different conformations) while there are 4 species in β. The presented phenylpiracetam example together with the other reported cases of solid solutions discussed suggest that the solid solution phenomenon could be a consequence of the high prevalence of organic molecules to crystallize in centrosymmetric space groups. The structures of phenylpiracetam *enant*−A and *enant*−B show that apparent centrosymmetry is achieved by an extensive variety of phenylpiracetam conformations present in the solid state. Furthermore, as the substituents of the chiral center are not directly involved in the formation of the supramolecular synthons, change of the configuration of the molecule preserves the hydrogen bond network. As a result, disordered structures form contradicting usually observed molecule arrangement in crystals in a strictly ordered fashion. However, this assures apparent centrosymmetry which seems to be of a greater importance in this case.

Common structural origin of the first kind of solid solutions of enantiomers is established allowing one to unambiguously justify it for similar cases where no thermodynamical evidence is present in the form of a phase diagram; therefore, SCXRD can be used to discover and characterize other solid solutions. Nevertheless, the present study also raises questions regarding whether and how to predict if a chiral molecule is able to form such disordered structures, and is it possible to intentionally design them.

ASSOCIATED CONTENT

Supporting Information

The Supporting Information is available free of charge on the ACS Publications website at DOI: 10.1021/acs.cgd.6b01867.

Additional PXRD results, results of the heat capacity measurements, formulas for the Gibbs free energy difference calculation (PDF)

Accession Codes

CCDC 1523460−1523462 contains the supplementary crystallographic data for this paper. These data can be obtained free of charge via www.ccdc.cam.ac.uk/data_request/cif, or by emailing data_request@ccdc.cam.ac.uk, or by contacting The Cambridge Crystallographic Data Centre, 12, Union Road, Cambridge CB2 1EZ, UK; fax: +44 1223 336033.

AUTHOR INFORMATION

Corresponding Author

*E-mail: toms.rekis@lu.lv.

ORCID

Toms Rekis: 0000-0001-5128-4611

Notes

The authors declare no competing financial interest.

ACKNOWLEDGMENTS

Work was supported by University of Latvia, grant No. 6012-AS5.2/48 and by University of Latvia Foundation awarding Toms Rekis a Kurt Hagen's Scholarship.

REFERENCES

(1) Jacques, J.; Collet, A.; Wilen, S. *Enantiomers, racemates, and resolutions*; Wiley, 1981.

(2) Kitaigorodsky, A. *Mixed Crystals*; Springer, 1984; pp 1−390.

(3) Coquerel, G. Review on the heterogeneous equilibria between condensed phases in binary systems of enantiomers. *Enantiomer* **2000**, *5*, 481−498.

(4) Esteves de Castro, R. A.; Canotilho, J.; Barbosa, R. M.; Silva, M. R.; Beja, A. M.; Paixão, J. A.; Redinha, J. S. Conformational Isomorphism of Organic Crystals: Racemic and Homochiral Atenolol. *Cryst. Growth Des.* **2007**, *7*, 496−500.

(5) Vogt, F. G.; Copley, R. C. B.; Mueller, R. L.; Spoors, G. P.; Cacchio, T. N.; Carlton, R. A.; Katrincic, L. M.; Kennady, J. M.; Parsons, S.; Chetina, O. V. Isomorphism, Disorder, and Hydration in the Crystal Structures of Racemic and Single-Enantiomer Carvedilol Phosphate. *Cryst. Growth Des.* **2010**, *10*, 2713−2733.

(6) de Diego, H. L.; Bond, A. D.; Dancer, R. J. Formation of solid solutions between racemic and enantiomeric citalopram oxalate. *Chirality* **2011**, *23*, 408−416.

(7) Brandel, C.; Amharar, Y.; Rollinger, J. M.; Griesser, U. J.; Cartigny, Y.; Petit, S.; Coquerel, G. Impact of Molecular Flexibility on

DOI: 10.1021/acs.cgd.6b01867
Cryst. Growth Des. 2017, 17, 1411−1418

Double Polymorphism, Solid Solutions and Chiral Discrimination during Crystallization of Diprophylline Enantiomers. *Mol. Pharmaceutics* **2013**, *10*, 3850−3861.
(8) Taratin, N. V.; Lorenz, H.; Kotelnikova, E. N.; Glikin, A. E.; Galland, A.; Dupray, V.; Coquerel, G.; Seidel-Morgenstern, A. Mixed Crystals in Chiral Organic Systems: A Case Study on (R)- and (S)-Ethanolammonium 3-Chloromandelate. *Cryst. Growth Des.* **2012**, *12*, 5882−5888.
(9) Wermester, N.; Aubin, E.; Pauchet, M.; Coste, S.; Coquerel, G. Preferential crystallization in an unusual case of conglomerate with partial solid solutions. *Tetrahedron: Asymmetry* **2007**, *18*, 821−831.
(10) Huang, J.; Chen, S.; Guzei, I. A.; Yu, L. Discovery of a Solid Solution of Enantiomers in a Racemate-Forming System by Seeding. *J. Am. Chem. Soc.* **2006**, *128*, 11985−11992.
(11) Bredikhin, A. A.; Bredikhina, Z. A.; Zakharychev, D. V.; Gubaidullin, A. T.; Fayzullin, R. R. Chiral drug timolol maleate as a continuous solid solution: Thermochemical and single crystal X-ray evidence. *CrystEngComm* **2012**, *14*, 648−655.
(12) Chion, B.; Lajzerowicz, J.; Bordeaux, D.; Collet, A.; Jacques, J. Structural aspects of solid solutions of enantiomers: the 3-hydroxymethyl- and 3-carboxy-2,2,5,5-tetramethylpyrrolidinyl 1-oxyl systems as examples. *J. Phys. Chem.* **1978**, *82*, 2682−2688.
(13) Rekis, T.; Berzins, A.; Orola, L.; Actins, A.; Seidel-Morgenstern, A.; Lorenz, H. On the formation of phenylpiracetam solid solutions: thermodynamic and structural considerations; *Proceedings 23rd Int Workshop on Industrial Crystallization (BIWIC 2016)*, 2016; pp 106−111.
(14) Sheldrick, G. M. A short history of SHELX. *Acta Crystallogr., Sect. A: Found. Crystallogr.* **2008**, *64*, 112−122.
(15) Kaemmerer, H.; Lorenz, H.; Black, S. N.; Seidel-Morgenstern, A. Study of System Thermodynamics and the Feasibility of Chiral Resolution of the Polymorphic System of Malic Acid Enantiomers and Its Partial Solid Solutions. *Cryst. Growth Des.* **2009**, *9*, 1851−1862.
(16) Bredikhin, A. A.; Bredikhina, Z. A.; Zakharychev, D. V. Crystallization of chiral compounds: Thermodynamical, structural and practical aspects. *Mendeleev Commun.* **2012**, *22*, 171−180.
(17) Gallis, H.; Bougrioua, F.; Oonk, H.; van Ekeren, P.; van Miltenburg, J. Mixtures of d- and l-carvone: I. Differential scanning calorimetry and solid-liquid phase diagram. *Thermochim. Acta* **1996**, *274*, 231−242.
(18) Oonk, H.; Tjoa, K.; Brants, F.; Kroon, J. The carvoxime system. *Thermochim. Acta* **1977**, *19*, 161−171.
(19) Li, Y.; Zhao, Y.; Zhang, Y. Solid Tryptophan as a Pseudoracemate: Physicochemical and Crystallographic Characterization. *Chirality* **2015**, *27*, 88−94.
(20) Flack, H. D. Chiral and Achiral Crystal Structures. *Helv. Chim. Acta* **2003**, *86*, 905−921.
(21) Hilfiker, R. *Polymorphism: In the Pharmaceutical Industry*; Wiley, 2006; pp 1−414.
(22) Qi, M.-H.; Hong, M.-H.; Liu, Y.; Wang, E.-F.; Ren, F.-Z.; Ren, G.-B. Estimating Thermodynamic Stability Relationship of Polymorphs of Sofosbuvir. *Cryst. Growth Des.* **2015**, *15*, 5062−5067.
(23) Ivantchev, S.; Kroumova, E.; Madariaga, G.; Pérez-Mato, J.; Aroyo, M. SUBGROUPGRAPH: A computer program for analysis of group-subgroup relations between space groups. *J. Appl. Crystallogr.* **2000**, *33*, 1190−1191.
(24) Pidcock, E. Achiral molecules in non-centrosymmetric space groups. *Chem. Commun.* **2005**, *27*, 3457−3459.
(25) Kitaigorodsky, A. *Organic chemical crystallography*; Consultants Bureau, 1961.
(26) Brock, C.; Dunitz, J. Towards a grammar of crystal packing. *Chem. Mater.* **1994**, *6*, 1118−1127.
(27) Filippini, G.; Gavezzotti, A. A quantitative analysis of the relative importance of symmetry operators in organic molecular crystals. *Acta Crystallogr., Sect. B: Struct. Sci.* **1992**, *48*, 230−234.

DOI: 10.1021/acs.cgd.6b01867
Cryst. Growth Des. 2017, 17, 1411−1418

V

Rekis, T.; Bērziņš, A.; Orola, L.; Actiņš, A.;
Seidel-Morgenstern, A.; Lorenz, H.

On the formation of phenylpiracetam solid solutions:
thermodynamic and structural considerations

Proceedings 23rd Int Workshop on Industrial Crystallization (BIWIC 2016) **2016**, 106–111

On the formation of phenylpiracetam solid solutions: thermodynamic and structural considerations

T. Rekis[1,2], A. Berzins[1], L. Orola[1], A. Actins[1], A. Seidel-Morgenstern[2], H. Lorenz[2]

[1]University of Latvia, Riga, Latvia;
[2]Max Planck Institute for Dynamics of Complex Technical Systems, Magdeburg, Germany;
toms.rekis@lu.lv

The present study shows a rare case of solid solutions formed by the pharmaceutically active ingredient phenylpiracetam. Two structurally independent solid solutions (α and β) have been discovered. Homochiral crystal forms (limiting cases of solid solutions — $\alpha_{x=0}$ and $\beta_{x=0}$, respectively) were found to be enantiotropically related. The transition temperature was calculated using data from isobaric heat capacity, melting temperature and enthalpy of melting measurements. Consequently, α shows complete miscibility in the solid state, while β shows miscibility near pure enantiomer composition region at temperatures above the transition point. The structures of phenylpiracetam crystal forms were determined, revealing that the studied molecule occupies in total six different conformations in the solid state. The structural origin of solid solution formation is discussed.

1 Introduction

Crystallization of racemic substances frequently brings up some interesting issues. Enantiomers of any chiral compound are indistinguishable with respect to achiral environments, but represent different building blocks when it comes to the formation of a crystal structure. Rarely solid solutions may form[1], where enantiomers are distributed randomly within the crystal. Thermal methods of analysis can be employed to identify and characterise them by studying the solid–liquid equilibrium for a given enantiomer system[2, 3]. The origin of the lack of molecular site stereoselectivity arises from the crystal structure. The two enantiomers are found to be homeomorphic — able to interchange each other within a molecular site. Comprehensive structure and phase diagram studies therefore can bring some clarity on the aspects of solid solution existence and conditions governing their formation. Here we report a case of two solid solutions formed by the active pharmaceutical ingredient phenylpiracetam — a mild nootropic drug (Figure 1).

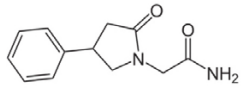

Fig. 1: Molecular structure of phenylpiracetam.

2 Experimental Methods

2.1 Materials

Racemic and homochiral phenylpiracetam (>99.8 %) was supplied by JSC *Olainfarm* (Olaine, Latvia). Organic solvents were purchased from commercial sources.

2.2 Single crystals

Single crystals of homochiral phenylpiracetam forms (*hom*–A and *hom*–B) were grown by slow evaporation of an ethanol solution at ambient conditions.

2.3 Single crystal X-ray diffraction

The data were collected at 173 K on a Bruker Nonius Kappa CCD diffractometer using Mo-Kα radiation (graphite monochromator, wavelength of 0.710 73 Å) (*Bruker*, Germany). The structures were solved by direct method and refined by full-matrix least squares on F^2 for all data, using SHELX-2014 software suite. The non-hydrogen atoms were refined anisotropically.

2.4 Powder X-ray diffraction

PXRD patterns were determined on a Bruker D8 Advance diffractometer (*Bruker*, Germany) using copper radiation (Cu-Kα) at a wavelength of 1.5418 Å equipped with a LynxEye position sensitive detector (*Bruker*, Germany). The tube voltage and current were set to 40 kV and 40 mA. The diffraction patterns were recorded using a scanning rate of 0.5 s/0.02° from 3° to 35° on 2θ scale.

2.5 Thermal methods of analysis

DSC curves were recorded on a SETARAM DSC 131 instrument (*SETARAM Instrumentation*, France) at heating rates of 0.5 to 5 K min^{-1}. 4 to 10 mg samples were used in closed aluminium crucibles. Melting temperatures and enthalpies of melting were calculated from 5 independent runs. Confidence interval was calculated based on a Student's t-distribution with a 5 % significance level.
The isobaric heat capacity measurements were performed on a SETARAM DSC 111 instrument (*SETARAM Instrumentation*, France) operating with a Tian-Calvet type sensor. Around 80 mg sample was used in closed 150 µL aluminium crucibles. For liquid phase heat capacity measurements, the sample was first heated above the melting point and then slowly supercooled. The measurements were performed in a stepwise mode in 8 K steps with a heating rate of 5 K min^{-1}.

2.6 Melt phase diagram

Mixtures of different compositions were dissolved in ethanol and recrystallized at room and elevated temperature (100 °C), then ground in a mortar. The DSC analyses were performed as described above. For solidus and eutectic line construction the onset temperatures were plotted in the phase diagram. The DSC peak maxima were used for liquidus line construction.

3 Results and Discussion

3.1 Characterization of phenylpiracetam crystal forms

Investigation of racemic and homochiral phenylpiracetam reveals that the racemic mixture crystallises in one form (*rac*–A), however, two different crystal forms *hom*–A and *hom*–B can be obtained for a homochiral sample. PXRD patterns and DSC curves of all three crystalline phases are given in Figure 2. Nearly identical PXRD patterns of *rac*–A and *hom*–A indicate great structural similarity of those crystalline phases, indicating possible solid solution formation. DSC study shows that the melting of *hom*–A is accompanied by a subsequent recrystallization of *hom*–B, which is observed as an exothermic peak. Melting points and enthalpies of melting are listed in the Table 1. As there are two single component phases (*hom*–A and *hom*–B) in the scope of studied system, the question arises, whether there is a monotropic or an enantiotropic relationship between

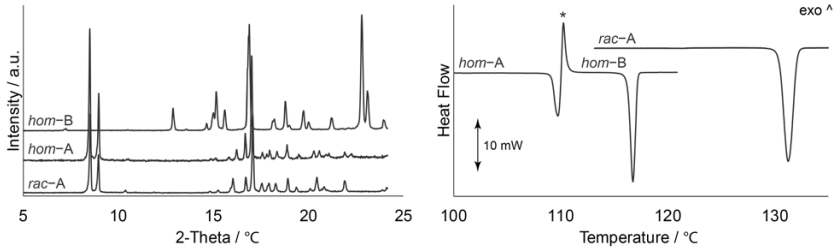

Fig. 2: PXRD patterns and DSC curves of racemic and homochiral phenylpiracetam crystalline phases.

Tab. 1: Melting points and enthalpies of melting of phenylpiracetam crystal forms.

Form	Melting point / °C	ΔH^{f} / kJ mol^{-1}
rac–A	130.4	29.1
hom–A	109.196(13)	24.9(9)
hom–B	116.32(6)	22.2(7)

them. Taking into account that the enthalpy of melting is higher for the lower melting form (Table 1), it is suggested[4] that *hom*–A and *hom*–B are enantiotropically related. The relationship was confirmed by slurrying *hom*–B seeded with *hom*–A for a few days at room temperature in a solvent, after which only the characteristic PXRD peaks of *hom*–A was observed. The transition point was determined based on purely thermodynamic approach by calculating the Gibbs free energy difference of *hom*–A and *hom*–B as a function of temperature using isobaric heat capacity measurements and determined melting temperatures and enthalpies of melting. The transition point for *hom*–A and *hom*–B transition is 70(13) °C (large uncertainty arises from the large error for the enthalpy of melting).

3.2 Melt phase diagram of phenylpiracetam enantiomers

The phase diagram (Figure 3) shows existence of solid solutions of phenylpiracetam enantiomers around the racemic and near the pure enantiomer concentration regions. There is a relatively narrow miscibility gap between the phenylpiracetam enantiomer solid solutions α and β. Close to the eutectic temperature the biphasic region exists between around 2 and 9 % enantiomeric composition. The eutectic invariant is observed at 114.4(4) °C and around 3 : 97 enantiomeric composition. The metastable equilibrium of solid solution α can also be observed. As the enantiotropic relationship holds, samples of a composition below 0.1 mole fraction of the opposite enantiomer crystallized at room temperature show absence of eutectic melting. At temperatures below the enantiotropic transition point phenylpiracetam enantiomers show complete miscibility in the solid state.

3.3 Structures of phenylpiracetam crystal forms

Crystal structures of *hom*–A and *hom*–B were determined. Selected crystallographic data are presented in Table 2. The overall structures of phenylpiracetam crystal forms are built by packing together chains in case of *hom*–A and layers in case of *hom*–B (Figure 4). There is a large variety of phenylpiracetam conformers within only the two crystal structures. Asymmetric unit of *hom*–B contains two symmetrically independent molecules, while there are even four different conformers present in *hom*–A crys-

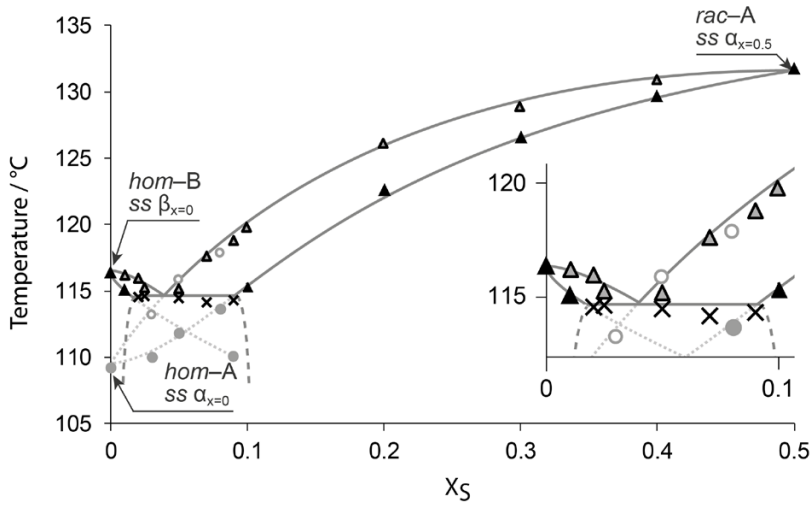

Fig. 3: Melt phase diagram of phenylpiracetam enantiomer system (△ liquidus of the stable equilibrium, ▲ solidus of the stable equilibrium, ✕ eutectics, ○ liquidus of the metastable equilibrium, ● solidus of the metastable equilibrium; the lines are guides for the eyes; the polymorphic phase transition temperature is omitted for clarity).

tal structure. Single enantiomer conformers in pairs are approximate mirror images to each other, as a result conformers can be replaced by their opposite chirality homeomorphic counterparts. Similar structural feature is present in most of the other solid solution structures reported in the literature[5–7]. In Fig. 4 it is seen that the chiral carbon substituents are not directly involved in the hydrogen bond network neither in *hom*–A, nor in *hom*–B structures. Therefore, it is possible to preserve the hydrogen bonds and their geometry by changing the chirality of the molecule. Furthermore, unlike hydrogen bonds, dispersion interactions are not directional, therefore the changes introduced by the molecule replacement may not be so significant.

4 Conclusions

Enantiomers of pharmaceutically active ingredient phenylpiracetam show complete miscibility in the solid state below 70(13) °C (solid solution α). Above this temperature solid solution β exists near the pure enantiomer composition region and solid solution α is stable around the racemic composition. The structural origin of the two solid solutions is the same as found in most of the other solid solutions reported in the literature — pairs of conformers that are approximate mirror images are present. Furthermore, enantiomers in both crystal structures can be replaced by each other preserving the hydrogen bond network, which could be the origin of the lack of molecular site stereoselectivity.

Tab. 2: Selected crystallographic data of phenylpiracetam crystal structures.

	hom–B *ss* $\beta_{x=0}$	*hom*–A *ss* $\alpha_{x=0}$
Crystal system	Orthorhombic	Triclinic
Space group	$P2_12_12_1$	$P1$
a / Å	8.1318(2)	6.11810(10)
b / Å	11.4712(3)	10.8017(3)
c / Å	24.0264(7)	17.2658(5)
α / °	90	76.5724(12)
β / °	90	84.5852(11)
γ / °	90	81.4105(18)
V / Å^3	2241.22(10)	1095.27(5)
Calculated density / g cm^{-3}	1.294	1.324
Z, Z'	8, 2	4, 4
Reflections collected	5126	6863
Reflections with $I > 2\sigma(I)$	3348	5954
Final R $(I > 2\sigma(I))$	0.0603	0.0409
Goodness of fit F^2	1.037	1.082

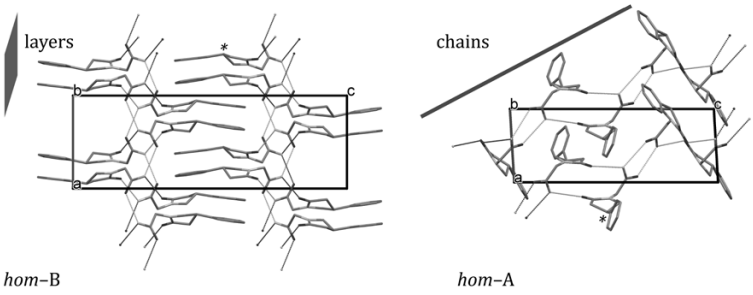

Fig. 4: Representation of packing in *hom*–A and *hom*–B structures (asymmetric carbon marked with an asterisk).

References

(1) Bredikhin, A. A.; Bredikhina, Z. A.; Zakharychev, D. V. Crystallization of chiral compounds: Thermodynamical, structural and practical aspects. *Mendeleev Communications* **2012**, *22*, 171–180.

(2) Taratin, N. V.; Lorenz, H.; Kotelnikova, E. N.; Glikin, A. E.; Galland, A.; Dupray, V.; Coquerel, G.; Seidel-Morgenstern, A. Mixed Crystals in Chiral Organic Systems: A Case Study on (R)- and (S)-Ethanolammonium 3-Chloromandelate. *Crystal Growth & Design* **2012**, *12*, 5882–5888.

(3) Brandel, C.; Amharar, Y.; Rollinger, J. M.; Griesser, U. J.; Cartigny, Y.; Petit, S.; Coquerel, G. Impact of Molecular Flexibility on Double Polymorphism, Solid Solutions and Chiral Discrimination during Crystallization of Diprophylline Enantiomers. *Molecular Pharmaceutics* **2013**, *10*, 3850–3861.

(4) Hilfiker, R., *Polymorphism: In the Pharmaceutical Industry*, 2006, pp 1–414.

(5) Bredikhin, A. A.; Bredikhina, Z. A.; Zakharychev, D. V.; Gubaidullin, A. T.; Fayzullin, R. R. Chiral drug timolol maleate as a continuous solid solution: Thermochemical and single crystal X-ray evidence. *CrystEngComm* **2012**, *14*, 648–655.

(6) Vogt, F. G.; Copley, R. C. B.; Mueller, R. L.; Spoors, G. P.; Cacchio, T. N.; Carlton, R. A.; Katrincic, L. M.; Kennady, J. M.; Parsons, S.; Chetina, O. V. Isomorphism, Disorder, and Hydration in the Crystal Structures of Racemic and Single-Enantiomer Carvedilol Phosphate. *Crystal Growth & Design* **2010**, *10*, 2713–2733.

(7) Huang, J.; Chen, S.; Guzei, I. A.; Yu, L. Discovery of a Solid Solution of Enantiomers in a Racemate-Forming System by Seeding. *Journal of the American Chemical Society* **2006**, *128*, 11985–11992.

VI

Rekis, T.; Oša, G.; Bērziņš, A.; Actiņš, A.

Pimobendāna polimorfās kristāliskās A formas iegūšanas paņēmiens

Patents LV A61K31/501 14737, **2013**

LV 14737

(19) LATVIJAS REPUBLIKAS
PATENTU VALDE

(11) LV 14737 B

(51) Int.Cl A61K31/501
A61P9/00
C07D403/04

Latvijas patents uz izgudrojumu
2007.g. 15.februāra Latvijas Republikas likums

(12) Īsziņas

(21) Pieteikuma numurs: P-13-86

(22) Pieteikuma datums: 25.06.2013

(41) Pieteikuma publikācijas datums: 20.10.2013

(45) Patenta publikācijas datums: 20.12.2013

(73) Īpašnieks(i):
LATVIJAS UNIVERSITĀTE
Raiņa bulvāris 19, Rīga LV-1586, LV

(72) Izgudrotājs(i):
Toms RĒĶIS (LV),
Gunita OŠA (LV),
Agris BĒRZIŅŠ (LV),
Andris ACTIŅŠ (LV)

(74) Pilnvarotais vai pārstāvis:
Aleksandra FORTŪNA
FORAL Intelektuālā īpašuma aģentūra, SIA
a/k 98, Rīga LV-1050, LV

(54) Virsraksts: **PIMOBENDĀNA POLIMORFĀS KRISTĀLISKĀS A FORMAS IEGŪŠANAS PAŅĒMIENS**

(57) Kopsavilkums: Izgudrojums attiecas uz pimobendāna iegūšanas paņēmieniem. Tiek piedāvāts pimobendāna polimorfās kristāliskās A formas iegūšanas paņēmiens, kas ietver šādus soļus:
(i) pimobendāna izšķīdināšana polārā šķīdinātājā temperatūrā, kas tuva šķīdinātāja viršanas temperatūrai, karsta ūdens pievienošana mazās porcijās, izturot ap 60 °C temperatūrā, šķīduma atdzesēšana līdz istabas temperatūrai un kristālu izdalīšana, kurus skalo ar acetonu un žāvē, iegūstot pimobendāna monohidrātu;
(ii) solī (i) iegūtā pimobendāna monohidrāta suspendēšana virstošā polārā aprotiskā šķīdinātājā;
(iii) solī (ii) iegūtās suspensijas atdzesēšana līdz istabas temperatūrai, filtrēšana, skalošana ar acetonu, žāvēšana un pimobendāna kristāliskās A formas izdalīšana.

IZGUDROJUMA APRAKSTS

Tehnikas joma

Izgudrojums attiecas uz pimobendāna iegūšanas paņēmieniem, konkrēti, uz pimobendāna polimorfās kristāliskās A formas iegūšanas paņēmieniem.

Tehnikas līmenis

Pimobendāns ar strukturālu formulu:

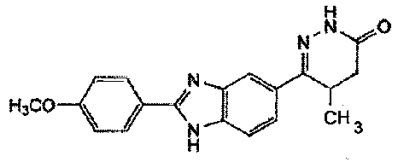

(1)

ir zināms kā aktīva farmaceitiska viela, kuru izmanto sirds mazspējas ārstēšanai, kā arī ir veterinārais preparāts, kuru izmanto suņu sirds mazspējas ārstēšanai.

Ir zināms pimobendāna kristāliskas A formas iegūšanas paņēmiens (EP 2338493), kurš satur šādas stadijas: pimobendāna monohidrāts tiek izšķīdināts 1,4-dioksānā, pēc tam šķīdumu vāra, un filtrātu iegūst ar karstās filtrācijas palīdzību, tad tas tiek atdzesēts no 15 līdz 20° C, veidojas nogulsnes, kuras filtrē un žāvē zem zema spiediena no 60 līdz 70° C temperatūrā, un pimobendāna kristālisko dioksāna solvātu iegūst balta pulvera veidā. Pimobendāna kristāliskais dioksāna solvāts tiek samaisīts ar toluolu, karsēts līdz viršanas temperatūrai un tiek pakļauts karstai filtrācijai, tad iegūtais produkts tiek mazgāts ar toluolu un žāvēts zema spiediena no 11 līdz 120° C temperatūrā, kā rezultātā pimobendāna kristāliskā A forma tiek iegūta balta pulvera veidā.

Ir zināms uzlabots pimobendāna kristāliskās A formas ražošanas paņēmiens (WO 2011/124638), kas satur šādas stadijas:

(a) solvāta savienojuma ar formulu (1) nodrošināšana;

(b) pēc izvēles atlikušā ūdens aizvākšana ar azeotropisku destilāciju;

(c) minētā savienojuma apstrādāšana, lai ar atkārtotu kristalizāciju no suspensijas iegūtu ne-solvāta kristālisko savienojumu ar formulu (1), pie kam šķīdinātājs ir izvēlēts no grupas, kas sastāv no lineāra vai sazarota C_{1-4}alkohola, tāda kā metanols, etanols, 1-propanols, 2-propanols un n-butanols; vai C_{1-4}alkil esteris, tāds kā butilacetāts vai etilacetāts; un to maisījumi;

(d) ne-solvāta kristāliskā savienojuma ar formulu (1) izolēšana,

ar noteikumu, ka tad, ja solvāta savienojums ar formulu (1) ir hidratēts savienojums ar formulu (1), atlikušais ūdens (b) solī tiek aizvākts ar azeotropisku destilāciju.

Izgudrojuma izklāsts

Viens no izgudrojuma mērķim ir racionālāka kristalizācijas procesa izveide, kas ļautu ekonomiskāk izmantot ražošanas resursus (par ~5%). Ražošanas procesā pimobendāna A polimorfo formu, ko tālāk izmanto kā aktīvo substanci tabletēs, iegūst no dioksāna solvāta. Tika veikta A formas sintēzes optimizācija, jo suspendējot pimobendāna dioksāna solvātu toluolā, iespējams iegūt arī nestehiometrisko solvātu g, kas nav piemērots kā aktīva farmaceitiska viela gatavā forma, un kura veidošanās ir nevēlama. Izgudrojuma ietvaros veicot jaunu pimobendāna kristālisko formu meklējumus, tika iegūtas piecas nesolvatētās formas, četri hidrāti un četri solvāti ar dažādiem šķīdinātajiem. Vienā aspektā šis izgudrojums attiecas uz procesu, lai iegūtu pimobendāna polimorfo A formu, kura izdalīšana notiek ar zināmiem paņēmieniem, piemēram, filtrāciju, centrifugēšanu, dekantēšanu.Citā aspektā izgudrojums attiecas uz farmaceitiskām kompozīcijām, kas satur pimobendāna polimorfo A formu, kas iegūta saskaņā ar piedāvāto paņēmienu. Vēl citā aspektā šis izgudrojums attiecas uz šādi iegūto pimobendāna polimorfo A formu izmantošanu veterināra preparāta ražošanai, kas paredzēts suņu sirds mazspējas ārstēšanai.

Piedāvātais paņēmiens pimobendāna polimorfās kristāliskās formas A iegūšanai, kas ietver šādus secīgus soļus:

(i) pimobendāna izšķīdināšanu polārā šķīdinātājā (metanolā, etanolā, n-propanolā vai *izo*-propanolā) temperatūrā, kas tuva šķīdinātāja viršanas temperatūrai, pēc tam karsta ūdens mazās porcijās pievienošanu, uzturot temperatūru ap 60° C, šķīduma atdzesēšanu līdz istabas temperatūrai, izturēšanu un no tā kristālu izdalīšanu, kurus skalo ar acetonu un žāvē, iegūstot pimobendāna monohidrātu;

(ii) iepriekšējā solī iegūtā pimobendāna monohidrāta suspendēšanu virstošā polārā aprotiskā šķīdinātājā (3-pentanona, nitrometāna, acetonitrila, 2-butanona, etilacetāta);
(iii) iepriekšējā solī iegūtās suspensijas atdzesēšanu līdz istabas temperatūrai, filtrēšanu, skalošanu ar acetonu, žāvēšanu un pimobendāna kristāliskās A formas izdalīšanu.

Piedāvāto paņēmienu īsteno šādi: pimobendāns tiek izšķīdināts metanolā (etanolā, *n*-propanolā, *izo*-propanolā) temperatūrā, kas tuva šķīdinātāja viršanas temperatūrai, un tam tiek pievienots karsts ūdens mazās porcijās, turklāt šķīduma temperatūra tiek uzturēta aptuveni 60 C. Šķīdums lēnām tiek atdzesēts līdz istabas temperatūrai 4 stundu laikā, līdz ir izveidojušies viegli pelēki vidēja izmēra kristāli. Tos skalo ar acetonu un žāvē 80 C un tiek iegūts pimobendāna monohidrāts. Pimobendāna monohidrātu var atdalīt ar iepriekšējā tehnikas līmeņa paņēmieniem, piemēram, filtrāciju, centrifugēšanu, pārliešanu.

Izgudrojuma realizācijas piemēri.

1.piemērs.
Pimobendāna monohidrāta iegūšana pārkristalizējot

Pimobendāns (0,20 g) tiek izšķīdināts (5 mL) metanolā (etanolā, *n*-propanolā, *izo*-propanolā) temperatūrā, kas tuva šķīdinātāja viršanas temperatūrai. Tiek pievienots karsts ūdens (5 mL) mazās porcijās, un šķīduma temperatūra uzturēta vismaz 60 °C. Šķīdums lēnām tiek dzesēts līdz istabas temperatūrai 4 stundu laikā, līdz ir izveidojušies viegli pelēki vidēja izmēra kristāli. Tos skalo ar acetonu (10 mL) un žāvē 80 °C. Tiek iegūts 0,18 g pimobendāna monohidrāta (iznākums 90 %).

2.piemērs.
Pimobendāna polimorfa iegūšana no pimobendāna hidrāta

Pimobendāna monohidrāts (0,20 g), kas pagatavots kā piemērā 1, suspendē virstošā 3-pentanonā (nitrometānā, acetonitrilā, 2-butanonā, etilacetātā). Pēc vienas stundas suspensiju atdzesē līdz istabas temperatūrai un filtrē, nogulsnes skalo ar acetonu (3 mL) un žāvē 80 °C. Iznākums ir 76 %.

3.piemērs.

Pimobendāna polimorfa iegūšana pārkristalizējot

Pimobendānu (0,11 g) izšķīdina virstošā acetonitrilā (7 mL). Brīdī, kad paradās pirmie kristāli, šķīdumu lēnām atdzesē līdz istabas temperatūrai. Nogulsnes filtrē, skalo ar acetonu (2 mL) un žāvē 80 °C. Iznākums ir 88 %.

Pretenzijas

1.Pimobendāna polimorfās kristāliskās A formas iegūšanas paņēmiens, kas ietver šādus soļus:

(i) pimobendāna izšķīdināšana polārā šķīdinātājā temperatūrā, kas tuva šķīdinātāja viršanas temperatūrai, pēc tam karsta ūdens pievienošana mazās porcijās, izturot ap 60° C temperatūrā, šķīduma atdzesēšana līdz istabas temperatūrai, kristālu izdalīšana no tā, kristālu skalošana ar acetonu un žāvēšana, iegūstot pimobendāna monohidrātu;

(ii) (i) solī iegūtā pimobendāna monohidrāta suspendēšana virstošā polārā aprotiskā šķīdinātājā;

(iii) (ii) solī iegūtās suspensijas atdzesēšana līdz istabas temperatūrai, filtrēšana, skalošana ar acetonu, žāvēšana un pimobendāna kristāliskās A formas izdalīšana.

2. Paņēmiens saskaņā ar 1. pretenziju, kur polārais šķīdinātājs ir metanols, etanols, n-propanols vai *izo*-propanols.

3. Paņēmiens saskaņā ar 1.un 2. pretenziju, kur polārais aprotiskais šķīdinātājs ir 3-pentanons, nitrometāns, acetonitrils, 2-butanons vai etilacetāts.

4. Farmaceitiskā kompozīcija, kas ietver polimorfās kristāliskās A formas pimobendānu, kas iegūts saskaņā 1.-3.pretenzijā aprakstīto paņēmienu.

5. Veterinārais preparāts, kas ietver polimorfās kristāliskās A formas pimobendānu, kas iegūts saskaņā ar 1.-3.pretenzijā aprakstīto paņēmienu.

Promocijas darbs "Enantiomēru atpazīšana kristāliskā stāvoklī: izvēlētu mazu organisku molekulu enantiomēru veidoto cieto šķīdumu strukturālā un termodinamiskā daba" izstrādāts Latvijas Universitātē, Maksa Planka Kompleksu tehnisku sistēmu dinamikas institūtā un Boloņas Universitātē.

Ar savu parakstu apliecinu, ka pētījums veikts patstāvīgi, izmantoti tikai tajā norādītie informācijas avoti un iesniegtā darba elektroniskā kopija atbilst izdrukai.

Autors: _____ /Toms Rēķis/ _____
(paraksts) (datums)

Rekomendēju darbu aizstāvēšanai.

Vadītāja: _____ / Dr.chem. Liāna Orola/ _____
(paraksts) (datums)

Darbs iesniegts Ķīmijas fakultātes Promocijas padomē: _____
(datums)

Padomes sekretārs _____ /Dr.chem. Jāzeps Logins/
(paraksts)

Darbs aizstāvēts LU Ķīmijas fakultātes Promocijas padomes sēdē:
10.05.2018. prot. Nr. _____

Padomes sekretārs _____ /Dr.chem. Jāzeps Logins/
(paraksts)